THEORY OF CYCLIC VOLTAMMETRY AT MACROPOROUS ELECTRODES

Inaugural-Dissertation
to obtain the academic degree

Doctor rerum naturalium
(Dr. rer. nat.)

submitted to the Department
of Biology, Chemistry, Pharmacy of
Freie Universität Berlin

by

Tim Tichter

August 2020

1st REVIEWER: Prof. Dr. Ing. Christina Roth
Universität Bayreuth, Germany

2nd REVIEWER: Prof. Dr. Beate Paulus
Freie Universität Berlin, Germany

SUPERVISOR: Prof. Dr. Ing. Christina Roth
Universität Bayreuth, Germany

DATE OF DEFENSE: OCTOBER 12TH 2020

Berlin, ...

This thesis was written in original TEX language developed by Donald E. Knuth and typset using a custom version of the LATEX template by Leslie Lamport accessible at `https://hci.rwth-aachen.de/karrer-thesistemplate`. The body text is set in 12pt *Latin Modern Roman*.

I hereby declare that I have created this work completely on my own and used no other sources or tools than the ones listed, and that I have marked any citations accordingly.

.....

Berlin, August *2020*
Tim Tichter

Abstract

Investigating the electrokinetic performance of novel electrode materials by means of diffusional cyclic voltammetry has emerged to the standard approach in electrochemistry. The straightforward implementation of the method in a three-electrode compartment provides scientists with a feasible ex-situ technique for assessing reaction kinetics in terms of potential-dependent redox currents. Providing that well-defined diffusion conditions are complied, i.e. the experiments are conducted at planar electrodes in a semi-infinite diffusion domain, characteristic features such as the separation, symmetry and magnitude of the redox peaks can be related unambiguously to the electrode kinetics. However, as soon as non-planar electrodes or electrodes with finite diffusion domains are employed an equivocation between the measured redox peaks and the intrinsic electrode kinetics emerges. Consequently, a quantitative interpretation of cyclic voltammetry data becomes exceptionally arduous. In particular porous structures like felts and foams, predominantly utilized as electrode materials in the field of battery research, exhibit an intimidating ambiguity of the polarographic current signal. Therefore, the majority of experimentalists restrict themself to a qualitative interpretation of cyclic voltammetry data in terms of arbitrarily chosen onset-potentials. Scientists who are still targeting to quantify the electrode kinetics usually aim to exploit alternative techniques such as electrochemical impedance spectroscopy. However, from a theoretical perspective this approach is not capable of solving the dilemma either since the experiments are subjected to the same diffusion complication, examined with a different potential perturbation only. Consequently, developing a theory of cyclic voltammetry for porous electrodes is inevitable to permit a quantitative analysis of experimental results.

This thesis consists of the cumulative work on the theory of cyclic voltammetry at macroporous electrodes with emphasis on felt-like structures. It is demonstrated that linking the high sensitivity of cyclic voltammetry with a sophisticated

mathematical diffusion model allows for an electrochemical and morphological characterization of porous electrodes simultaneously, promoting the so-called „*electrochemists spectroscopy* “ to the next level. All theoretical concepts are supported by experimental data acquired for the electrochemical redox-reactions of vanadium(II)/ vanadium(III) and oxovanadium(IV)/ dioxovanadium(V), relevant in the field of vanadium redox-flow battery research.

In a first approximation, porous electrodes are treated as random arrays of microelectrodes in a finite diffusion space with a statistically fluctuating size. A systematic investigation of simulated and experimentally acquired cyclic voltammetry data for both, porous and non-porous electrodes, draws an enlightening picture on the complex interplay of electrode porosity and reaction kinetics. With this knowledge, precise values for the heterogeneous rate constant of the oxovanadium(IV)/ dioxovanadium(V) redox reaction are obtained. These values usually scatter over orders of magnitude in the recent literature, most likely due to an inconsequent interpretation of data.

In another study, a strategy for real-space simulation of cyclic voltammetry at carbon felt electrodes is presented. For this purpose, in-situ micro X-ray computed tomography is exploited to construct a template of the three-dimensional diffusion domain inside a porous electrode. This renders any statistical assumptions obsolete. To perform the simulations, two self-reliant computational methods, namely digital simulation and convolutive modeling, are combined. The resulting method offers significant advantages with respect to computation time, programming effort and mathematical complexity. Since effects of electrochemical double-layer charging, nonlinear contributions of ohmic resistances, coupled chemical reactions and limited electron transfer kinetics can be accounted for readily, the novel approach covers an extraordinarily wide range of electrochemical situations.

The exceptional endowment of simulating polarographic experiments at porous electrodes was finally implemented into an open source program named „*Polarographica* “. This software provides the experimentalists community with a straightforward way of interpreting cyclic voltammetry data of porous electrodes in terms of a fitting routine. Since many other electroanalytical techniques are supported in the environment of *Polarographica* as well, it will eventually lead to a more decent interpretation of cyclic voltammetry data, based on mathematical models instead of ambiguous current peaks and arbitrarily chosen onset-potentials.

Zusammenfassung

Die Zyklische Voltammetrie hat sich als Standardmethode für die Charakterisierung der kinetischen Leistung neuartiger Elektrodenmaterialien durchgesetzt. Die einfache Umsetzung des Verfahrens in einem Drei-Elektroden-Aufbau ermöglicht Experimentatoren eine Evaluation der intrinsischen Reaktionskinetik von Elektrokatalysatoren über potenzialabhängige Redoxströme. Sofern dabei die elektrochemischen Untersuchungen unter wohldefinierten Diffusionsbedingungen an planaren Elektroden in halbunendlicher Diffusion erfolgen, korrelieren Separation, Symmetrie und Magnitude einer voltammetrischen Redoxkurve quantitativ und eineindeutig mit der Elektrodenkinetik. Werden hingegen nicht-planare Elektroden oder Elektroden mit finiten Diffusionsdomänen genutzt, so besteht eine Mehrdeutigkeit des gemessenen Stromsignals, welche die quantitative Bewertung der Elektrodenkinetik als außerordentlich mühsam gestaltet. Dies ist insbesondere für poröse Elektrodenmaterialien wie Filze oder Schäume der Fall, welche überwiegend im Bereich der Batterietechnik Einsatz finden. Aus diesem Grund beschränkt sich die Mehrheit der Experimentatoren gegenwärtig auf eine rein qualitative Interpretation der voltammetrischen Daten anhand von — oftmals willkürlich definierten — Onset-Potenzialen. Wissenschaftler/innen, die dennoch eine quantitative Analyse der Elektrodenkinetik anstreben, weichen hingegen zumeist auf alternative Methoden wie die elektrochemische Impedanzspektroskopie aus. Von einer theoretischen Perspektive vermag dieser Ansatz jedoch ebenfalls nicht das Dilemma zu lösen, da die Experimente denselben komplizierten Diffusionbedingungen unterworfen sind. Aus diesem Grund erscheint die Entwicklung einer ausgereiften Theorie der Zyklischen Voltammetrie für poröse Elektrodenstrukturen als unumgänglich, wenn eine quantitative Interpretation der Messergebnisse gewünscht ist.

Die vorliegende Dissertaion enthält die gesammelten Ergebnisse zur Theorie der Zyklischen Voltammetrie an makroporösen Elektroden mit dem Schwerpunkt

auf filzartigen Strukturen. Es wird gezeigt, dass die Kombination der hohen Sensitivität der Zyklischen Voltammetrie mit einem ausgereiften Diffusionsmodell eine simultane Charakterisierung der elektrochemischen Kinetik sowie der Morphologie von porösen Elektrodenmaterialien ermöglicht. Sämtliche theoretische Konzepte werden dabei stets von experimentellen Daten für die elektrochemischen Reaktionen der Vanadium(II)/Vanadium(III) und Oxovanadium(IV)/Dioxovanadium(V) Redoxpaare, welche im Bereich der Vanadium Redox-Fluss Batterien zum Einsatz kommen, begleitet.

In einer ersten Näherung werden poröse Elektroden als ein Netzwerk aus Mikroelektroden mit finiten Diffusionsdomänen von statistisch fluktuierender Größe betrachtet. Eine systematische Untersuchung von simulierten und experimentell gewonnenen Daten generiert dabei ein aufschlussreiches Bild der komplexen Zusammenhänge von diffusivem Massentransport, Elektrodenporosität und intrinsischer katalytischer Aktivität. Auf diese Weise werden schließlich akkurate Werte für die Reaktionsgeschwindigkeitskonstanten des heterogenen Ladungstransfers der Oxovanadium(IV)/Dioxovanadium(V) Redoxreaktion an Kohlenstoffelektroden erhalten, welche in der aktuellen Literatur um Größenordnungen streuen.

In einer weiteren Studie wird eine Strategie für die Simulation polarographischer Experimente in filzartigen Kohlenstoffelektroden präsentiert, welche die reale, dreidimensionale Struktur des Diffusionsraumes einer porösen Elektrode berücksichtigt. Zu diesem Zweck wird zunächst die tatsächliche Diffusionsdomäne eines Kohlenstofffilzes mittels in-situ Röntgentomographie rekonstruiert, wodurch sämtliche statistische Annahmen über interne Diffusionsräume obsolet werden. Anschließend werden zwei voneinander unabhängige Methoden der Berechnung voltammetrischer Experimente, d.h. die Digitale Simulation und die Konvolutive Modellierung, kombiniert. Die resultierende Methode bietet dabei signifikante Vorteile bezüglich der Berechnungsdauer, des Programmieraufwandes und der mathematischen Komplexität. Da in diesem Modell eine Implementierung von elektrochemischen Doppelschichtkapazitäten, nicht-linearen Beiträgen von Ohmschen Widerständen, gekoppelten chemischen Reaktionen und finiter Elektrontransfer Kinetik auf einfachste Art und Weise erfolgen kann, deckt es einen außerordentlich weiten Teil experimenteller Konstellationen ab.

Die Fähigkeit, polarographische Experimente an porösen Elektroden zu simulieren, wurde schließlich in ein Open-Source-Programm mit dem Namen „*Polarographica*“ implementiert. Diese Software bietet eine unkomplizierte Routine für die Interpretation von Zyklovoltammetrie-Daten poröser Elektroden, welche anstelle von willkürlich gewählten Onset-Potentialen auf mathematischen Modellen basiert und künftig zu verlässlicheren Ergebnissen führen kann.

Contents

Chapter 1

Introduction

Before deriving and discussing the theoretical concept of diffusional cyclic voltammetry at macroporous electrode structures in any depth, this chapter will provide an overview on the relevance, features and limitations of this electroanalytical technique for the field of energy conversion and storage with emphasis on the vanadium redox-flow system. Subsequently, the correlation between the five individual publications related to this cumulative work will be elucidated and assembled to the outline of this thesis.

1.1 Motivation

Abstain from fossil fuels! Towards renewable energy sources! Save the global climate! These and similar paradigma are the epitome of a modern and sustainable human culture. Simultaneously, they challenge the scientific community to develop economically and ecologically efficient systems for energy conversion and storage in order to provide a continuous supply of intermittant *'green energy'* derived from wind and solar power. Starting from portable electronics such as smartphones and computers towards electric cars and right up to stationary battery stacks in power plants – energy storage is indispensible in our daily life.

Depending on the technical requirements and the amount of energy to be accumulated, an abundance of technologies is available, e.g. lithium ion batteries [1]–[3], lead accumulators[4], fuel cells [5]–[8], supercapacitors [9]–[13] and flow batteries [14]–[20]. Among these, flow batteries and in particular the vanadium redox-flow battery (VRFB) system are considered as promising devices for a stationary large-scale energy storage [14], [15], [19]–[21]. Owing to the inherent independence of capacity and power, the low-cost factor and the comparably large cycle-lifetime this system has gathered a significant industrial interest [15]. However, the rather poor overall efficiency [14], [15] of this technology impedes its wide range application. Consequently, improving the performance of the VRFB technology is considered as a hot-topic in recent electrochemistry research. The majority of studies is thereby dedicated to increase the intrinsic electrokinetic activity of the typically carbon-based electrode materials. In this context a plethora of modifications involving a) chemical etching, either alkaline [22]–[25] or acidic [26]–[29], b) surface functionalization techniques via plasma treatments [30], [31] c) surface halogenation [32], d) nitrogen doping [33]–[37] and e) surface impregnation techniques with carbon nanoparticles [38]–[49] and/or literally any kind of metal and metal compound [50]–[62] is proposed. However, it is worth to note that, except from the heat treatments, none of these so-called activation methods has made it to a commerical large scale application yet. This might be attributed to the fact that the majority of novel electrode materials is investigated in ex-situ setups only and that depending on the wettability [63] and porosity [64]–[71] of the electrode, the classical electrochemical characterization techniques are likely to be misinterpreted owing to their inherent ambiguity.

When referring to electrochemical characterization techniques, typically two methods, namely cyclic voltammetry (CV) and electrochemical impedance spectroscopy (EIS) are implied. Both of them are virtually as good as each other and should always lead to consistent results. However, since EIS requires for the handling of complex numbers, experimentalists might be discouraged to utilize

it on a first glance [72]. In contrast, CV pretends to be the preferable method since it enables a fast assessment of the electrode kinetics in terms of potential dependent redox currents [73]. However, this is valid only as long as exceptionally well-defined mass transfer conditions are fulfilled – in other words, provided that the electroanalytical experiment is carried out at a planar electrode in a semi-infinite diffusion domain. Furthermore, the electrochemical reaction is restricted to a one-step, one electron process in absence of any coupled homogeneous kinetics. Only under this particular circumstance, magnitude, separation and shape of the respective current wave are unambiguously linked to the electrodes kinetics [74]–[76]. In contrast, interpreting cyclic voltammetry data at non-planar electrodes [77], [78] with optionally finite diffusion domains [79], [80] and coupled chemical reactions [76], [81], [82] will pose a formidable challenge. This is mainly caused by the fact that depending on the geometry of the electrode under investigation the diffusive mass transport of the respective depolarizer will behave substantially different. As a consequence, the measured current signal turns into a highly complex function of the electrode geometry, the diffusion domain size and the electrode kinetics [76]–[85]. A respective example is depicted in figure 1.1. A planar electrode with an impermeable finite diffusion domain will exhibit a narrow peak-to-peak separation as well as a low current magnitude in a CV, since the mass transport decreases as soon as the concentration profile hits the outer boundary [79], [80]. In contrast, the CV of a cylindrical electrode will show a larger peak-to-peak separation and an increased peak current when compared to a planar electrode, since the mass transport increases due to the additional radial diffusion contribution [77], [78]. Neglecting these geometric effects one would, however, term the cylindrical electrode as less active owing to the larger peak-to-peak separation in the CV – which is obviously not true. Now, bearing this in mind, one could go one step further and pose the questions: „How about a cylindrical electrode with an impermeable finite diffusion domain?“ and in particular: „How about a felt electrode which consists of thousands of cylindrical microelectrodes in direct proximity?“. Certainly, it can be expected that in these cases the model of planar semi-infinite diffusion will provide results which are entirely opaque. Therefore it is somewhat astonishing that many experimentalists are still tempted to analyze CV data of macroporous electrodes in terms of peak separations or other — almost arbitrarily chosen — parameters like onset potentials only. Concerning the VRFB system this ambiguous way of interpreting experimental results might be the particular reason for the vast discrepancy of kinetic data [86] and the related multitude of the aforementioned *'activation methods'*. Simultaneously, it might have disengaged other scientists from utilizing CV in general and to regard in-operando electrochemistry in sophisticated

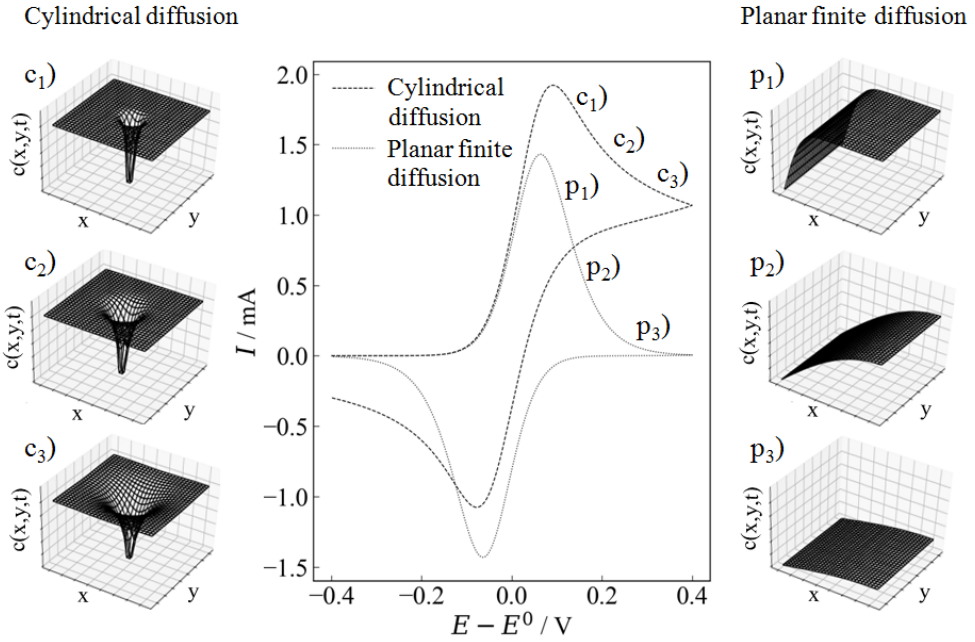

Figure 1.1: Qualitative effect of the electrode geometry on the concentration profiles and the current response during a CV experiment. In case of a cylindrical electrode the radial diffusion contribution provides a larger mass transport which enforces a slow depletion and an increased magnitude of the CV current wave. In contrast, a planar finite diffusion domain results in a lack of electrochemically active species as soon as the concentration profile hits the outer boundary, which results in a fast decay and a low magnitude in the CV current. The points c_1), c_2) and c_3) and p_1), p_2) and p_3) correspond to the local two-dimensional concentration profiles during the forward potential sweep of a CV at a cylindrical electrode in a semi-infinite and a planar electrode in a finite diffusion domain, respectively.

setups as the only proper approach instead [87]. Although this practice will reflect the most realistic scenario, it will introduce an abundance of other uncertainties, which will finally prevent a conclusive determination of the intrinsic electrode kinetics. If scientists therefore still aspire to utilize cyclic voltammetry for assessing the electrode kinetics, the development of a reliable method for the interpretation of experimental data is mandatory.

Contributing such a strategy was exactly the motivation of this thesis. It was intended that linking the intrinsically high sensitivity of cyclic voltammetry with a sophisticated diffusion model should allow for an accurate electrochemical characterization of porous electrodes. The theoretical concept presented in this context captures an electrochemical reaction at any degree of reversibility optionally coupled to a) chemical reactions preceeding and following the electron transfer,

b) unequal diffusion coefficients of the electrochemically active species, c) finite heterogeneous electron transfer kinetics, d) nonlinear effects of ohmic resistances, e) interfacial double-layer capacities (ideal and non-ideal) and f) parallel reactions, competing the desired reaction. It therefore covers an exceptionally wide range of experimental settings and will eventually lead to a significantly more precise interpretation of experimental results.

1.2 Outline

The experimental implementation of diffusional cyclic voltammetry will be outlined in chapter 2. Furthermore, this chapter elucidates the classical pitfalls in the qualitative interpretation of experimental data acquired via this electroanalytical technique. Chapter 3 reviews the theoretical development of diffusional cyclic voltammetry with emphasis on two standard mathematical concepts utilized in this context: a) convolutive modelling and b) digital simulation. Highlighting the advantages and drawbacks of both of these methods this chapter will provide a resumeé of detailed derivations on the fundamentals of diffusional CV in order to familiarize the reader with the complex interplay of electrode kinetics and diffusive mass transfer. In chapter 4, the vanadium redox-flow system will be intruduced since the involved redox-reactions are the reference for all theoretical concepts developed in the present work. Finally, chapter 5 will summarize the results of the five individual publications related to this cumulative thesis. At first, the two research papers entitled

'Finite Heterogeneous Rate Constants for the Electrochemical Oxidation of VO^{2+} at Glassy Carbon Electrodes'.

and

'Rotating Ring-Disc Electrode Measurements for the Quantitative Electrokinetic Investigation of the V^{3+}-Reduction at Modified Carbon Electrodes'

will be discussed in detail. These particular publications focus on the assessment of electrokinetic and hydrodynamic parameters of the vanadium(II)/vanadium(III) (V^{2+}/V^{3+}) and oxovanadium(IV)/dioxovanadium(V) ($VO^{2+}/VO_2{}^{+}$) redox-reactions

at planar glassy carbon model electrodes. Since both studies experimentally circumvent the issue of electrode porosity, estimated hydrodynamic and electrokinetic parameters are regarded as highly accurate reference points for all the following works involving porous structures. Furthermore, by utilizing diffusional cyclic voltammetry in combination with other advanced electroanalytical techniques such as Fourier transform alternating current cyclic voltammetry (FT-ACCV), chronoamperometry (CA) and electrochemical impedance spectroscopy (EIS) the two publications provide valuable insights into the electrode kinetics of the respective vanadium reactions at carbon surfaces. The first publication focussing entirely on macroporous electrode structures, entitled

'Theory of Cyclic Voltammetry in Random Arrays of Cylindrical Microelectrodes Applied to Carbon Felt Electrodes for Vanadium Redox-Flow Batteries',

represents a method-oriented approach for describing the diffusion phenomena in carbon felts. The porous electrodes are thereby treated as an array of cylindrical microelectrodes. Individual electrode fibers are in turn regarded as one-dimensional sub-structures in a finite diffusion domain with a statistically fluctuating size. For this purpose, the theory of an electrochemical reaction at a cylindrical microelectrode in a finite diffusion domain, coupled to preceeding and following homogeneous kinetics, was derived for the first time. The core of this derivation is based on Laplace integral transformation techniques. Since the respective Laplace-domain solution does, however, not possess an analytical time domain solution, the concept of numerical inverse Laplace transformation was introduced. By systematically investigating experimentally acquired and simulated data, this publication impressively demonstrates that CV is capable of resolving electrode kinetics and porosity effects of macroporous electrodes simultaneously. In this manner, it substantially increases the experimental benefit of CV. In a follow-up publication entitled

'Universal Algorithm for Simulating and Evaluating Cyclic Voltammetry at Macroporous Electrodes by Considering Random Arrays of Microelectrodes',

the theoretical concept of cyclic voltammetry at felt electrodes was extended to electrode foams (arrays of spherical pores), layered structures (arrays of electrode sheets) and capillary electrodes (arrays of cylindrical pores). By thoroughly investigating the statistical diffusion domain effect it is shown that electrodes consisting of cylindrical pores and spherical pores will behave qualitatively different than arrays of microcylindrical electrodes and electrode sheets. Furthermore, the statistical diffusion domain effect is proven to be one possible source of the tailing

in experimental CV curves which cannot be explained by classical finite diffusion domain models. In order to provide the strategy of CV simulation at porous electrodes to the experimentalists community, this publication also reports on the free software tool *Polarographica* which was created as a part of the present work and which is already released at *GitHub*. This software provides a graphical user interface for facile simulation and evaluation of CV data. Since *Polarographica* also supports the classical non-porous diffusion models as well as many other electroanalytical techniques, it will eventually lead to a more reliable evaluation of experimental data. Regarding the two aforementioned publications on cyclic voltammetry at porous electrodes it is worth to note that all porous-network models presented, rely on a statistical assumption of the diffusion domain. Furthermore, the effect of coupled ohmic resistances as well as interfacial double layer capacities is not considered so far. These deficiencies were tackled in the fifth and final publication related to this work, entitled

> *'Real-Space Simulation of Cyclic Voltammetry in Carbon Felt Electrodes by Combining Micro CT Data, Digital Simulation and Convolutive Modeling'.*

In this study, the internal diffusion domain of a porous felt electrode was reconstructed from micro X-ray tomographic images. This real-space template renders any statistical assumption on the diffusion domain obsolete. To utilize it for the simulation of electroanalytical experiments, a numerical algorithm based on digital simulation and convolutive modeling was developed. In this strategy, the Douglas–Gunn modification of the three-dimensional Crank–Nicolson algorithm is exploited first to calculate the mass transfer controlled current of the porous network. Based on this real-space diffusion controlled current, the mass transfer function related to the electrode under investigation is calculated subsequently. This particular function is utilized in turn as the base for classical convolutive modeling. This strategy preserves the great advantage of convolutive modeling – the use of a master equation. Furthermore, it circumvents the most crucial inverse Laplace transformation step which is usually linked to convolutive modeling, since it avoids solving the diffusion equation by means of Laplace integral transformation techniques. Finally, the novel procedure allows for including non-linear contributions of ohmic resistances as well as interfacial double layer capacities and therefore covers an exceptionally huge diversity of experimental scenarios.

Chapter 2

Fundamentals

Before targeting the theoretical fundamentals of diffusional cyclic voltammetry, this chapter will familiarize the reader with the experimental implementation and the features of this particular electroanalytical technique. Based on a qualitative overview on the complex interplay of diffusive mass transfer and electrode kinetics, the classical practice of interpreting CV data is outlined. Finally, the common pitfalls in the evaluation of experimental CV data are elucidated.

2.1 Measuring Cyclic Voltammetry

The term *voltammetry* basically originates from the two quantities potential (measured in *Volt*) and current (measured in *Ampere*) which are monitored during an electroanalytical — *voltammetric* — experiment. The designation *cyclic voltammetry* refers to one particular type of voltammetry, where the potential of an electrode under investigation is periodially swept at a time-variant triangular wave (cf. figure 2.1 (A)) [88]. Cyclic voltammetry is typically conducted in a so called three-electrode compartment consisting of an electrode under investigation (working electrode, WE), an electrode closing the electric circuit to the working electrode (counter electrode, CE) and a non-polarizable high impedance electrode serving as external potential anchor (reference electrode, RE). The time-variant potential perturbation is compelled by an instrument known as potentiostat (cf. figure 2.2). This device adjusts the potential difference between the working electrode/counter electrode couple in a way that the voltage between the working electrode/reference electrode pair, which is sensed over a high-impedance connection, follows the desired time-dependent triangular wave[1][2]. The upper and lower inflection points of the potential wave are termed anodic (upper) and cathodic (lower) switching potential, respectively. The rate of potential chage is referred to as sweep rate or scan rate of the experiment. Switching potentials and potential sweep rate are therefore the three free variables during a CV experiment.

Since current and potential are related functionally, the potentiostat can be regarded as an active element which forces any amount of current to pass through the working electrode to achieve a given voltage with respect to the reference electrode. Therefore, one can term cyclic voltammetry as a current controlled technique [88]. Since the current is governed by the flow of charges (electrons), required to obey any electrochemical process, it represents the experimentally observable quantity in a CV measurement. Figure 2.1 (B) depicts the time dependent current response of a classical CV experiment, which follows the potential wave shown in figure 2.1 (A). Plotting the potential versus the current yields the classical *'Bird-neck'* shaped current-voltage curve of a CV experiment as depicted in figure 2.1 (C).

[1] The potential wave is triangular only in case of cyclic voltammetry. It might be adjusted to any desired shape by modifying the program defined by a function generator implemented in the potentiostat.

[2] A perfectly triangular potential wave is a theoretical assumption. Under experimentally relevant conditions, the potential wave is never completey triangular, but rather a staircase wave. However, modern potentiostats are usually able to sufficiently approximate the triangular potential wave by actively smoothing the input signal.

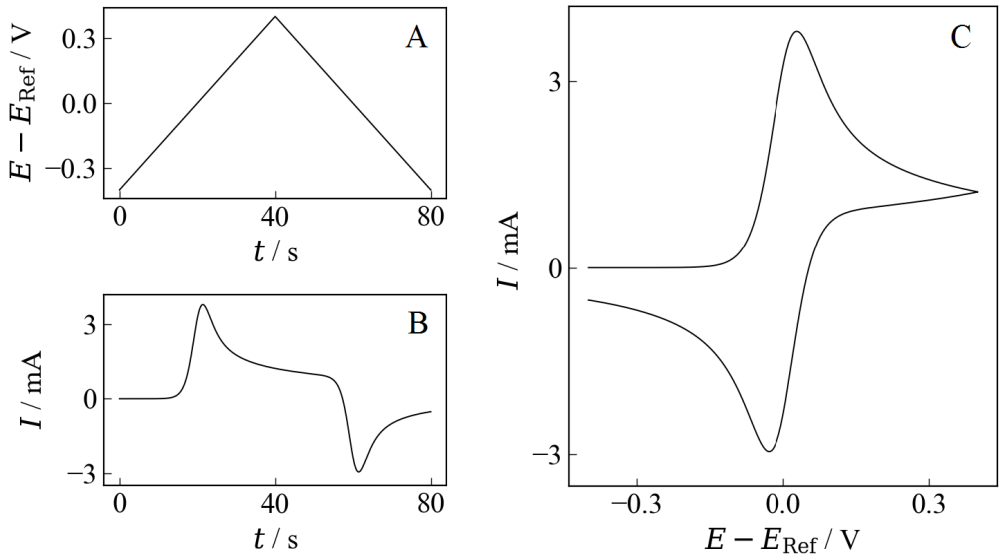

Figure 2.1: (A) Time-variant triangular potential wave between a working electrode and an arbitrary reference electrode of a cyclic voltammetry experiment. (B) Time-dependent Faradaic current of an electrochemically reversible reaction at a planar electrode in semi-infinite diffusion space related to the potential perturbation depicted in panel (A), (C) *'Bird-neck'* shaped current-voltage curve of the cyclic voltammetry experiment depicted in panel (A) and (B).

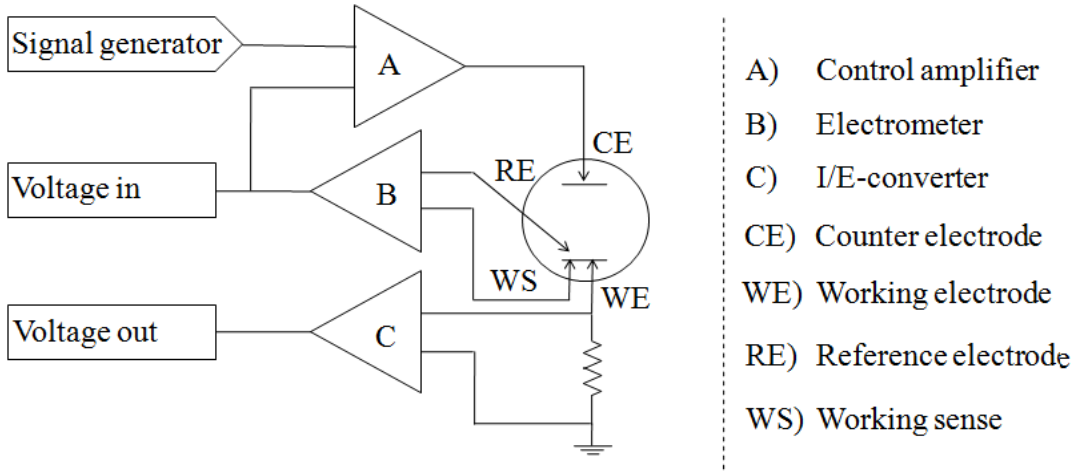

Figure 2.2: Sketch of a potentiostat. The desired potential perturbation is introduced by the signal generator. The working electrode potential is monitored between working sense and reference electrode.

2.2 Interpreting Cyclic Voltammetry

The outstanding advantage of diffusional cyclic voltammetry stems from the exceptionally high sensitivity paired with the comparably low experimental effort [88]. Therefore, CV has emerged to a standard technique in almost any — not necessarily electrochemical — laboratory. It can be utilized for a plethora of applications ranging from electrochemical sensing and trace analysis up to mechanistic investigations of chemical and electrochemical reactions. Cyclic voltammetry features that the position, magnitude and shape of the characteristic current peaks are functionally related to the electrode kinetics, to the electrolyte concentration and to the number of electrons transferred, as long as

- the electroanalytical experiment is conducted at a planar electrode in a semi-infinite diffusion domain,
- the electroanalytical experiment is conducted in a stagnant electrolyte in absense of any convection
- the electrochemical reaction consists of a single-step electron transfer which is not coupled to any chemical kinetics,
- the electrochemical reaction does not involve any adsorption or desorption steps,
- the electrochemical reaction is either strictly reversible (without any activation barrier) or irreversible (kinetically hindered to fulfill the Tafel criterion),
- the concentration of the product is negligible when compared to the educt,
- the only quantity contributing to the total current is Faradaic (no double layer charging),
- migration of ions is negligible — mass transfer is selectively governed by diffusion
- the electrode is homogeneously active over 100% of its area,
- no Ohmic resistances are involved.

Regarging this rather restrictive list, one might get curious on which constraints are the most descisive ones and under which circumstances CV will provide misleading results. In fact, all of the points are extraordinarily important, even if some parametrs can be fine-tuned experimentally to meet the desired requirements. This will be outlined in the following sections.

Qualitative origin of the current/voltage curve

Any CV response can be bisected into two linear potential scans[3] which are termed either anodic (positive potential direction) or cathodic (negative potential direction) sweep. The current response related to each of these individual scanning directions can be regarded as a combination of a reaction controlled and a diffusion controlled sub-region[4]. However, in principle the entire current response in a CV depends on the flux of the active species towards the electrode which is governed by the concentration gradient at the electrodes´ surface. This particular concentration gradient is introduced by the potential perturbation which leads the experiment. The complex interplay of potential perturbation, surface concentrations, the resulting concentration profiles and the fluxes are depicted in figure 2.3. In panel (A) of figure 2.3 the time-dependent triangular potential perturbation of an exemplary CV experiment is displayed. In this particular case the forward scan is chosen to be anodic whereas the reverse scan is cathodic. The rate of potential change was set to be $\nu = 1\ \mathrm{V\,s^{-1}}$. For the sake of simplicity, the example considers an electrochemically reversible electrode reaction. This implies that the surface concentrations are unambiguously related and instantaneously adjusted according to the Nernst equation [74] (equation 2.1).

$$E(t) = E^0 + \frac{RT}{nF} \ln\left(\frac{c_\mathrm{O}(x=0,t)}{c_\mathrm{R}(x=0,t)}\right) \tag{2.1}$$

In equation 2.1, $E(t)$ is the time dependent electrode potential, E^0 is the standard electrode potential, n is the number of electrons transferred, F is Faradays constant, T is the absolute temperature, R is the gas constant and $c_\mathrm{O}(x=0,t)$ and $c_\mathrm{R}(x=0,t)$ are the time-dependent surface concentrations of the oxidized and reduced species, respectively. The time-dependent surface concentration of the electrochemically active species being consumed at the electrode surface and being calculated on the base of equation 2.1 is depicted in figure 2.3 (B). Of course, it can be seen that the most significant change in the surface concentration is achieved when the ratio of the reduced species (here the educt) to the oxidized species (here the product) approaches one.

[3] An electrochemical technique which consists of one linear potential scan only is termed linear-sweep voltammetry (LSV) and represents a half-CV.

[4] At this stage, the extensively used term *'kinetically controlled'*, is deliberately avoided and replaced by *'reaction controlled'*, since an electrochemically reversible reaction will not exhibit any sign of kinetic limitation.

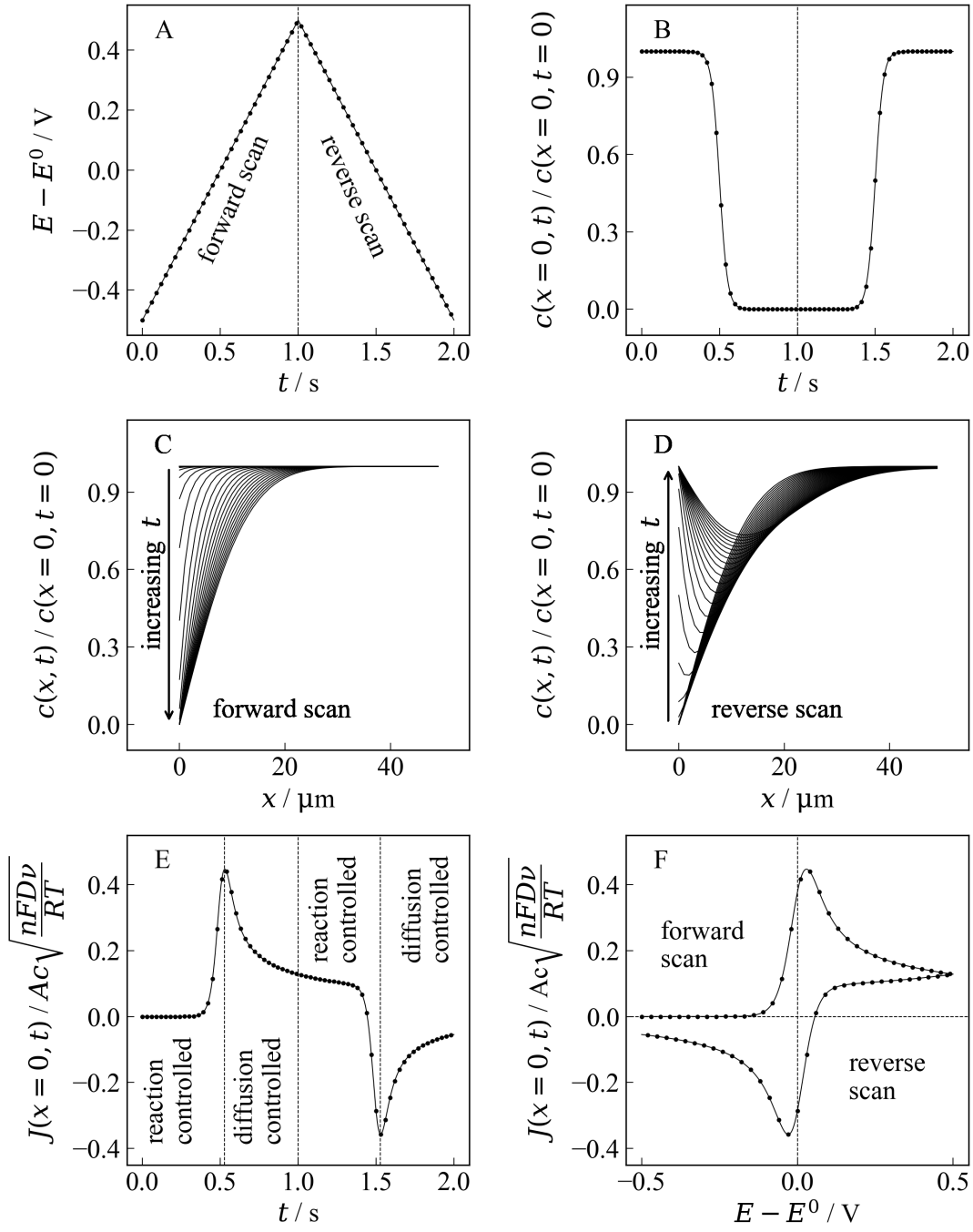

Figure 2.3: (A) Time-dependent potential. (B) Educt surface concentration of a reversible reaction. (C) Educt concentration profile during the forward potential sweep. (D) Educt concentration profile during the reverse potential sweep. (E) Time-dependent dimension-less flux of the educt governed the concentration gradient at the electrode surface. (F) Dimension-less flux of the educt versus the applied potential.

This is fulfilled at $c_{\mathrm{R}}(x = 0, t) = 0.5 \times c_{\mathrm{O}}(x = 0, t = 0)$ if the educt c_{R} is the only species present at $t = 0$. Assuming an initially homogeneous distribution of the electrochemically active species inside the electrolyte, any variation in the surface concentration will entail compensation processes in order to obey the equipartition theorem. Therefore, any loss of educt species at the electrode surface will enforce a diffusive flux of the same towards the electrode [89]. This diffusive flux is in turn proportional to the concentration gradient and is therefore strongly dependent on the concentration profile which is depicted in figure 2.3 (C) for the forward and in figure 2.3 (D) for the reverse scan, respectively. Since the reversibility criterion compells that any amount of electrochemically active species which reaches the electrode surface by diffusion will be instantaneously converted to obey the Nernst equation, the related Faradaic current is directly proportional to the flux, or better, to the concentration gradient at $x = 0$. The time-dependent dimensionless flux of the examplary CV is depicted in figure 2.3 (E). The regions termed *'reaction controlled'* are related to the concentration profiles, where the surface concentration of the electrochemically active species being consumed is significantly different from zero. In contrast, the regions termed *'diffusion controlled'* are related to the concentration profiles, where the surface concentration of the electrochemically active species being consumed is approximately zero. Even though this terminology is convenient, it has to be underlined that the current is always related to the flux and that a strict demarcation between reaction and diffusion control is not possible. Since the two quantities *'potential'* and *'diffusive flux'* are time dependent, the latter can be represented as a function of the former one. This results in the classical cyclic flux/voltage (alias current/voltage) curve which is depicted for the normalized flux in figure 2.3 (F). In this particular representation, the respective forward and reverse potential scan of a CV experiment are neatly separated at the point of potential inflection. The resulting flux/voltage or current/voltage curve possesses two disctinct redox peaks which can be readily utilized for either qualitative or quantitative investigation of the electrode reaction as long as the aforementioned rectrictions are satisfied.

Qualitative interpretation of cyclic voltammetry

When regarding realistic reactions the reversibility criterion, which was assumed so far, has to be questioned since almost any chemical conversion requires for an activation energy. Therefore, it has to be expected that the surface concentration does *particularly not* follow the Nernst equation at each and every time instance

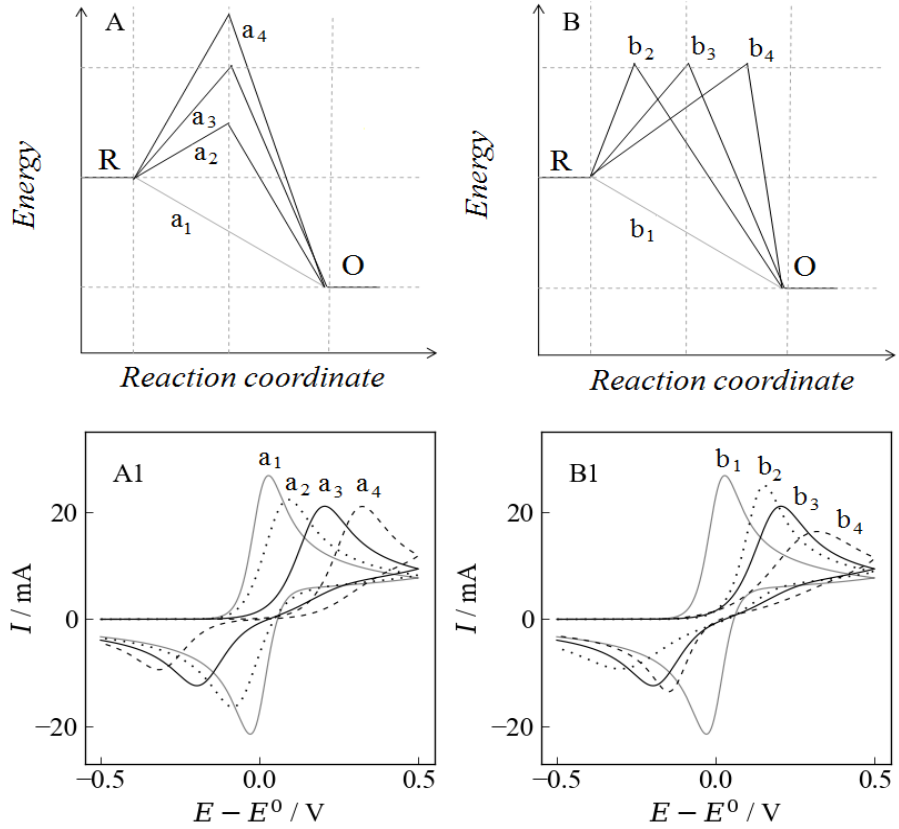

Figure 2.4: (A) and (A1): influence of the height of the activation barrier (scenarios a_1 to a_4) on the peak separation of the current/voltage curve in a CV experiment. (B) and (B1) influence of the symmetry of the activation barrier (scenarios b_1 to b_4) on the shape of the current/voltage curve in a CV experiment. R and O denote the reduced and oxidized species, respectively. The curves a_1 and b_1 do not possess any acivation barrier at all. It can be seen that a high activation barrier (a_4) forces a large peak-to-peak separation in the CV and an early transition state (b_2) favours the forward reaction (here the oxidation).

during a potential sweep. Consequently, also the concentration gradient and the related flux of the electrochemically active species will depend on the electrode kinetics, meaning on the height and the symmetry of the activation barrier of the reaction. Since the height of the activation barrier is proportional to the amount of energy required to surpass it and since the potential is a measure for the energy per charge, it can be expected that the surface concentrations will adjust at comparably larger potentials with respect to the reversible case [88], [89]. In terms of a CV experiment, this implies that a kinetically controlled system will require for more time to respond to the time-variant potential excitation.

Consequently, the respective redox peak in the current-voltage curve of a CV will be more separated as the height of the potential barrier (or the rate of potential change) increases. This scenario is depicted in figure 2.4 (A) and (A1). It can be seen that all potential barriers depicted in figure 2.4 (A) are symmetric and likewise the corresponding CV responses are somewhat uniform as well. In case of a non-symmetric potential barrier — corresponding to an early or a late transition state, respectively — also the CV response will be distorted. This scenario is depicted in figure 2.4 (B) and (B1), respectively. It is mainly caused by the fact that one half reaction is kinetically more feasible than the other one. Regarding the practical application of CV in the context of battery catalyst research these qualitative features imply that a peak separation as small as possible and a current wave as symmetric as possible are desired since they translate to a low activation barrier which does not disfavour one particular reaction.

Quantitative interpretation of cyclic voltammetry

Apart from the qualitative view on CV, also a quantitative interpretation of the current/voltage curves, in particular of the forward scan, is possible as long as the restrictions stated on page 12 are satisfied. Then, and only then, the so-called Randles-Ševčík relations[5] apply [74], [75]. These link the peak current of an electrochemically reversible $I_{\mathrm{p,rev}}$ or irreversible $I_{\mathrm{p,irr}}$ reaction to the applied rate of potential change, ν, as:

$$I_{\mathrm{p,rev}} = 0.446\, nFAc\sqrt{\frac{nF\nu D}{RT}} \tag{2.2}$$

and

$$I_{\mathrm{p,irr}} = 0.496\, nFAc\sqrt{\frac{\alpha nF\nu D}{RT}}. \tag{2.3}$$

In equations 2.2 and 2.3, A is the electrode area, and D is the diffusion coefficient of the electrochemically active species. The parameters n, F, R, T and c have their usual meaning. In equation 2.3, α represents the electron transfer coefficient. This parameter is a quantitative measure for the symmetry of the activation barrier of the reaction under investigation [88]. It is of course absent in equation 2.2, since a reversible reaction does not obey any kinetic limitations and therefore does not

[5]These are named after J. Randles [90] and A. Ševčík [91] who independently pioneered the theory of cathode ray polarography in 1948.

possess any activation barrier. In case of an electrochemically irreversible reaction α can also be accessed from the shape of the current-voltage curve according to

$$\alpha = \frac{1.85\,RT}{nF(E_{\mathrm{p,irr}/2} - E_{\mathrm{p,irr}})}, \tag{2.4}$$

where $E_{\mathrm{p,irr}/2}$ is the potential of the half peak current [74]. Since the peak position in the CV of an electrochemically irreversible reaction is unambiguously related to the potential sweep rate (with α as proportionality factor [74]), the electron transfer coefficient can be also calculated from the derivative of the peak potential according to

$$\alpha = \frac{RT}{2\,nF}\left(\frac{\partial E_{\mathrm{p,irr}}}{\partial \ln(\nu)}\right)^{-1}. \tag{2.5}$$

In contrast, for an electrochemically reversible reaction the peak position will be independent of the potential sweep rate and no α can be obtained.
With the knowledge of α in case of an electrochemically irreversible reaction, the standard rate constant, k^0, can be calculated via

$$k^0 = 2.182\sqrt{\frac{\alpha nF D\nu}{RT}}\exp\left(\frac{\alpha nF(E_{\mathrm{p,irr}} - E^0)}{RT}\right), \tag{2.6}$$

which is a rearranged and more handy version of the equation given by Matsuda and Ayabe [74]. This quantity is a quantitative measure for the height of the activation barrier. In case of an electrochemically reversible reaction with no activation barrier $k^0 \to \infty$.

Ambiguity of CV and limits of the Randles-Ševčík relations

The interpretation of cyclic voltammetry data poses a formidable challenge if one, two or even more of the constraints given on page 12 are not fulfilled. This is illustrated qualitatively for two selected examples, which are the origin for the most common pitfalls in the interpretation of CV, in this sub-paragraph. Scenario I) is dedicated to the case if the reversibility/irreversibility constraint is not fulfilled. Scenario II) emphasizes the effect of a non-semi-infinite diffusion domain with an impermeable outer boundary in front of the electrode.

When regarding the reversibility/irreversibility constraint, one could pose the question of what eventuates if the electrode reaction under investigation is neither

electrochemically reversible nor irreversible and what actually determines electrochemical reversibility. For this purpose, figure 2.5 depicts the forced transition of an electrochemical system from the reversible state to the irreversible state. In figure 2.5, the combined influence of electrode kinetics and potential sweep rate are depicted. For this purpose, panels (A), (B) and (C) show the simulated dimension-less flux (or current) of a CV in a planar semi-infinite diffusion domain for $\alpha = 0.5$, $\alpha = 0.3$ and $\alpha = 0.7$, respectively. The standard rate constant was set to $k^0 = 10^{-4}$ cm s^{-1}. The simulations were performed at 15 potential sweep rates spanning a logarithmic grid from $\nu = 1$ µV s^{-1} to $\nu = 1$ kV s^{-1}. It can be seen that the CV peak separation gets larger as the potential sweep rate increases, i.e. the system becomes more irreversible even without changing k^0. This is caused by the fact that the rate of the electrochemical reaction gets surpassed by the timescale of the experiment as the potential sweep rate gets sufficiently large. This scanrate dependence of the dimension-less flux peak is depicted in panel (D) for the respective combinations of α and k^0 shown in panels (A), (B) and (C). It can be seen that the system behaves reversible[6] for potential sweep rates of $\nu < 0.1$ mV s^{-1}. As the potential sweep rate becomes sufficiently large (in the present case referring to $k^0 = 10^{-4}$ cm s^{-1} at $\nu > 10$ V s^{-1}), the system becomes electrochemically irreversible[7]. Since the electrochemical system behaves neither reversible nor irreversible in the intermediate region, this transient range is termed *'quasi-reversible'*. In this region, the classical Randles-Ševčík relations do not apply which renders assessing k^0 and α from experimental CV data exceptionally complicated. In order to quantify electrochemical reversibility, Matsuda and Ayabe have introduced the parameter $\Lambda = k^0 \left(RT/nFD\nu\right)^{0.5}$ [74]. If $\Lambda > 15$, the reaction is classified as reversible. In contrast, if $\Lambda < 0.01$ the reaction is termed irreversible. It is worth to note that in the present example the quasi-reversible region covers the entire range of experimentally reasonable potential sweep rates. This is caused by the fact that the standard rate constant was deliberately chosen ill-suited which may — or may not — also apply to a real electrochemical system investigated via CV. Since from an experimental point of view, the value of k^0 is not known a-priori, particular caution has to be paid when using the Randles-Ševčík relations.

Subsequently to the potential-sweep rate dependence of the reversibility of an electrochemical reaction, the effects of a non-semi-infinite diffusion

[6]For a reversible reaction the dimensionless flux peak approaches the limit of 0.446 which corresponds to the reversible Randles-Ševčík parameter. Furthermore, the shape of the CV curves become independent of α. [74]

[7]Electrochemically irreversible behaviour translates to a dimensionless flux peak which approaches the irreversible limit of $0.496\,\alpha^{0.5}$ [74].

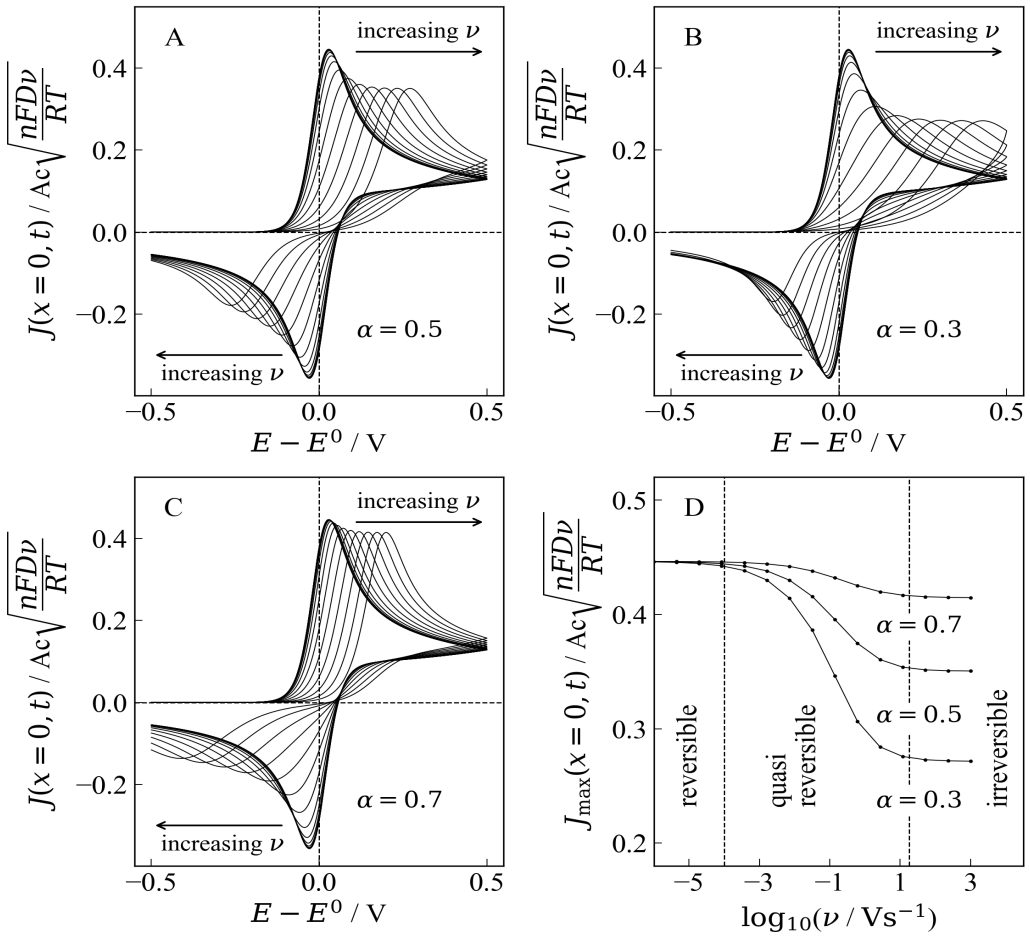

Figure 2.5: (A), (B) and (C): CV curves simulated for three different values of the electron transfer coefficient α and one intermediate standard rate constant of $k^0 = 10^{-4}$ cm s^{-1} at 15 potential sweep rates spanning a logarithmic grid from $\nu = 1$ µV s^{-1} to $\nu = 1$ kV s^{-1}. (D) Dependence of the dimension-less flux peak (or current peak) of the forward scan on the potential sweep rate. It can be seen that for potential sweep rates of $\nu < 0.1$ mV s^{-1} the system behaves reversible (the dimensionless flux peak approaches the reversible Randles-Ševčík parameter of 0.446 and the shape of all CV curves becomes independent of α). In contrast, at potential sweep rates of $\nu > 10$ V s^{-1} the system becomes irreversible (the dimensionless flux peak approaches the irreversible limit of $0.496\,\alpha^{0.5}$ and the shape of the individual CV responses approaches the characteristic curvature). In the intermediate region the system behaves neither reversible nor irreversible. Instead, it traverses from one limit to the other. This dynamic region is the *'quasi-reversible'* range in which the Randles-Ševčík relations do not apply. In the present example, where the standard rate constant is deliberately chosen ill-suited, this region covers the entire range of experimentally reasonable potential sweep rates.

domain will be outlined qualitatively at next. This scenario corresponds to an electrochemical reaction which takes place at an electrode with an impermeable wall in direct proximity to the reactive surface so that the mass transfer of electrochemically active species is somewhat hindered. Experimentally it translates to either a) a thin layer cell, classically utilized in spectroelectrochemical applications or in a more abstract picture to b) a homogeneously layered electrode structure, which can be regarded as the most simple model of a porous electrode. The corresponding concentration profiles as well as the related CV curves are depicted for a strictly reversible reaction in figure 2.6.

Figure 2.6 (A) and (A1) serve as reference and correspond to the forward and the backward CV scan of a reaction which takes place in a semi-infinite diffusion domain. In this context, the term *'semi-infinite'* implies that the concentration profile will never hit the outer boundary (located at $x = 50$ µm in the present example) during the timescale of the experiment and that the diffusive mass transfer will not be limited in any occasion. In contrast, figure 2.6 (B) and (B1) correspond to a reaction in a significantly smaller diffusion domain, where the impermeable boundary is located at $x = 3$ µm in front of the active electrode surface. The CV curves resulting from scenario (A) and (B) are depicted in figure 2.6 (C) and labeled as a) and b) accordingly. The additional grey CV curves correspond to ten diffusion domain sizes spanning a logarithmic grid which ranges from $x_{\mathrm{min}} = 1$ µm to $x_{\mathrm{max}} = 50$ µm. It can be seen that a smaller diffusion domain size will decrease the CV peak separation and height simultaneously. Mathematically, this scenario was first ever described in the work by Aoki et al. [79], [80]. Qualitatively, it can be ascribed to the lack of active species reaching the electrode surface as soon as the zone of dilution in the concentration profile hits the outer boundary. In the most extreme scenario — a diffusion domain size which approaches zero[8] — the current response will not show any sign of diffusive mass transfer. Consequently, it will reduce to the Nernstian surface wave. In this manner, the smallest diffusion domain size of $x = 1$ µm, already results in a CV response which does almost look like two Gaussian curves. Therefore, taking this diffusion domain effect into consideration, it is readily possible to achieve peak separations of $\Delta E_{\mathrm{p,rev}} < 58$ mV, which is the thermodynamic limit of a reversible CV in a semi-infinite diffusion domain. This finally implies that in a finite diffusion domain the peak separation of a CV is not unambiguously kinked to the electrode kinetics anymore. Instead, it is a complex function of both, the diffusion domain size and the intrinsic electrode kinetics.

[8]This is just a mathematical consideration. In real systems the diffusion domain size is at least at the size of one effective ion radius.

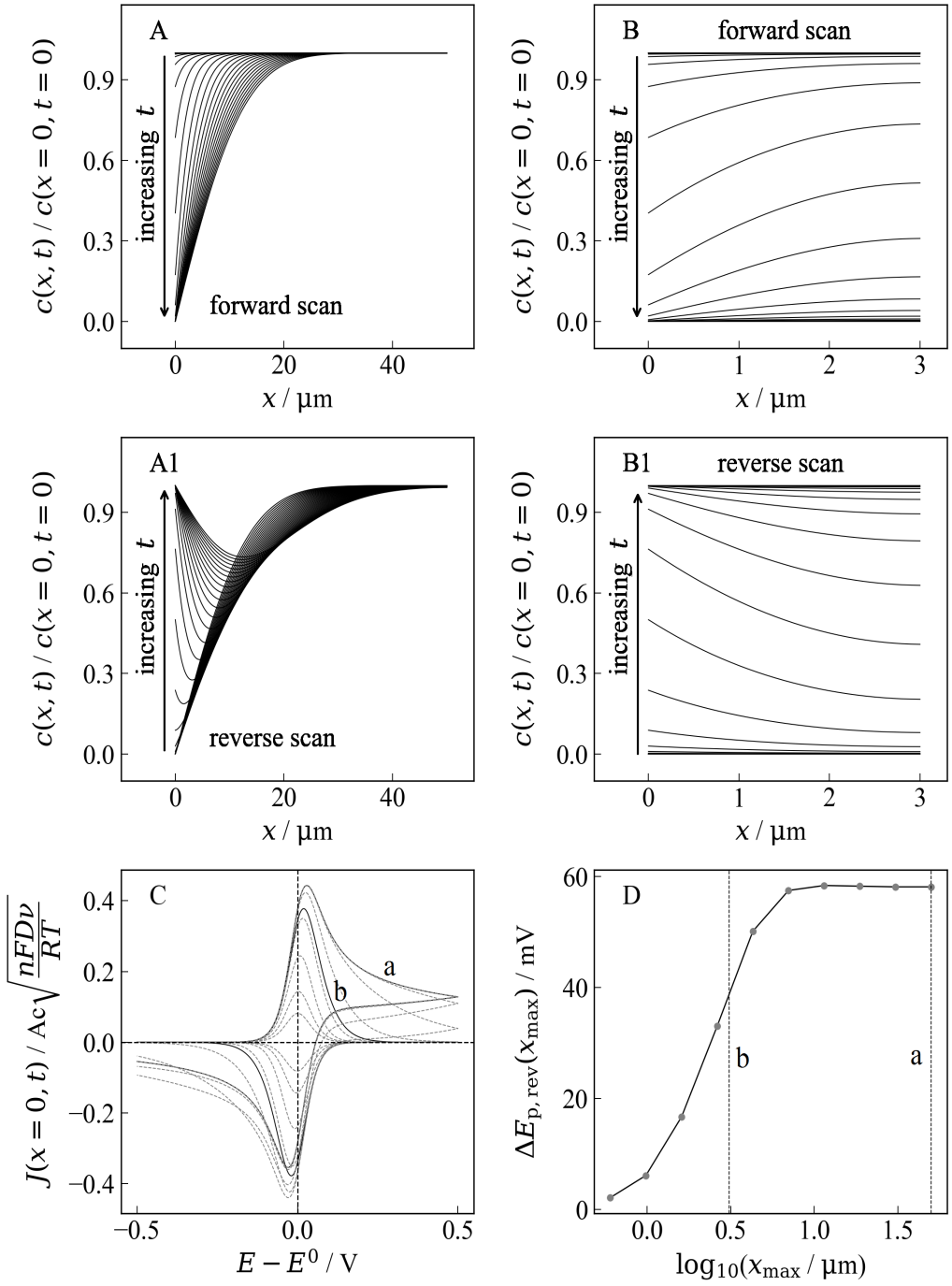

Figure 2.6: (A), (A1) and (B), (B1): Forward and reverse scan of a reversible electrode reaction in a semi-infinite and a finite diffusion space, respectively.(C) Dimension-less flux of the educt versus the applied potential for diffusion domain sizes ranging from $x_{\min} = 1$ µm to $x_{\max} = 50$ µm. (D) Dependence of the peak-to-peak separation on the diffusion domain size.

Considering the complex interplay of electrode kinetics together with the additional diffusion domain effect, is proven that a unique — Randles-Ševčík like — interpretation of CV curves in terms of peak positions and peak heights will be impossible for non-planar electrodes in non-semi infinite diffusion spaces. Consequently, it is demonstrated the classical approach of comparing peak-to-peak separation for assessing the kinetic performance of electrode materials with different morphologies will inevitably provide misleading or at least highly questionable results. Therefore, taking it in a nutshell, one might be tempted to say:

„Measuring CV is an easy task while the correct interpretation will be a lucky-punch.“.

Chapter 3

Theoretical Background

This chapter will provide an overview on the electrochemical and mathematical fundamentals of diffusional cyclic voltammetry. Emphasizing two methods utilized for the simulation of CV — namely convolutive modeling and digital simulation — the reader will be provided with detailed derivations on the mathematics of diffusive mass transfer. These fundamental concepts can be regarded as the ancestor of the theory developed in all the publications related to this thesis and are therefore of utmost importance.

3.1 Electrochemical Fundamentals

When regarding any kind of electroanalytical experiment one requires for a decent model of the electrochemical driving force of the reactions involved. In the most simple case, the underlying process will be kinetically unlimited. Consequently, the reaction will always obey the restrictions of thermodynamic reversibility. Electrochemically speaking this implies that the Nernst equation will be valid at each and every potential. In case of a kinetic limitation, the system will be controlled by the activation barrier. In this case, one might utilize the Butler–Volmer model of electrode kinetics. These two scenarios will be treated in the following sub-paragraphs. The derivation introduced at this stage was particularly developed for this thesis and gives rise to a unique notation. Of course, it is virtually as good as the derivations provided by textbooks such as the monograph by Bard and Faulkner [88].

Thermodynamic reversibility and the Nernst equation

Thermodynamic reversibility of an electrochemical reaction implies that any process which compensates an external potential perturbation will be directly linked to the Gibbs-free energy of the system. This quantity can be formulated according to its total differential as

$$\mathrm{d}G = \left(\frac{\partial G}{\partial p}\right)_{T,n} \mathrm{d}p + \left(\frac{\partial G}{\partial T}\right)_{p,n} \mathrm{d}T + \sum_i \left(\frac{\partial G}{\partial n_i}\right)_{T,p} \mathrm{d}n_i. \tag{3.1}$$

Considering that the electrochemical reaction takes place in a condensed phase (electrolyte), it immediately follows that $\mathrm{d}p = 0$. Assuming further, that the experiment is conducted under isothermal conditions, it also follows that $\mathrm{d}T = 0$. Consequently, equation 3.1 simplifies to

$$\mathrm{d}G_{p,T} = \sum_i \left(\frac{\partial G}{\partial n_i}\right)_{T,p} \mathrm{d}n_i. \tag{3.2}$$

The partial differential coefficient in equation 3.2 can be recognized as the chemical potential of species i according to:

$$\left(\frac{\partial G}{\partial n_i}\right)_{T,p} = \mu_i = \mu_i^0 + RT \cdot \ln(a_i), \tag{3.3}$$

so that one can alternatively write

$$\mathrm{d}G_{p,T} = \sum_i \mu_i \mathrm{d}n_i. \tag{3.4}$$

In equation 3.4, a_i represents the activity of species i, which is replaced in all the following considerations by the normalized concentration according to $a_i \stackrel{!}{=} c_i/c^0$, where c^0 is the standard concentration.[1]. Introducing the reaction extent as $\mathrm{d}\xi = \mathrm{d}n_i/\nu_i$, where ν_i represents the stoichiometric coefficients of the reacting species one can write alternatively:

$$\mathrm{d}G_{p,T} = \sum_i \mu_i \nu_i \mathrm{d}\xi. \tag{3.5}$$

Finally, considering that the tangent line in G is defined by

$$\Delta G = \left(\frac{\partial G}{\partial \xi}\right)_{T,p}, \tag{3.6}$$

equation 3.5 can be rewritten as

$$\Delta G = \sum_i \mu_i \nu_i. \tag{3.7}$$

The partial differential quotient in equation 3.7 can be introduced only because p and T are considered as constant. For a simple electrode reaction of

$$R \underset{+\mathrm{ne}^-}{\overset{-\mathrm{ne}^-}{\rightleftharpoons}} O, \tag{3.8}$$

where R is the reduced and O is the oxidized species, respectively, the sum in equation 3.7 consists of two terms only and can be written as

$$\Delta G = \mu_\mathrm{O} - \mu_\mathrm{R} = \mu_\mathrm{O}^0 - \mu_\mathrm{R}^0 + RT \cdot \ln\left(\frac{c_\mathrm{O}}{c_\mathrm{R}}\right). \tag{3.9}$$

With the respective definition of $\Delta G^0 = \mu_\mathrm{O}^0 - \mu_R^0$ it immediately follows:

$$\Delta G = \Delta G^0 + RT \cdot \ln\left(\frac{c_\mathrm{O}}{c_\mathrm{R}}\right). \tag{3.10}$$

[1]This might be a fair approximation as long as dilute electrolyte solutions are involved. In this case, the electrolyte can be considered as fully dissociated and the interactions between the molecules or ions of the electrochemically active species are assumed to be negligible.

Considering equation 3.10 in an electrochemical sense, one can link the electric potential difference U[V] to the difference in the chemical potentials by Faradays´ constant and the number of electrons transferred as proportionality factors. In this manner, one arrives at

$$U = \pm\frac{\Delta G}{nF}. \tag{3.11}$$

The ± sign in equation 3.11 arises from the ambiguity in the connection of the device measuring the electric potential difference and the unambiguity of the sign of ΔG. Therefore, an additional definition is required. This can be formulated as:

$$U_{\mathrm{an-ca}} = \frac{\Delta G}{nF} \tag{3.12}$$

and

$$U_{\mathrm{ca-an}} = -\frac{\Delta G}{nF}, \tag{3.13}$$

where the indices 'an' and 'ca' give rise to the potential differences of anode with respect to cathode (equation 3.12) or cathode with respect to anode (equation 3.13). In this context, the anode corresponds to the electrode where the oxidation takes place and the cathode to the electrode where the reduction occurs. Therefore, the anode can be considered as the electron donating site (negative potentials) and the cathode to the electron accepting site (positive potentials). Referring the electric potentials of any electrode reaction to one uniquely chosen reference system — the standard hydrogen electrode — gives rise to:

$$U_{\mathrm{el-SHE}} = \pm\frac{\Delta G}{nF} = E. \tag{3.14}$$

In equation 3.14, again, the ± sign occurs, since it is not defined a-priori, whether or not the electrode under investigation (index 'el') will be the anode or the cathode with respect to the standard hydrogen electrode (index 'SHE'). The variable E introduced in equation 3.14 terms the measured potential difference U as E, which is the common formulation in the literature.

It is, however, exceptionally worth to note that equation 3.14 gives rise to another, yet *unambiguous*, formulation which can be written as

$$E = E^0 + \frac{RT}{nF} \cdot \ln\left(\frac{c_\mathrm{O}}{c_\mathrm{R}}\right), \tag{3.15}$$

where

$$E^0 = \pm\frac{\Delta G^0}{nF}. \tag{3.16}$$

Equation 3.15 is unambiguous since the logarithmic term always contains the ratio of oxidized to reduced species, owing to the previous definition of anodic and cathodic reactions (equations 3.12, 3.13 and 3.14). The parameter E^0 also represents a fixed and therefore unambiguous value of an electrode potential — the one with respect to the standard hydrogen electrode. It is the potential which emerges when the ratio of oxidized to reduced species approaches unity and is therefore termed standard electrode potential.

Equation 3.15 is basically the so-called Nernst equation. This particular formulation does, however, require for two additional modifications to be the startingpoint for all further derivations. Considering that the electric potential will only be determined by the ratio of the electrochemically active species at the electrode surface, one has to write

$$E = E^0 + \frac{RT}{nF} \cdot \ln\left(\frac{c_\mathrm{O,S}}{c_\mathrm{R,S}}\right), \tag{3.17}$$

where the index 'S' translates to a surface concentration. Considering an electrochemical equilibrium, where the surface concentration of the electrochemically active species is equal to the respective concentration in the bulk of the electrolyte (index 'B') one can alternatively introduce the corresponding equilibrium potential as

$$E^\mathrm{eq} = E^0 + \frac{RT}{nF} \cdot \ln\left(\frac{c_\mathrm{O,B}}{c_\mathrm{R,B}}\right). \tag{3.18}$$

Since equations 3.17 and 3.18 accurately describe an electochemical system which may, or may not be in an equilibrium state, they can be utilized for all the following derivations, where a potential perturbation usually forces a deviation from an initial — equilibrated — state.

Electrode kinetics and the Butler–Volmer equation

Subsequently to discussing the electrochemical equilibrium condition and the Nernst equation, this sub-paragraph is dedicated to the derivation of the Butler–Volmer relation. This particular equation represents the fundamental theory of electrode kinetics. Starting with the formulation of the Gibbs free energy of equation 3.10 and noting that at equilibrium conditions $\Delta G = 0$, one can write:

$$\Delta G^0 = -RT \cdot \ln\left(\frac{c_{\mathrm{O,B}}}{c_{\mathrm{R,B}}}\right). \tag{3.19}$$

Noting that this circumstance will correspond to a certain ratio of $c_{\mathrm{O,B}}/c_{\mathrm{R,B}} = K$, the equilibrium constant, one can alternatively write

$$\Delta G^0 = -RT \cdot \ln(K) = -RT \cdot \ln\left(\frac{k^0_{\rightarrow}}{k^0_{\leftarrow}}\right), \tag{3.20}$$

where $k^0_{\rightarrow}$ and $k^0_{\leftarrow}$ denote the individual standard rate constants of the forward (oxidation) and backward (reduction) reaction, respectively. Referring to the standard electrode potential, this implies that

$$E^0 = \frac{RT}{nF} \cdot \ln\left(\frac{k^0_{\leftarrow}}{k^0_{\rightarrow}}\right). \tag{3.21}$$

Introducing this into equation 3.18 and rearranging the resulting expression into an exponential form, one arrives at:

$$\frac{k^0_{\leftarrow} c_{\mathrm{O,B}}}{k^0_{\rightarrow} c_{\mathrm{R,B}}} = \exp\left(\frac{nFE^{\mathrm{eq}}}{RT}\right). \tag{3.22}$$

The next step towards the Butler–Volmer equation is to split the exponent in equation 3.22, by introducing an arbitrary parameter, α, which will later on translate to the electron transfer coefficient. Doing so, one can obtain:

$$\frac{k^0_{\leftarrow} c_{\mathrm{O,B}}}{k^0_{\rightarrow} c_{\mathrm{R,B}}} = \exp\left(\frac{\alpha nFE^{\mathrm{eq}}}{RT}\right) \cdot \exp\left(\frac{(1-\alpha)nFE^{\mathrm{eq}}}{RT}\right), \tag{3.23}$$

which is mathematically identical to equation 3.22. This expression can be rearranged to give the very important relation:

$$0 = c_{\mathrm{R,B}}\, k^0_{\rightarrow} \exp\left(\frac{\alpha n F E^{\mathrm{eq}}}{RT}\right) - c_{\mathrm{O,B}}\, k^0_{\leftarrow} \exp\left(\frac{-(1-\alpha) n F E^{\mathrm{eq}}}{RT}\right). \tag{3.24}$$

Equation 3.24 is of utmost importance, since it relates the reaction rates in the forward direction (here an oxidation) and in the reverse direction (here a reduction) with the electrode potential. The product of the individual standard rate constants with the respective exponential terms can be translated to an Arrhenius type of equation which states that an electrode reation is exponentially accelerated or decelerated by the electrode potential. Therefore, one might also write

$$0 = v = v_{\rightarrow} - v_{\leftarrow} \tag{3.25}$$

which corresponds to a zero total reaction rate in equilibrium. From equations 3.24 and 3.25 it is now readily seen, that in case of a non equilibrium potential, the total reaction rate will differ from zero. Likewise, the respective surface concentrations will differ from their bulk value. Therefore, one has to state:

$$v = c_{\mathrm{R,S}}\, k^0_{\rightarrow} \exp\left(\frac{\alpha n F E}{RT}\right) - c_{\mathrm{O,S}}\, k^0_{\leftarrow} \exp\left(\frac{-(1-\alpha) n F E}{RT}\right), \tag{3.26}$$

which can be finally rearranged to give the electric current by multiplying with nFA. In this manner one finally obtains the most simple form of the Butler–Volmer equation as

$$I = nFA\left\{c_{\mathrm{R,S}}\, k^0_{\rightarrow} \exp\left(\frac{\alpha n F E}{RT}\right) - c_{\mathrm{O,S}}\, k^0_{\leftarrow} \exp\left(\frac{-(1-\alpha) n F E}{RT}\right)\right\}. \tag{3.27}$$

Equation 3.27 is not too handy, as it does not include any reference potential in a straightforward way. However, it can be rearranged readily by inserting the known expression of the standard electrode potential. Hence, bearing in mind equation 3.21, one might substitute

$$(k^0_{\rightarrow})^{\alpha} = (k^0_{\leftarrow})^{\alpha} \exp\left(\frac{-\alpha n F E^0}{RT}\right) \tag{3.28}$$

and

$$(k^0_{\leftarrow})^{(1-\alpha)} = (k^0_{\rightarrow})^{(1-\alpha)} \exp\left(\frac{(1-\alpha) n F E^0}{RT}\right). \tag{3.29}$$

Substituting these two expressions into equation 3.27 and defining the unified standard rate constant of the reaction as $k^0 = (k^0_{\rightarrow})^{(1-\alpha)} \cdot (k^0_{\leftarrow})^{\alpha}$, one arrives at

$$I = nFAk^0 \Bigg\{ c_{\mathrm{R,S}} \exp\left(\frac{\alpha n F (E - E^0)}{RT}\right) - c_{\mathrm{O,S}} \exp\left(\frac{-(1-\alpha) n F (E - E^0)}{RT}\right) \Bigg\}. \quad (3.30)$$

Equation 3.30 is the most commonly utilized version of the Butler–Volmer equation, which will be also the base for all the following considerations.

Equilibrium conditions and the exchange current

Assuming that the total current will be zero at equilibrium, one can rewrite equation 3.30 as

$$I^{\mathrm{eq}} = nFAk^0\, c_{\mathrm{R,B}} \exp\left(\frac{\alpha n F (E^{\mathrm{eq}} - E^0)}{RT}\right) = nFAk^0\, c_{\mathrm{O,B}} \exp\left(\frac{-(1-\alpha) n F (E^{\mathrm{eq}} - E^0)}{RT}\right), \quad (3.31)$$

where I^{eq} stands for the exchange current. This quantity represents the amount of current which flows in the anodic and cathodic direction at equilibrium conditions. Of course, the electrode potential E in equation 3.30 will be replaced by its equilibrium value E^{eq} and the surface concentrations will be equal to the bulk concentrations. Dividing equation 3.30 by I^{eq} and rearranging the result yields an additional formulation of the Butler–Volmer equation, where the electrode potentials are referred to their equilibrium value. This expression is given by

$$I = I^{\mathrm{eq}} \Bigg\{ \left(\frac{c_{\mathrm{R,S}}}{c_{\mathrm{R,B}}}\right) \exp\left(\frac{\alpha n F (E - E^{\mathrm{eq}})}{RT}\right) - \left(\frac{c_{\mathrm{O,S}}}{c_{\mathrm{O,B}}}\right) \exp\left(\frac{-(1-\alpha) n F (E - E^{\mathrm{eq}})}{RT}\right) \Bigg\}. \quad (3.32)$$

Reversible limit of the Butler–Volmer equation

When regarding equation 3.30, two extreme cases can be distinguished. In scenario a), the standard rate constant will be very large, ($k^0 \to \infty$), and in case b) it will be very small. Considering a), it immediately follows that $I/(nFAk^0) \to 0$. As a consequence, equation 3.30 simplifies to

$$c_{\mathrm{R,S}} \exp\left(\frac{\alpha nF(E-E^0)}{RT}\right) = c_{\mathrm{O,S}} \exp\left(\frac{-(1-\alpha)nF(E-E^0)}{RT}\right), \tag{3.33}$$

which can be rearranged to give the Nernst equation (equation 3.17). This implies that in case of very large reaction rates (very low activation barriers), the Nernst equation will be valid at each and every potential which corresponds to *electrochemical reversibility*. The transition from equation 3.30 to equation 3.17 can therefore be regarded as the quantitative analogon of the qualitative explanation of electrochemical reversibility given on page 15.

Irreversible limit of the Butler–Volmer equation: The Tafel-criterion

In case of a very small standard rate constant of an electrochemical reaction, equation 3.30 suggests that a significant deviation of the electrode potential E from E^0 will be required to achieve a noticable current. Since the respective anodic and cathodic exponential terms carry an opposite sign, it is readily seen that an acceleration of the reaction in one direction will decelerate the reverse reaction. As a consequence one can expect that the reverse reaction will become negligible when compared to the forward reaction if the absolute difference of $E - E^0$ increases. Assuming that the surface concentrations would be always equal to the bulk concentrations[2], equation 3.32 simplifies to

$$I = I^{\mathrm{eq}}\left\{\exp\left(\frac{\alpha nF(E-E^{\mathrm{eq}})}{RT}\right) - \exp\left(\frac{-(1-\alpha)nF(E-E^{\mathrm{eq}})}{RT}\right)\right\}. \tag{3.34}$$

[2]This is just hypothetical and implies that the mass transfer would be infinitely fast in order to immediately compensate any consumption or production of electrochemically active species at the electrode surface.

Taking the definition, that the reverse reaction is equal to (or less than) one percent of the forward reaction, equation 3.34 can be rearranged to give:

$$0.01 = \frac{\exp\left(\frac{\alpha n F(E - E^{\mathrm{eq}})}{RT}\right)}{\exp\left(\frac{-(1-\alpha) n F(E - E^{\mathrm{eq}})}{RT}\right)} \tag{3.35}$$

From equation 3.35, it immediately follows that at $T = 298$ K, the backwards reaction can be neglected if the absolute difference of $n\,|E - E^0| \geq 118$ mV. This limit is also called Tafel-criterion. Since any realistic electrode reaction will always be subjected to mass transfer, which is excluded in equation 3.35 by definition, the following sub-paragraphs will emphasize this particular effects.

3.2 Cyclic Voltammetry with Forced Convection

When performing cyclic voltammetry experiments, typically stagnant electrolyte solutions — electrolytes in absense of any convection — are employed. These usually demand a complicated mathematical description of the diffusive mass transfer. However, instead of modeling the diffusive part of an electroanalytical experiment in any depth, it is also possible to simplify it experimentally as long as the electrode under investigation is planar and exposed to a semi-infinite diffusion domain. Indeed, this assumption does not account for any porosity effects of the electrode which this thesis is dedicated to, but is, however, an exceptionally valuable tool for obtaining reference measurements for systems involving porous structures. For this reason it is included in the present theory chapter. The implementation of a forced convection is usually accomplished by exploiting a rotating electrode which introduces a well-defined forced convection of the electrolyte, so that the diffusive mass transfer can be treated as a time-independent quantity. Owing to the principle and the geometry this type of electrode is called rotating disc electrode (RDE). A sketch of a RDE, the related steady-state concentration gradient as well as the corresponding flux are depicted in figure 3.1. It can be seen that the rotation of the electrode introduces a forced convection of the electrolyte solution. Since the convective flux can be regarded as a quantity which depends on the distance perpendicular to the electrode surface, one can equate it with the

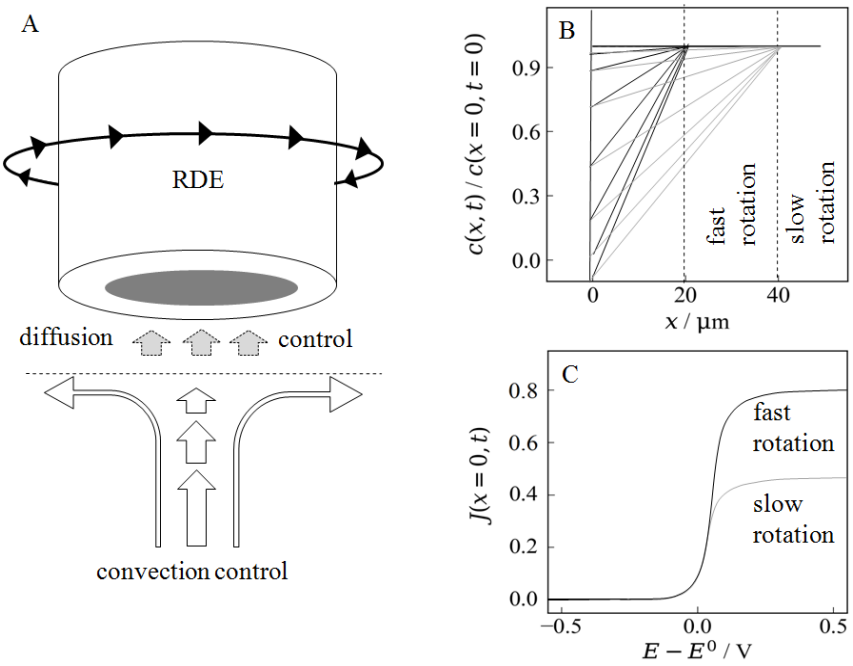

Figure 3.1: (A) Sketch of a rotating disc electrode (RDE). (B) Concentration gradients during a potential sweep experiment at an RDE for two different rotation frequencies. (C) Flux of the reduced species towards the electrode during an anodic potential sweep at two different roation frequencies. The dotted line in panels (A) and (B) marks the diffusion layer thickness, where convective and diffusive mass transfer equate. As the rotation speed of the electrode increases, the diffusion layer thickness decreases and causes an enhanced flux.

diffusive mass transfer to obtain the so-called diffusion layer thickness. This quantity is represented by the dashed line in figure 3.1 (A) and corresponds to the point at which the diffusive flux surpasses the convective mass transfer. This quantity will depend on the rotation speed of the electrode. As long as the electrode is rotated at a certain angular frequency, the constant diffusion layer thickness will introduce a linear concentration gradient (cf. figure 3.1 (B), which does exclusively depend on the concentration of the electrochemically active species at the electrode surface. Consequently, as soon as the surface concentration of the species consumed approaches zero, the concentration gradient will be time invariant. In this case a flux (or current) plateau will be reached which is termed *limiting current*. Since the concentration gradient is proportional to the rotation speed of the electrode in some, yet not defined, manner the limiting current will depend on the rotation rate as well. Considering that the electroanalytical experiment is conducted at a potential sweep rate sufficiently slow to provide a steady state concentration

gradient at each and every potential instance, the potential-dependent flux (or current) will be proportional to the inverse shape of the concentration profile. This behaviour is depicted in figure 3.1 (C). The grey curve corresponds to a low rotation speed of the electrode (low limiting current) and the black curve to a larger rotation speed (larger limiting current). Equating the limiting currents with the ratio of surface-to-bulk concentration one can recognize that

$$\frac{c_{i,\mathrm{S}}}{c_{i,\mathrm{B}}} = 1 - \frac{I}{I_{\mathrm{lim},i}}, \tag{3.36}$$

where $I_{\mathrm{lim},i}$ denotes the corresponding anodic or cathodic limiting current, respectively. This limiting current can be expressed in terms of the Levich-equation[3]. This equation originates from the hydrodynamics of a rotating disc [92] and is given by

$$I_{\mathrm{lim},i} = 0.201\, nFAc_{i,\mathrm{B}} D_i^{2/3} \eta^{-1/6} \sqrt{\omega}. \tag{3.37}$$

In equation 3.37, η stands for the kinematic viscosity of the electrolyte solution and ω denotes the angular rotation frequency of the electrode. The other variables have their usual meaning. Introducing equation 3.36 into equation 3.32 results in

$$I = I^{\mathrm{eq}} \Bigg\{ \left(1 - \frac{I}{I_{\mathrm{lim,an}}}\right) \exp\left(\frac{\alpha n F (E - E^{\mathrm{eq}})}{RT}\right) - \left(1 - \frac{I}{I_{\mathrm{lim,ca}}}\right) \exp\left(\frac{-(1-\alpha) n F (E - E^{\mathrm{eq}})}{RT}\right) \Bigg\}. \tag{3.38}$$

In equation 3.38, the respective limiting currents might be substituted by the Levich equation. Now, considering a sluggish electrode reaction which will require for a comparably large deviation of E from its equilibrium value to attain a current significantly different from zero, one of the exponential terms in equation 3.38 will become negligible according to the Tafel criterion. Suppose an anodic reaction, this translates to

$$I = I^{\mathrm{eq}} \left(1 - \frac{I}{I_{\mathrm{lim,an}}}\right) \exp\left(\frac{\alpha n F (E - E^{\mathrm{eq}})}{RT}\right). \tag{3.39}$$

[3] A derivation of the Levich equation is not part of this thesis, since focusing on hydrodynamics in any depth will be out of the scope.

Defining the kinetic anodic current to be

$$I_{\text{kin,an}} = I^{\text{eq}} \exp\left(\frac{\alpha n F(E - E^{\text{eq}})}{RT}\right), \tag{3.40}$$

one can rearrange equation 3.39 to

$$\frac{1}{I} = \frac{1}{I_{\text{kin,an}}} + \frac{1}{I_{\text{lim,an}}}, \tag{3.41}$$

which represents the Koutecký-Levich equation [88]. This particular equation is of utmost importance for the work related to chapter 5.1, where RDE measurements are conducted to obtain a set of kinetic reference parameters for the following work on porous electrodes. For this purpose, it might be rearranged once more in terms of the kinetic current to give

$$I_{\text{kin,an}} = \frac{I \cdot I_{\text{lim, an}}}{I_{\text{lim,an}} - I}. \tag{3.42}$$

This expression can be finally linearized to give

$$\ln\left(\frac{I \cdot I_{\text{lim, an}}}{I_{\text{lim,an}} - I}\right) = \ln\left(I^{\text{eq}}\right) + \frac{\alpha n F}{RT}(E - E^{\text{eq}}). \tag{3.43}$$

The outstanding advantage of equation 3.43 emerges from the feasibility of accessing I^{eq} (and therefore k^0) from the offset and α from the slope of a simple line equation which can be readily generated from experimental data.

3.3 Mathematics of Diffusion

In contrast to sub-chapter 3.2 which was dedicated to avoiding the complex interplay of diffusion phenomena and electrode kinetics under transient conditions by introducing forced convection, this sub-chapter will solely discuss the diffusive part of an electrochemical reaction in a stagnant electrolyte. In this context, the diffusion equation needs to be solved to certain boundary conditions, defined by the experiment. For this purpose, two different strategies, namely a) the Crank-Nicolson method which falls under the category of digital simulation and b) the Laplace transformation technique will be introduced.

The diffusion equation

When referring to the diffusion equation, typically Ficks´ second law is implied[4], which is a second order partial differential equation [94] and can be stated as

$$\frac{\partial c(x,y,z,t)}{\partial t} = D\nabla^2\, c(x,y,z,t). \tag{3.44}$$

In equation 3.44, ∇^2 corresponds to the Laplacian operator which contains the second order spatial derivatives according to

$$\nabla^2 = \left(\frac{\partial^2}{\partial x^2} + \frac{\partial^2}{\partial y^2} + \frac{\partial^2}{\partial z^2}\right). \tag{3.45}$$

Depending on the symmetry of the diffusion domain employed, equation 3.44 can be simplified. In this context, three totally symmetric electrode geometries will be regarded in the following, namely a) a planar electrode, b) a spherical electrode and c) a cylindrical electrode. In case of c), the cylinder is significantly longer than wide, so that the radial diffusion part can be considered as the only quantity contributing to the mass transport. In scenario a) the case of a one-dimensional diffusion problem at a planar electrode, the only coordinate which is left will be the distance from the active electrode surface — suppose x. Therefore it is $c(x,t)$ instead of $c(x,y,z,t)$. In this manner, one can alternatively write:

$$\frac{\partial c(x,t)}{\partial t} = D\frac{\partial^2 c(x,t)}{\partial x^2}. \tag{3.46}$$

In case of b), the diffusion equation 3.44 can be transformed into polar coordinates $c(x,y,z,t) \equiv c(r,\phi,\theta,t)$. If the electrode will be of spherical (or hemispherical) shape, the only quantity which governs the mass transfer will be the radial distance, $r = \sqrt{x^2+y^2+z^2}$. Therefore one can reduce $c(r,\phi,\theta,t)$ to $c(r,t)$ and arrives at

$$\frac{\partial c(r,t)}{\partial t} = D\left[\frac{\partial^2 c(r,t)}{\partial r^2} + \frac{2}{r}\frac{\partial c(r,t)}{\partial r}\right]. \tag{3.47}$$

[4]The difusion equation is named after Adolf Fick, who published his pioneering work on diffusive mass transfer in 1855 [93]

In scenario c), a cylindrical electrode, the diffusion equation will be reduced to a two-dimensional problem before applying the transformation to polar coordinates such that $c(x, y, z, t) \equiv c(x, y, t)$. In this manner, one obtains finally

$$\frac{\partial c(r,t)}{\partial t} = D\left[\frac{\partial^2 c(r,t)}{\partial r^2} + \frac{1}{r}\frac{\partial c(r,t)}{\partial r}\right]. \tag{3.48}$$

Equations 3.46, 3.47 and 3.48 can be employed whenever the system possesses the respective planar, spherical or cylindrical symmetry. For the sake of simplicity, the strategies of solving the diffusion equation via digital simulation and Laplace transformation techniques will be elucidated on the base of equation 3.46 only.

Digital simulation: The Crank–Nicolson algorithm

The idea of solving the diffusion equation in the context of electrochemical applications by means of *'digital simulation'* is usually associated with the seminal work of Feldberg in 1964 [95]. However, it is worth to note that Randles also utilized a similar approach already 16 years earlier in 1948 [90]. By approximating the partial derivatives in equation 3.46 by their finite difference quotients, Feldberg proposed an explicit algorithm which successively yields the time dependent concentration profile in front of the electrode according to

$$c_{i,t+\Delta t} \approx c_{i,t} + \frac{D\Delta t}{\Delta x^2} \cdot \Big(c_{i+1,t} - 2c_{i,t} + c_{i-1,t}\Big), \tag{3.49}$$

where the index i counts the space increments Δx which denote the distance from the electrode surface. Equation 3.49 is termed explicit, since it approximates the concentration at a new time instance $t + \Delta t$ on the base of the previously known values only. In a mathematical sense, equation 3.49 is somewhat inconvenient since it provides first order accuracy in time and a second order accuracy in space and is therefore unconditionally unstable[5]. Consequently, it requires considerably small increments of Δt to converge. It therefore represents a straightforward but awfully inefficient way of approximating the desired solution.

[5]Conditional stability means that the solution depends on the choice of the respective time and space increments of the finite difference approximations. In case of equation 3.49 one requires for $D\Delta t/\Delta x^2 \leq 0.5$ to ensure numerical stability. If Δt is chosen too large, approximating the spatial derivative by three grid points only (cf. equation 3.49) would be insufficient.

An alternative — and significantly more efficient — way of solving the diffusion equation is given by the implicit Crank–Nicolson algorithm. This method was introduced by John Crank and Phyllis Nicolson in 1947 [96] and pioneered in the context of electrochemistry by Heinze, Rudolph and Störzbach [97]–[99]. It is based on averaging the old (known) and new (yet unknown) concentration values at each individual point in space. In this manner, it achieves a second order accuracy in space and time. The respective finite difference approximation of equation 3.46 can be formulated as

$$c_{i,t+\Delta t} - c_{i,t} \approx \frac{D\Delta t}{2\Delta x^2} \cdot \Big(c_{i+1,t} - 2c_{i,t} + c_{i-1,t} + c_{i+1,t+\Delta t} - 2c_{i,t+\Delta t} + c_{i-1,t+\Delta t} \Big). \quad (3.50)$$

The solution of equation 3.50 follows after separating all the known and yet unknown concentration values. Introducing $\lambda = D\Delta t/\Delta x^2$, one might equate

$$-\lambda c_{i+1,t+\Delta t} + 2(1+\lambda)c_{i,t+\Delta t} - \lambda c_{i-1,t+\Delta t} = \lambda c_{i+1,t} + 2(1-\lambda)c_{i,t} + \lambda c_{i-1,t}. \quad (3.51)$$

Taking into account all — suppose N — spatial grid points, one can rearrange equation 3.51 into a tridiagonal matrix notation according to

$$\begin{pmatrix} \beta & \lambda & 0 & \cdots & 0 \\ \lambda & \beta & \lambda & 0 & \vdots \\ 0 & \ddots & \ddots & \ddots & 0 \\ \vdots & 0 & \lambda & \beta & \lambda \\ 0 & \cdots & 0 & \lambda & \beta \end{pmatrix} \cdot \begin{pmatrix} c_{1,t} \\ c_{2,t} \\ \vdots \\ c_{N-2,t} \\ c_{N-1,t} \end{pmatrix} + \begin{pmatrix} \lambda c_{0,t} \\ 0 \\ \vdots \\ 0 \\ \lambda c_{N,t} \end{pmatrix} = \begin{pmatrix} \epsilon & -\lambda & 0 & \cdots & 0 \\ -\lambda & \epsilon & -\lambda & 0 & \vdots \\ 0 & \ddots & \ddots & \ddots & 0 \\ \vdots & 0 & -\lambda & \epsilon & -\lambda \\ 0 & \cdots & 0 & -\lambda & \epsilon \end{pmatrix} \cdot \begin{pmatrix} c_{1,t+\Delta t} \\ c_{2,t+\Delta t} \\ \vdots \\ c_{N-2,t+\Delta t} \\ c_{N-1,t+\Delta t} \end{pmatrix} + \begin{pmatrix} \lambda c_{0,t+\Delta t} \\ 0 \\ \vdots \\ 0 \\ \lambda c_{N,t+\Delta t} \end{pmatrix}. \quad (3.52)$$

In equation 3.52 it is $\beta = 2(1-\lambda)$ and $\epsilon = 2(1+\lambda)$. The points located at $i = 0$ and $i = N$ represent the boundary conditions at the electrode surface and at the end of the diffusion layer, respectively. The boundary at the electrode surface is thereby defined by the Nernst or Butler–Volmer equation. Since the matrix notation in equation 3.52 accounts for all space grid points simultaneously, it offers an unconditionally stable way of solving the diffusion equation. Consequently, it is favoured, when compared to its explicit analogon. The tridiagonal matrices in equation 3.52 can be regarded as a set of $N-2$ linear equations which can be solved very efficiently by utilizing the Thomas algorithm [100]. The diffusive flux (and the related current) can be generated on the flow according to Ficks first law as

$$J(x=0,t) = -\frac{D}{\Delta x}\Big(c_{1,t} - c_{0,t}\Big) \tag{3.53}$$

or more precise as

$$J(x=0,t) = -\frac{D}{2\Delta x}\Big(-3c_{0,t} + 4c_{1,t} - c_{2,t}\Big). \tag{3.54}$$

Thereby, equation 3.54 includes a three point approximation of the concentration gradient at the electrode surface, which is of second order accuracy [89]. It is therefore more precise than equation 3.53, which consists of a two point approximation with first order accuracy, only.

When regarding equation 3.52 and equation 3.53, it is worth to note that the only concentration values, mandatory for computing the diffusive flux, are located at $x = 0$ and $x = \Delta x$. However, each time iteration requires for computation of the entire concentration profile in front of the electrode which will be of course significantly time consuming. Furthermore, since the resulting flux (or current) is numerically estimated at each time iteration it will be obtained as a set of discrete points only. These two drawbacks can be avoided in a very limited number of circumstances by exploiting Laplace integral transformation techniques which will be discussed in the following sub-paragraph.

The Laplace transformation technique

Solving the diffusion equation by means of Laplace integral transformation techniques offers an exceptionally elegant strategy, against which the digital simulation approach appears like a brute force method. Apart from satisfying the electrochemists mathematical curiosity, this approach can yield analytical (or semi-analytical) expressions for a variety of experimental circumstances. These are — of course — preferred when compared to entirely numerical results.

The Laplace transformation of a function $f(t)$ is defined by the following integral

$$\bar{f}(s) = \mathcal{L}\Big\{ f(t) \Big\}(s) = \int_0^\infty f(t)\, \mathrm{e}^{-st} \mathrm{d}t, \tag{3.55}$$

where $\mathcal{L}$ denotes the Laplace transformation operator and s is the Laplace transformed variable related to the time t [101]. Performing the Laplace transformation of an integral in time will result in

$$\begin{aligned}
\mathcal{L}\Big\{ \int_0^t f(\tau)\mathrm{d}\tau \Big\}(s) &= \int_0^\infty \Big(\int_0^t f(\tau)\mathrm{d}\tau \Big) \mathrm{e}^{-st} \mathrm{d}t \\
&= \int_0^\infty \Big(F(t) - F(0) \Big) \mathrm{e}^{-st} \mathrm{d}t \\
&= -\frac{F(t)}{s} \mathrm{e}^{-st} \Big|_0^\infty + \frac{1}{s} \int_0^\infty \Big(f(t) - sF(0) \Big) \mathrm{e}^{-st} \mathrm{d}t \\
&= \frac{F(0)}{s} + \frac{F(0)}{s} \mathrm{e}^{-st} \Big|_0^\infty + \frac{1}{s} \int_0^\infty f(t)\, \mathrm{e}^{-st} \mathrm{d}t \\
&= \frac{\bar{f}(s)}{s},
\end{aligned} \tag{3.56}$$

where τ is an auxiliary variable for t, to avoid the same nomenclature in the integrand and the integration limit. In contrast, applying transformation 3.55 to a derivative in time yields

$$\begin{aligned}
\mathcal{L}\Big\{ \frac{\mathrm{d}f(t)}{\mathrm{d}t} \Big\}(s) &= \int_0^\infty \frac{\mathrm{d}f(t)}{\mathrm{d}t} \mathrm{e}^{-st} \mathrm{d}t \\
&= f(t)\, \mathrm{e}^{-st} \Big|_0^\infty + s \int_0^\infty f(t)\, \mathrm{e}^{-st} \mathrm{d}t \\
&= -f(0) + s\bar{f}(s).
\end{aligned} \tag{3.57}$$

When regarding the relations in equations 3.56 and 3.57, the great advantage of the Laplace transformation becomes obvious, which is given by converting a differential equation into an algebraic expression [101]. Therefore, one can realize that an integration in the time domain will correspond to a simple division by the Laplace transformed variable in the Laplace domain. Vice versa, a differentiation in the time domain is achieved by a multiplication by transformed variable in the Laplace domain. Since the Laplace transformation is usually related to time-dependent problems, it will not affect any n^{th}-order spatial

derivatives. For example, consider the Laplace transformation of the n^{th} spatial derivative of a function $f(x,t)$. This will be given by

$$\begin{aligned}\mathcal{L}\left\{\frac{\partial^n f(x,t)}{\partial x^n}\right\}(s) &= \int_0^\infty \frac{\partial^n f(x,t)}{\partial x^n}\,\mathrm{e}^{-st}\mathrm{d}t \\ &= \frac{\partial^n}{\partial x^n}\int_0^\infty f(x,t)\,\mathrm{e}^{-st}\mathrm{d}t \\ &= \frac{\partial^n \bar{f}(x,s)}{\partial x^n}.\end{aligned} \tag{3.58}$$

Regarding equations 3.57 and 3.58, the outstanding power of the Laplace transformation for solving the diffusion equation emerges. By removing the partial derivative with respect to time on the left hand side of equations 3.44-3.48 the respective partial differential equations can be transformed into ordinary differential equations (ODEs). As an example, equation 3.46 can be converted into

$$-\bar{c}(x,0) + s\bar{c}(x,s) = D\frac{\partial^2 \bar{c}(x,s)}{\partial x^2}. \tag{3.59}$$

This expression is much more facile to treat mathematically when compared to equation 3.46, since it involves spatial derivatives only. Therefore, an efficient routine of solving the diffusion equation might be to first perform a Laplace transform, to subsequently solve the diffusion problem in the Laplace domain and to finally perform an inverse Laplace transformation to obtain the desired time-dependent result.

The formula for the inversion of the Laplace transformation — the so-called Bromwich integral [101], [102] — is given by the following line integral parallel to the imaginary axis

$$f(t) = \mathcal{L}^{-1}\left\{\bar{f}(s)\right\}(t) = \frac{1}{2\pi\mathrm{i}}\int_{\gamma-\mathrm{i}\infty}^{\gamma+\mathrm{i}\infty}\bar{f}(s)\,\mathrm{e}^{st}\mathrm{d}s, \tag{3.60}$$

where $\mathrm{i} = \sqrt{-1}$ and γ is a constant to be chosen so that all singularities of $\bar{f}(s)$ are located at the left hand side of the respective line integral. Since a direct evaluation of the Bromwich integral can be exceptionally complicated, one typically refers to tables of Laplace/inverse Laplace transform pairs — like to recipes in a mathematical cookbook. For two particular examples, relevant in the context of electrochemistry, detailed derivations of Laplace transformation/inverse Laplace transformation pairs are provided in appendix A of this work.

Properties of the Laplace transformation

Subsequently to introducing the Laplace transformation technique for solving the diffusion equation, this sub-paragraph will emphasize two important properties of this particular integral transformation [101], [102], which are urgently required in the context of electrochemical applications namely a) frequency shifting and b) convolution. Regarding a), one might consider a function $f(t)$, which is multiplied by an exponentially decaying term in the time domain and which is going to be Laplace transformed. This scenario can be written as

$$\begin{aligned}\mathcal{L}\Big\{f(t)\,\mathrm{e}^{-at}\Big\}(s) &= \int_0^\infty f(t)\,\mathrm{e}^{-(s+a)t}\mathrm{d}t \\ &= \bar{f}(s+a).\end{aligned} \tag{3.61}$$

Equation 3.61 will be required when treating electrochemical reactions coupled to homogeneous kinetics.

Regarding b), the convolution is required whenever an inverse Laplace tranformation (or Laplace transformation) is applied to a product of two functions — suppose f and g. In case of an inverse Laplace transformation, suppose $\mathcal{L}^{-1}\{\bar{f}(s)\bar{g}(s)\}(t)$. Then, the desired time-dependent solution is given by

$$\begin{aligned}\mathcal{L}^{-1}\Big\{\bar{f}(s)\bar{g}(s)\Big\}(t) &= \int_0^t f(\tau)g(t-\tau)\mathrm{d}\tau \\ &= \int_0^t f(t-\tau)g(\tau)\mathrm{d}\tau.\end{aligned} \tag{3.62}$$

In equation 3.62, τ represents a dummy integration variable for the time t. The functions $f(t)$ and $g(t)$ are the individual inverse Laplace transformations according to $f(t) = \mathcal{L}^{-1}\{\bar{f}(s)\}(t)$ and $g(t) = \mathcal{L}^{-1}\{\bar{g}(s)\}(t)$. Equation 3.62 is called the convolution theorem. It is of utmost importance when treating electroanalytical experiments under transient conditions, i.e. when the diffusive mass transfer is coupled (convoluted) with a potential sweep.

3.4 Diffusional Potential Step Methods

Before discussing the concept of transient boundary conditions required for simulating cyclic voltammetry experiments, this subsection will be dedicated to large-amplitude potential step methods. These can be regarded as an experimental extreme case, which forces the surface concentration of the electrochemically active species to zero as soon as the experiment starts (at any $t > 0$). Then, considering that the restrictions outlined on page 12 are satisfied, the resulting analytic solution for the flux of the electrochemically active species will be given in terms of the Cottrell equation [103] which will be derived by means of the Laplace transformation technique, at next.

For this purpose the Laplace transformation of the one-dimensional diffusion equation at a planar electrode, given in equation 3.59, is recovered. For the consumption of the reduced species at the electrode surface during an anodic potential step it follows

$$\bar{c}_{\mathrm{R}}(x,s) = \bar{c}_{\mathrm{R,B}} + \frac{D_{\mathrm{R}}}{s}\frac{\partial^2 \bar{c}_{\mathrm{R}}(x,s)}{\partial x^2}, \tag{3.63}$$

where $\bar{c}_{\mathrm{R,B}} = c_{\mathrm{R}}(x,0)/s$. This ODE possesses the general solution of

$$\bar{c}_{\mathrm{R}}(x,s) = C_{+}\exp\left(x\sqrt{\frac{s}{D_{\mathrm{R}}}}\right) + C_{-}\exp\left(-x\sqrt{\frac{s}{D_{\mathrm{R}}}}\right) + \bar{c}_{\mathrm{R,B}}, \tag{3.64}$$

with C_{+} and C_{-} as constants to be determined by the boundary conditions of the experiment. Regarding that $c_{\mathrm{R}}(x \to \infty, t) = c_{\mathrm{R,B}}$ in a semi-infinite diffusion domain, it follows that $C_{+} \overset{!}{=} 0$. Furthermore, considering that the potential step enforces $c_{\mathrm{R}}(x = 0, t > 0) = 0$, one can determine C_{-} by setting $x = 0$, as $C_{-} = -c_{\mathrm{R,B}}$. In this manner, equation 3.64 can be simplified to

$$\bar{c}_{\mathrm{R}}(x,s) = \bar{c}_{\mathrm{R,B}}\left(1 - \exp\left(-x\sqrt{\frac{s}{D_{\mathrm{R}}}}\right)\right) \tag{3.65}$$

Since the current is related to the flux of electrochemically active species at the electrode surface, introducing the Laplace transformed version of Ficks first law yields

$$\bar{I}(s) = -nFA\bar{J}_{\mathrm{R}}(x=0,s) = nFAD_{\mathrm{R}}\left(\frac{\partial \bar{c}_{\mathrm{R}}(x,s)}{\partial x}\right)_{x=0}. \tag{3.66}$$

Performing the spatial derivative in equation 3.66 to the Laplace transformed concentration given in equation 3.65 and subsequently setting $x = 0$ provides

$$\bar{I}(s) = nFA\sqrt{sD_{\mathrm{R}}}\bar{c}_{\mathrm{R,B}}. \tag{3.67}$$

Recognizing that $\bar{c}_{\mathrm{R,B}} = c_{\mathrm{R,B}}/s$, one can alternatively write

$$\bar{I}(s) = \frac{nFA\sqrt{D_{\mathrm{R}}}c_{\mathrm{R,B}}}{\sqrt{s}}. \tag{3.68}$$

Finally, performing the inverse Laplace transformation[6] on equation 3.68 with $\mathcal{L}^{-1}\{1/\sqrt{s}\}(t) = 1/\sqrt{\pi t}$ [104] results in the so-called Cottrell equation given by

$$I(t) = \frac{nFA\sqrt{D_{\mathrm{R}}}c_{\mathrm{R,B}}}{\sqrt{\pi t}}. \tag{3.69}$$

This expression functionally relates the current of a potential step experiment to the respective experiment duration. It unambiguously shows that the current decays with the inverse square root of the time as soon as the surface concentration of the electrochemically active species approaches zero. It therefore describes the depleting part of the current wave of a CV at a planar electrode in a semi-infinite diffusion domain. Furthermore, it is one of the rare cases, where an entirely analytic solution of the current wave can be derived.

Apart from finding an analytical solution to equation 3.68, one could also attempt to solve it numerically. On a first glance, this appears redundant, since an analytical solution offers a much more valuable tool for describing the system. However, since in the case of cyclic voltammetry a very similar numerical treatment is utilized, it is worth to introduce the respective concept right now. Starting with equation 3.67 as

$$nFA\sqrt{D_{\mathrm{R}}}\bar{c}_{\mathrm{R,B}} = \frac{\bar{I}(s)}{\sqrt{s}} \tag{3.70}$$

suggests to utilize equation 3.62 with $\bar{f}(s) = \bar{I}(s)$ and $\bar{g}(s) = 1/\sqrt{s}$. Defining further that $\chi(t) = I(t)/nFA\sqrt{D_{\mathrm{R}}}c_{\mathrm{R,B}}$ one arrives at

$$1 = \frac{1}{\sqrt{\pi}}\int_0^t \frac{\chi(\tau)}{\sqrt{t-\tau}}\mathrm{d}\tau. \tag{3.71}$$

[6] This relation is derived in section A.1 in appendix A.

It is readily seen that the denominator in the integrand of equation 3.71 will introduce a singularity at the upper integration limit. This can be, however, circumvented by an integration by parts which provides

$$\sqrt{\pi} = -2\sqrt{t-\tau}\,\chi(\tau)\Big|_0^t + 2\int_{\chi(0)}^{\chi(t)} \sqrt{t-\tau}\mathrm{d}\chi(\tau). \tag{3.72}$$

Now, discretizing the time variables t and τ, such that $t = i\Delta t$ and $\tau = j\Delta t$, where $j \leq i$ one can approximate equation 3.72 as Riemann–Stieltjes integral. Defining further that $M(t-\tau) = 2\sqrt{t-\tau}/\sqrt{\pi}$ is the so-called mass transfer function of the system, one arrives at

$$1 \approx \chi(0)M(i\Delta t) + \sum_{j=0}^{i-1} M((i-j)\Delta t)[\chi((j+1)\Delta t) - \chi(j\Delta t)]. \tag{3.73}$$

Recognizing that $M(0) = 0$, this expression can be rearranged to finally give a recurrance relation for the dimension-less current according to

$$\chi(i\Delta t) \approx \frac{1}{M(\Delta t)}\Big(1 - \sum_{j=1}^{i-1} \chi(j\Delta t)[M((i-j+1)\Delta t) - M((i-j)\Delta t)]\Big) \tag{3.74}$$

Another way of numerically solving the diffusion equation for a potential step experiment is given by the implicit Crank–Nicolson method [96] which was introduced in subsection 3.3. Defining the matrix of the known time instance in equation 3.52 (the one that contains the coefficient β) to be $\underline{\underline{M}}_{\mathrm{old}}$ and the matrix at the new time instance (the one which contains the coefficient ϵ) to be $\underline{\underline{M}}_{\mathrm{new}}$, one obtains

$$\underline{\underline{M}}_{\mathrm{old}} \cdot \begin{pmatrix} c_{1,t} \\ c_{2,t} \\ \vdots \\ c_{N-2,t} \\ c_{N-1,t} \end{pmatrix} + \begin{pmatrix} \lambda c_{0,t} \\ 0 \\ \vdots \\ 0 \\ \lambda c_{N,t} \end{pmatrix} = \underline{\underline{M}}_{\mathrm{new}} \cdot \begin{pmatrix} c_{1,t+\Delta t} \\ c_{2,t+\Delta t} \\ \vdots \\ c_{N-2,t+\Delta t} \\ c_{N-1,t+\Delta t} \end{pmatrix} + \begin{pmatrix} \lambda c_{0,t+\Delta t} \\ 0 \\ \vdots \\ 0 \\ \lambda c_{N,t+\Delta t} \end{pmatrix}. \tag{3.75}$$

Setting $c_{0,t} = c_{0,t+\Delta t} = 0$ one defines the boundary conditions of a Cottrellian potential step experiment at the electrode surface. For the boundary of the N^{th} spatial grid point one might set a constant concentration $c_{N,t} = c_{N,t+\Delta t} = c_{\mathrm{R,B}}$. This assumption appears fair, as long as a sufficient number of spatial grid points

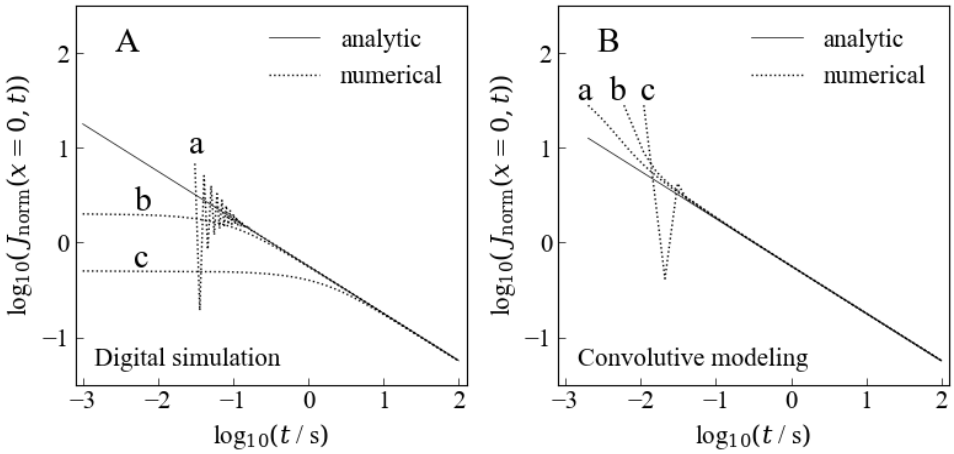

Figure 3.2: Time-dependent dimensionless flux (or current) of a Cottrellian potential step experiment simulated on (A) the base of digital simulation (equations 3.75 and 3.76) and (B) convolutive modeling (equation 3.74). The solid line represents the analytical current response based on the Cottrell equation 3.69. In panel (A), the simulations were performed with a) $\Delta x = 0.25$ μm, $\Delta t = 0.005$ s, $\lambda = 8.00$; b) $\Delta x = 5$ μm, $\Delta t = 0.005$ s, $\lambda = 0.02$ and c) $\Delta x = 20$ μm, $\Delta t = 0.08$ s, $\lambda = 0.02$, In panel B), it was used a) $\Delta t = 0.001$ s; b) $\Delta t = 0.005$ s and c) $\Delta t = 0.01$ s.

are employed to attain a semi-infinite diffusion domain[7]. The related dimensionless flux $\chi(t)$ will be calculated by normalizing equation 3.54 to the square root of the diffusion coefficient of the electrochemically active species. In analogy to equation 3.74, consider i timesteps of Δt in the experiment, such that $t = i\Delta t$ and therefore

$$\chi(i\Delta t) = \frac{\sqrt{D}}{2\Delta x}\Big(- 3c_{0,i\Delta t} + 4c_{1,i\Delta t} - c_{2,i\Delta t}\Big). \tag{3.76}$$

Equation 3.74 and 3.76 will be utilized now, for simulating the time-dependent current response of a Cottrellian potential step experiment. Reference values are generated on the base of the analytical result — equation 3.69. These are depicted in figure 3.2. In figure 3.2, it can be seen that the result of digital simulation depends on both, the choice of Δt and Δx, whereas convolutive modeling only depends on the choice of Δt. In the case of convolutive modeling, it is readily seen that if Δt decreases, the computation becomes more accurate.

[7]This implies that the concentration profile does not hit the outer boundary in the timescale of the experiment.

In the case of digital simulation, the choice of Δx basically determines at which point the numerical result converges. However, solely decreasing Δx, by keeping Δt constant will lead to unfavourably large values of the parameter λ which will finally result in catastrophal oscillations of the numerical result (curve a) in figure 3.2 (A)). However, it is worth to note that the numerical result will converge in any occasion due to the unconditional stability of the Crank–Nicolson algorithm. Nevertheless, owing to the straighforward implementation and mathematical elegance of convolutive modeling, this technique will be emphasized in the following.

3.5 Diffusional Cyclic Voltammetry

Since the concept of convolutive modeling is considered as the more decent approach for simulating the diffusive part of electroanalytical experiments, it will be employed in this sub-chapter. Convolutive modeling was basically pioneered by Matsuda [74] and Aoki [77]–[80] and generalized by Oldham [105] in the context of electrochemistry. In order to familiarize the reader with this particular technique the mathematics of CV in a planar semi-infinite diffusion domain will considered at next. Subsequently, the expressions for CV in a planar finite diffusion domain with an ideally impermeable outer boundary will be derived and utilized to introduce the co-called master-equation approach — a term first utilized by Oldham — which generalizes convolutive modeling of CV to any kind of diffusion domain as long as the respective mass transfer function is known.

Convolutive modeling of cyclic voltammetry at a planar electrode in semi-infinite diffusion space

The most simple situation of cyclic voltammetry emerges, when the electroanalytical experiment is conducted at an ideally planar electrode in a semi-infinite diffusion domain. Considering that the restrictions given on page 12 are fulfilled, one might directly start the derivation by recovering the modified[8] general solution

[8]Modified refers to the absence of the term containing C_+, owing to the semi-infinite diffusion domain.

of the Laplace transformed version of the diffusion equation which was given in equation 3.64 for an exemplary reduced species as

$$\bar{c}_{\mathrm{R}}(x,s) = C_{-}\exp\left(-x\sqrt{\frac{s}{D_{\mathrm{R}}}}\right) + \bar{c}_{\mathrm{R,B}}. \tag{3.77}$$

Relating the Laplace transformed flux (or current) to the Laplace transformed surface concentration in analogy to equation 3.66 yields

$$\begin{aligned}\bar{I}(s) &= nFAD_{\mathrm{R}}\left(\frac{\partial\bar{c}_{\mathrm{R}}(x,s)}{\partial x}\right)_{x=0} \\ &= -nFA\sqrt{sD_{\mathrm{R}}}C_{-}.\end{aligned} \tag{3.78}$$

This defines the constant C_{-} as

$$C_{-} = -\frac{1}{nFA\sqrt{D_{\mathrm{R}}}}\frac{\bar{I}(s)}{\sqrt{s}}, \tag{3.79}$$

such that the Laplace transformed surface concentration can be expressed as a function of the Laplace transformed current according to

$$\bar{c}_{\mathrm{R,S}} = \bar{c}_{\mathrm{R,B}} - \frac{1}{nFA\sqrt{D_{\mathrm{R}}}}\frac{\bar{I}(s)}{\sqrt{s}}. \tag{3.80}$$

In analogy, the Laplace transformed surface concentration of the oxidized species will be given by

$$\bar{c}_{\mathrm{O,S}} = \frac{1}{nFA\sqrt{D_{\mathrm{O}}}}\frac{\bar{I}(s)}{\sqrt{s}}, \tag{3.81}$$

if the experiment starts with a negligible amount of oxidized species in the bulk of the electrolyte. Performing the inverse Laplace transformation on equations 3.80 and 3.81 by applying the convolution theorem as outlined in equation 3.62 results in

$$c_{\mathrm{R,S}} = c_{\mathrm{R,B}} - \frac{1}{nFA\sqrt{D_{\mathrm{R}}}}\frac{1}{\sqrt{\pi}}\int_0^t \frac{I(\tau)}{\sqrt{t-\tau}}\mathrm{d}\tau \tag{3.82}$$

for the surface concentration of the reduced species. In a similar way, the surface concentration of the oxidized species is given by

$$c_{\mathrm{R,O}} = \frac{1}{nFA\sqrt{D_{\mathrm{O}}}}\frac{1}{\sqrt{\pi}}\int_0^t \frac{I(\tau)}{\sqrt{t-\tau}}\mathrm{d}\tau. \tag{3.83}$$

In analogy to equation 3.71, the denominator in the integrand of equations 3.82 and 3.83 will introduce a singularity at the upper integration limit which can be circumvented by an integration by parts. Assuming that $I(0) = 0$ (i.e. the experiment starts at equilibrium conditions), one obtains

$$c_{\mathrm{R,S}} = c_{\mathrm{R,B}} - \frac{1}{nFA\sqrt{D_{\mathrm{R}}}} \frac{2}{\sqrt{\pi}} \int_{I(0)}^{I(t)} \sqrt{t-\tau}\,\mathrm{d}I(\tau) \tag{3.84}$$

and

$$c_{\mathrm{O,S}} = \frac{1}{nFA\sqrt{D_{\mathrm{O}}}} \frac{2}{\sqrt{\pi}} \int_{I(0)}^{I(t)} \sqrt{t-\tau}\,\mathrm{d}I(\tau) \tag{3.85}$$

Recovering the Butler–Volmer equation as given in equation 3.30 and introducing the dimension-less electrode potential as

$$\xi(t) = \frac{nF}{RT}(E(t) - E^0) \tag{3.86}$$

results in

$$I(t) = nFAk^0 \Big\{ c_{\mathrm{R,S}}\, \mathrm{e}^{\alpha\xi(t)} - c_{\mathrm{O,S}}\, \mathrm{e}^{-(1-\alpha)\xi(t)} \Big\}. \tag{3.87}$$

In equation 3.87, the time dependent surface concentrations defined by equations 3.84 and 3.85 can be inserted. After slight rearrangement, one arrives at the following integral equation

$$\begin{aligned} I(t)\,\frac{\sqrt{D_{\mathrm{R}}}\,\mathrm{e}^{-\alpha\xi(t)}}{k^0} &= nFAc_{\mathrm{R,B}}\sqrt{D_{\mathrm{R}}} \\ &\quad - \left[1 + \sqrt{\frac{D_{\mathrm{R}}}{D_{\mathrm{O}}}}\mathrm{e}^{-\xi(t)}\right] \cdot \frac{2}{\sqrt{\pi}} \int_{I(0)}^{I(t)} \sqrt{t-\tau}\,\mathrm{d}I(\tau). \end{aligned} \tag{3.88}$$

Similar to equation 3.73, the integral in equation 3.88 can be transformed into a sum in order to evaluate it as Riemann–Stieltjes integral.

Therefore, taking the discretization of the time variables $t = i\Delta t$ and $\tau = j\Delta t$ with $j \leq i$, one arrives at

$$I(i\Delta t)\,\frac{\sqrt{D_\mathrm{R}}\,\mathrm{e}^{-\alpha\xi(i\Delta t)}}{k^0} \approx nFAc_{\mathrm{R,B}}\sqrt{D_\mathrm{R}} - \left[1+\sqrt{\frac{D_\mathrm{R}}{D_\mathrm{O}}}\mathrm{e}^{-\xi(i\Delta t)}\right]\cdot\frac{2\sqrt{\Delta t}}{\sqrt{\pi}}\sum_{j=0}^{i-1}\sqrt{i-j}\,[I((j+1)\Delta t)-I(j\Delta t)]. \quad (3.89)$$

Subsequently to rearranging the sum in equation 3.89 and isolating the $I(i\Delta t)$ term, one obtains the following recursion relation for the current of a potential sweep experiment like the one in a CV.

$$I(i\Delta t) \approx \frac{nFAc_{\mathrm{R,B}}\sqrt{D_\mathrm{R}} - \left[1+\sqrt{\frac{D_\mathrm{R}}{D_\mathrm{O}}}\mathrm{e}^{-\xi(i\Delta t)}\right]\cdot\mathfrak{S}}{\frac{\sqrt{D_\mathrm{R}}\,\mathrm{e}^{-\alpha\xi(i\Delta t)}}{k^0}+\frac{2\sqrt{\Delta t}}{\sqrt{\pi}}\cdot\left[1+\sqrt{\frac{D_\mathrm{R}}{D_\mathrm{O}}}\mathrm{e}^{-\xi(i\Delta t)}\right]}, \quad (3.90)$$

where $\mathfrak{S}$ denotes a convolution of lists[9] according to

$$\mathfrak{S} = \frac{2\sqrt{\Delta t}}{\sqrt{\pi}}\sum_{j=1}^{i-1} I(j\Delta t)\left(\sqrt{i-j+1}-\sqrt{i-j}\right) \quad (3.91)$$

Following the recursion relation of equation 3.90, the current response of a planar electrode in a semi-infinite diffusion domain to basically any time-variant potential perturbation can be computed. It is therefore not limited to CV experiments. The only requirement is then to modify the time-dependence of the electrode potential $E(t)$, and hence $\xi(t)$.

[9] A convolution of lists implies that the convolution integrals which were transformed into sums are solved recursively and that the respective intermediate solutions are stored in the computer memory as lists of discrete points.

Convolutive modeling of cyclic voltammetry at a planar electrode in a finite reflective diffusion space

Considering that the electroanalytical experiment is performed at a planar electrode in a finite diffusion domain with an impermeable outer boundary, it can be expected that the current will be a complicated function of the electrode kinetics and the diffusion domain size. This scenario was first ever described by Aoki [79], [80] and generalized by Bieniasz [106]. The mathematical treatment in terms of convolutive modeling will be, however, closely related to the semi-infinite case. This will be demonstrated right now to emphasize an additional outstanding advantage of convolutive modeling. The startingpoint will be again the general solution of the Laplace transformed diffusion equation (equation 3.64) for an exemplary reduced species as

$$\bar{c}_{\mathrm{R}}(x,s) = C_+ \exp\left(x\sqrt{\frac{s}{D_{\mathrm{R}}}}\right) + C_- \exp\left(-x\sqrt{\frac{s}{D_{\mathrm{R}}}}\right) + \bar{c}_{\mathrm{R,B}}. \tag{3.92}$$

In contrast to the scenario of a semi-infinite diffusion domain both constants — C_+ and C_- — need to be preserved here since the diffusion domain size will approach a maximum size, say $x = d$, instead of $x \to \infty$. Therefore, C_+ is particularily *not* zero. Now, again calculating the Laplace transformed current according to Ficks first law at $x = 0$ gives

$$\begin{aligned} \bar{I}(s) &= nFAD_{\mathrm{R}}\left(\frac{\partial \bar{c}_{\mathrm{R}}(x,s)}{\partial x}\right)_{x=0} \\ &= nFA\sqrt{sD_{\mathrm{R}}}(C_+ - C_-). \end{aligned} \tag{3.93}$$

Considering a no-flux boundary at $x = d$ implies that

$$0 = \left(\frac{\partial \bar{c}_{\mathrm{R}}(x,s)}{\partial x}\right)_{x=d} = C_+ \exp\left(d\sqrt{\frac{s}{D_{\mathrm{R}}}}\right) - C_- \exp\left(-d\sqrt{\frac{s}{D_{\mathrm{R}}}}\right). \tag{3.94}$$

Combining equations 3.93 and 3.94 allows for determining both constants C_+ and C_- as

$$C_+ = \frac{\bar{I}(s)}{nFA\sqrt{sD_{\mathrm{R}}}} \frac{\exp\left(-d\sqrt{\frac{s}{D_{\mathrm{R}}}}\right)}{\exp\left(-d\sqrt{\frac{s}{D_{\mathrm{R}}}}\right) - \exp\left(d\sqrt{\frac{s}{D_{\mathrm{R}}}}\right)} \tag{3.95}$$

and

$$C_{-} = \frac{\bar{I}(s)}{nFA\sqrt{sD_{\mathrm{R}}}} \frac{\exp\left(d\sqrt{\frac{s}{D_{\mathrm{R}}}}\right)}{\exp\left(-d\sqrt{\frac{s}{D_{\mathrm{R}}}}\right) - \exp\left(d\sqrt{\frac{s}{D_{\mathrm{R}}}}\right)}. \tag{3.96}$$

Substituting equations 3.95 and 3.96 back into equation 3.92 and evaluating the expression at $x = 0$ allows for calculating the surface concentrations according to

$$\bar{c}_{\mathrm{R,S}} = \bar{c}_{\mathrm{R,B}} - \frac{\bar{I}(s)}{nFA\sqrt{sD_{\mathrm{R}}}} \frac{\exp\left(d\sqrt{\frac{s}{D_{\mathrm{R}}}}\right) + \exp\left(-d\sqrt{\frac{s}{D_{\mathrm{R}}}}\right)}{\exp\left(d\sqrt{\frac{s}{D_{\mathrm{R}}}}\right) - \exp\left(-d\sqrt{\frac{s}{D_{\mathrm{R}}}}\right)}, \tag{3.97}$$

or extensively simplified by identifying the hyperbolic cotangent function as

$$\bar{c}_{\mathrm{R,S}} = \bar{c}_{\mathrm{R,B}} - \frac{\bar{I}(s)}{nFA\sqrt{D_{\mathrm{R}}}} \frac{\coth\left(d\sqrt{\frac{s}{D_{\mathrm{R}}}}\right)}{\sqrt{s}}. \tag{3.98}$$

In analogy, the surface concentration of the oxidized species can be obtained as

$$\bar{c}_{\mathrm{O,S}} = \frac{\bar{I}(s)}{nFA\sqrt{D_{\mathrm{O}}}} \frac{\coth\left(d\sqrt{\frac{s}{D_{\mathrm{O}}}}\right)}{\sqrt{s}}. \tag{3.99}$$

The most crucial step is now, to perform the inverse Laplace transformation of equations 3.98 and 3.99 to access the respective time-domain solution. The inverse Laplace transformation of the function convoluted with the current is given in terms of Jacobi theta functions[10] [79], [80], [104] and can be written as

$$\begin{aligned} \mathcal{L}^{-1}\left\{\frac{\coth\left(\sqrt{s}\right)}{\sqrt{s}}\right\}(s) &= \Theta_3(0|t) \\ &= 1 + 2\sum_{k=1}^{\infty} \exp(-\pi^2 k^2 t). \end{aligned} \tag{3.100}$$

[10] This particular derivation is included in section A.2 in appendix A.

However, for the sake of simplicity and generality, urgently required in the context of this thesis, suppose a function $m_{\mathrm{R}}(t)$, which defines

$$\mathcal{L}^{-1}\left\{\frac{\coth\left(d\sqrt{\frac{s}{D_{\mathrm{R}}}}\right)}{\sqrt{s}}\right\}(t) = m_{\mathrm{R}}(t) \tag{3.101}$$

and another function $m_{\mathrm{O}}(t)$ which defines

$$\mathcal{L}^{-1}\left\{\frac{\coth\left(d\sqrt{\frac{s}{D_{\mathrm{O}}}}\right)}{\sqrt{s}}\right\}(t) = m_{\mathrm{O}}(t). \tag{3.102}$$

In this manner, one would readily obtain the convolution integrals

$$c_{\mathrm{R,S}} = c_{\mathrm{R,B}} - \frac{1}{nFA\sqrt{D_{\mathrm{R}}}} \int_0^t I(\tau)\, m_{\mathrm{R}}(t-\tau)\mathrm{d}\tau \tag{3.103}$$

and

$$c_{\mathrm{O,S}} = \frac{1}{nFA\sqrt{D_{\mathrm{O}}}} \int_0^t I(\tau)\, m_{\mathrm{O}}(t-\tau)\mathrm{d}\tau. \tag{3.104}$$

In analogy to the planar electrode in a semi-infinite diffusion domain these expressions could be treated by an integration by parts to remove the singularity in the integrand, which defines the antiderivatives of m_{R} and m_{O} as M_{R} and M_{O}, respectively. The resulting expressions can also be inserted into the Butler–Volmer equation and finally rearranged to provide a recursion formula which is fairly similar to — but much more generalized than — equation 3.90. Owing to the generality of this recursion relation, it is termed *The Master Equation* of convolutive modeling. It is given as

$$I(i\Delta t) \approx \frac{nFAc_{\mathrm{R,B}}\sqrt{D_{\mathrm{R}}} - \mathfrak{S}_{\mathrm{R}} - \sqrt{\frac{D_{\mathrm{R}}}{D_{\mathrm{O}}}}\mathrm{e}^{-\xi(i\Delta t)}\mathfrak{S}_{\mathrm{O}}}{\frac{\sqrt{D_{\mathrm{R}}}\,\mathrm{e}^{-\alpha\xi(i\Delta t)}}{k^0} + M_{\mathrm{R}}(\Delta t) + M_{\mathrm{O}}(\Delta t)\sqrt{\frac{D_{\mathrm{R}}}{D_{\mathrm{O}}}}\mathrm{e}^{-\xi(i\Delta t)}}, \tag{3.105}$$

where $\mathfrak{S}_{\mathrm{R}}$ denotes a convolution of lists of the reduced species according to

$$\mathfrak{S}_{\mathrm{R}} = \sum_{j=1}^{i-1} I(j\Delta t) \Big(M_{\mathrm{R}}((i-j+1)\Delta t) - M_{\mathrm{R}}((i-j)\Delta t) \Big) \tag{3.106}$$

and $\mathfrak{S}_{\mathrm{O}}$ the respective convolution of lists for the oxidized species as

$$\mathfrak{S}_{\mathrm{O}} = \sum_{j=1}^{i-1} I(j\Delta t) \Big(M_{\mathrm{O}}((i-j+1)\Delta t) - M_{\mathrm{O}}((i-j)\Delta t) \Big). \tag{3.107}$$

Equation 3.105 can be considered as somewhat universal, since it allows for computing electroanalytical experiments to any kind of potential excitation and in any kind of diffusion domain, considering that the respective mass transfer functions are known a-priori. It is, however, different from the expressions given by Oldham [105], since it avoids a double-integration. When referring to porous electrodes, computing this particular mass transfer functions will be the emphasis of the final publication related to this thesis which is given in section 5.5 of chapter 5. However, before referring to CV porous electrodes, the following section will provide an overview on the theoretical work which has been published in this particular context.

3.6 Cyclic Voltammetry at Porous Electrodes

Subsequently to introducing two *'recipes'* for the mathematical treatment of diffusional cyclic voltammetry, this section will be dedicated to the very limited amount of publications on the theory of CV at porous electrode structures which was mainly pioneered by the group of Compton.

Probably the first study which emphasized the effect of electrode porosity on the current response of diffusional cyclic voltammetry has been published by this group in 2006 [64]. There, the authors proposed a theoretical model for describing an electrode which is accessible through randomly distributed cylindrical pores of uniform diameter in an insulating layer which covers the surface. The respective numerical computations of the electroanalytical experiments were performed on the base of digital simulation.

In 2007, the same group published an article on cyclic voltammetry at random arrays of microband electrodes inlayed into an inert surface [107]. This might not be associated with a porous electrode on a first glance, but does, however,

highlight the effects of a statistically distributed diffusion domain on CV which is extraordinarily important for porous electrodes. In 2008, three additional scientific reports of the Compton group were published which are dedicated to a) the influence of electrode porosity on CV [65], b) the influence of electrode roughness on CV [108] and c) to the theory for electrodes covered with a porous layer of carbon-nanotubes [109]. In the same year, a work very similar to c) was independently published by Holloway and Wildgoose [110].

In ref. [65], the authors proposed a theoretical model for describing an electrode which is covered with a porous layer of catalytically active material by assuming a regular array of hollow-cylindrical pores. In order to reduce the mathematical complexity, they treated each cylindrical pore as an individual sub-structure and approximated the diffusion domain by assuming translational symmetry of these sub-units. For their computations, they again utilized digital simulation. In 2009, another research paper on cyclic voltammetry at microelectrode arrays was published, which highlights the limitations of the diffusion domain approximation [111] which was introduced so far.

In 2014, the Compton group published a theoretical concept which treats porous electrodes as an array of hollow spheres[66]. They highlight the experimental relevance of this particular concept for electrocatalysts which have been synthesized via electroplating on micro-spherical particles. However, it might also hold for materials which have been synthesized via bubble templating. The authors point out, that the current response of such a porous electrode can exhibit two distinct current peaks, even if just one redox reaction is involved. This exceptionally important remark is ascribed to the two distinct diffusion modi which occur in parallel and which can be termed as internal spherical finite (in the individual pores) and planar semi-infinite (towards the entire electrode). Again, the calculations were performed via digital simulation.

In 2017, another study on porous electrodes was published by the Compton group [69]. In this paper, the authors investigated the theory of CV experiments which consist of multiple cycles in order to find out whether or not the current wave will converge to a constant shape within time. Since CV experiments are typically conducted for more than one cycle this study is fairly important for the experimentalists community as a time-variant CV will complicate any experimental evaluation.

Even though the latter four studies are a great pioneering work on the theory of porous electrodes, they do not provide any experimental reference. Furthermore, they are somewhat incomplete, since no distribution of pore sizes is considered which might be, however, of relevance when describing porous electrodes.

The first — and to the best of the authors knowledge only — publication which combined experimental and theoretical work on porous electrodes is the one from Smith et al. [67] which was published in 2015 and which is entitled *'The electrochemical characterisation of graphite felts '*. In this particular publication, the diffusion domain of a felt electrode was approximated by a planar finite reflective diffusion model — analog to a thin layer cell. The diffusion layer thickness in turn was estimated from the average pore volume of the felt and defined as the half-average void distance. Again, no statistical effects of the diffusion domain size were considered, i.e. a constant diffusion layer thickness was assumed. Nevertheless, it is remarkable, how well this rigorous approximation can already fit the presented experimental data when compared to the classical planar semi-infinite diffusion model. For this reason, this particular study can be regarded as the ancestor and the main motivation of the combined theoretical and experimental work presented in this thesis.

Chapter 4

The VRFB System

Since any theoretical model requires for an experimental validation, this chapter will be dedicated to the experimental reference of this thesis, the vanadium redox-flow system. However, it is worth to mention that the theoretical concepts derived in this work chronologically emerged in the exactly opposite order. This implies that the theory was created in order to accurately interprete experimentally acquired CV data of the VRFB system in terms of electrode kinetics. This chapter will be split into two subsections. At first, the working principle of redox-flow batteries will be introduced with emphasis on the vanadium redox-flow system. Subsequently, an overview on the extensive amount of *activation methods* for the improvement of this particular technology will be given.

4.1 Technical Implementation of the Vanadium Redox-Flow System

When referring to large-scale electrochemical energy storage systems, redox-flow batteries are promising candidates since they allow for an independent adjustment of capacity and power. In a redox-flow battery, the capacity is determined by the size of the electrolyte reservoirs, while the stacksize limits the maximum power output of the system [15]. The conversion between electrical and chemical energy occurs at the typically high surface area carbon felt electrodes (cf. figure 4.1) of an electrochemical cell under continous supply (flow) of the liquid electrolytes. The electrodes are separated by an ion-conducting membrane or separator which prevents the two electrolytes from mixing and which allows for a transport of the charge carrying ions to maintain electroneutrality.

The first real redox-flow battery utilized an electrolyte solution which contained the ferric/ferrous (Fe^{2+}/Fe^{3+}) redox couple in the positive and the chromic/chromous (Cr^{2+}/Cr^{3+}) redox couple in the negative half-cell [15], [112]. Unfortunately, this technology was prone to cross-contamination which resulted in a significant capacity fading over a short period of time. Consequently, a number of other redox-flow systems have been proposed, which have been reviewed by Wang in 2012 [15]. Among them, the vanadium redox-flow system is probably the most important and promising one. It was invented and pioneered by the group of Maria Skyllas-Kazacos in the 1980s [113]–[115] and recently gathers a significant industrial interest all around the world. It utilizes the four oxidation states of vanadium, separated as two redox couples in the so-called anolyte and catholyte, respectively. A sketch of a vanadium redox-flow battery is depicted in figure 4.2. Since it is based on only one active element, cross-contamination is not an issue. Furthermore, since it utilizes aqueous electrolytes, the common hazards of other electrochemical energy conversion and storage devices, i.e. internal shortning (related to Li-ion batteries) or risk of explosions (related to hydrogen based fuel cells) are not an issue.

The conversion of energy is achieved by changes in valence states of the vanadium species, which can be formulated in terms of the following redox reactions.

$$VO_2^+ + 2H^+ \underset{-e^-}{\overset{+e^-}{\rightleftharpoons}} VO^{2+} + H_2O \tag{4.1}$$

$$V^{3+} \underset{-e^-}{\overset{+e^-}{\rightleftharpoons}} V^{2+} \tag{4.2}$$

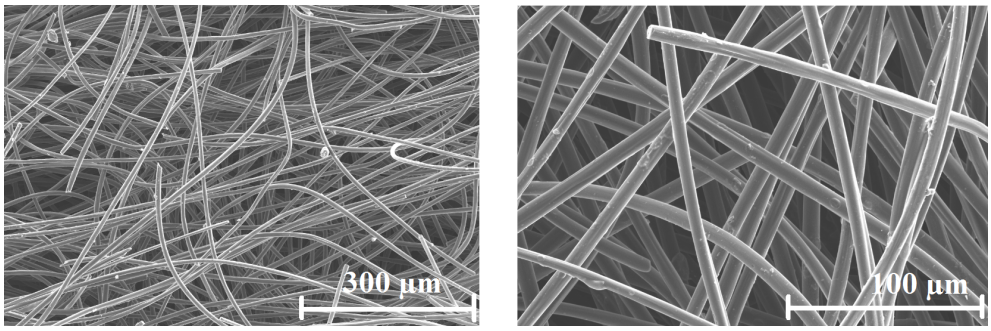

Figure 4.1: Scanning electron microscopy image of a carbon felt typically utilized as electrode material in a vanadium redox flow battery. The fibrous sructure of the electrode provides a stable network with a large active surface area for the desired electrochemical redox reactions of the vanadium species.

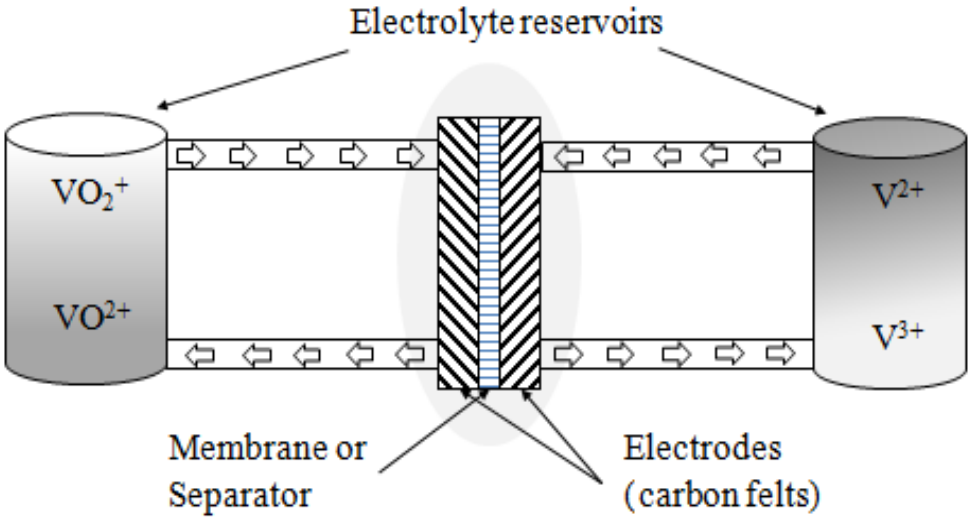

Figure 4.2: Sketch of a vanadium redox-flow battery during the discharging process. The positive redox couple ($VO^{2+}/VO_2{}^+$) and negative redox couple(V^{2+}/V^{3+}) are stored in aqueous electrolyte solutions in separate tanks. During the charging or discharging process, the electrolytes are pumped through the electrodes of the respective battery cell, where the electrochemical reactions take place. To preserve electroneutrality, counter-ions diffuse through the ion-conducting membrane in the opposite direction of the electric current.

The electrode reaction of the positive half-cell (equation 4.1 has a standard electrode potential of $E^0 = 1.005$ V vs. SHE, whereas the redox reaction of the negative side has a standard electrode potential of $E^0 = -0.255$ V. The total electrochemical redox-reaction can be formulated as

$$VO_2^+ + 2H^+ + V^{2+} \rightleftharpoons VO^{2+} + H_2O + V^{3+} \tag{4.3}$$

and has, of course, a standard cell voltage of 1.26 V. This potential difference is in the range of the stability window of water, which is why aqueous electrolytes can be employed. This fact, together with the low-cost factor of the electrode materials which are typically carbon felts renders the vanadium redox-flow system an overall cost efficient and attractive technology. Nevertheless, the low energy density of the electrolytes, the sluggish electrode kinetics as well as a whole bunch of degradation phenomena impede the wide range industrial application and the commercial breakthrough of the VRFB. Consequently, a significant effort has been taken to improve all the components related to this technology among which the most popular one lies in enhancing the electrode kinetics.

4.2 On *'Outstanding Activities'* and *'Improved Kinetics'*

In recent years, an impressive amount of scientific reports on the improvement of the sluggish electrode kinetics related to the vanadium redox flow system have been published. These include a) chemical treatments like alkaline [22]–[25] or acidic [26], [29] etching, surface hydroxylation [27] and halogenation [32], b) electrochemical etching techniques [116] or c) impregnation techniques with either carbon nanoparticles [35], [37], [46]–[48] or literally any kind of metal or metal compounds such as bismuth [55], iridium [50], niobium [53], titanium nitride [56], titanium carbide [61], titanium oxide [52], [54], [60] and zirconia [58] (this list is far from being exhaustive). Furthermore, thermal decomposition and carbonization techniques [33], [49] or plasma treatments [30], [31] have been proposed, which all lead to the same conclusion — *enhanced catalytic activity*. With a wink of the eye, the storyline of the majority of these studies can be summarized as follows:

- Take a commercial electrode material, suppose a carbon felt,
- etch/oxidize/coat or somehow modify its surface in an optionally advanced way and term the synthesis route as *facile* and *scalable*,
- characterize the novel electrode material by means of any technique which is accessible to you. In particular, do not miss out on XPS, Raman spectroscopy, IR spectroscopy, etc,
- investigate the electrocatalytic performance of the novel electrode material by means of standard electrochemical characterization techniques such as cyclic voltammetry and probably electrochemical impedance spectroscopy,
- interprete the CV data classically in terms of peak separations or by applying the Randles-Ševčík equation and verify a superior catalytic for your electrode material,
- finally, but optionally, propose a sophisticated reaction mechanism.

Even if this list is an exaggeration which might sound malicious, it is exceptionally worth to note that among the multitude of activation methods only the simple heat treatment has been commercialized to date. Furthermore, it appears questionable whether or not *carbonized waste-coffee beans* [117] and *carbonized corn protein* [118] or *graphene decorated carbon* [47] will save the global climate by *'outstandingly'* boosting the performance of a VRFB. In contrast, as pointed out in the previous chapters of this thesis, it is very much likely that the auspicious electrode kinetics

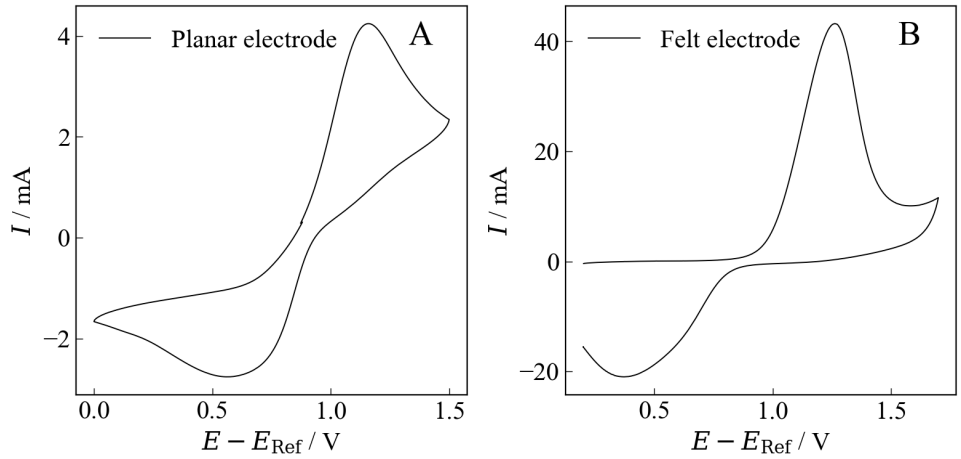

Figure 4.3: Cyclic voltammograms acquired for the electrochemical oxidation of VO^{2+} in 2 M H_2SO_4 at a potential sweep rate of 20 mV/s at (A) a planar glassy carbon electrode and (B) a carbon felt electrode (GFD4.6, SGL Carbon). The potentials are referred to a saturated silver/silver chloride electrode. After the oxidation peak, the current of the CV curve acquired at the planar electrode decays according to an inverse square root function, typical for a semi-infinite diffusion domain. In contrast, the current wave of the felt electrode decays much steeper owing to the effect of a finite diffusion domain. Furthermore, the current magnitude of the CV of the felt electrode is about ten times larger, when compared to the planar electrode which is caused by the huge internal surface area of a felt electrode.

may be caused by the inherent ambiguity of CV at porous electrodes which can easily lead to misinterpretation. To demonstrate this significant ambiguity, figure 4.3 depicts the CV measurements of the electrochemical oxidation of VO^{2+} at (A), a planar glassy carbon electrode and (B), a carbon felt electrode (GFD4.6, SGL Carbon). It can be seen that the two CV curves are substantially different with respect to shape, magnitude and separation of the redox peaks. Consequently, an interpretation of the felt electrode CV with the model of a planar electrode will certainly lead to incorrect results. For this particular reason, the essence of this thesis is to develop a theoretical model for cyclic voltammetry at porous electrodes which allows for a reliable characterization of the electrode kinetics.

Chapter 5

Discussion of Related Publications

This chapter will assemble the individual publications related to this thesis. The first two studies, presented in sections 5.1 and 5.2 are dedicated to a thorough investigation of the positive and negative VRFB half-cell reactions under well-defined semi-infinite diffusion conditions. Based on a combination of CV/LSV with other advanced electroanalytical techniques, exceptionally accurate values for hydrodynamic and electrokinetic parameters are obtained. These constitute the base for the three follow-up publications presented in sections 5.3, 5.4 and 5.5, where sophisticated diffusion models for CV at porous electrodes are derived and experimentally validated.

5.1 Finite Heterogeneous Kinetics

The first publication presented in this cumulative thesis, which is entitled

'Finite Heterogeneous Rate Constants for the Electrochemical Oxidation of VO^{2+} at Glassy Carbon Electrodes'.

comprises the preliminary studies on the positive VRFB half-cell reactions under well-defined diffusion conditions. Chronologically it was, however, the second last manuscript submitted and the last manuscript which had been accepted for publication. It is attached as original scientific research paper in section 6.1.

By experimentally avoiding the use of porous electrodes, this study provided highly accurate information on hydrodynamic and kinetic parameters of the electrochemical oxidation of the oxovanadyl cation at carbon surfaces. Furthermore, it led to an extension of the classical Butler–Volmer model of electrode kinetics by considering a maximum heterogeneous reaction rate which is independent of the electrode potential. It can be therefore regarded as a combined experimental and theoretical work on the VRFB related reactions. Furthermore, it builds a solid fundament for this thesis, since all the kinetic information acquired, served as reference for the following publications which involved porous electrode structures.

Motivation

Owing to the vast discrepancy in the kinetic data of the VRFB related reactions at porous electrodes, this study intended to exclude the complicated porous diffusion domain effects experimentally. For this purpose, planar electrodes in semi-infinite diffusion space were employed. Since the reactions related to the vanadium redox-flow system are usually termed as kinetically sluggish, it was assumed that the classical way of data interpretation by means of the irreversible Randles-Ševčík-, the Koutecky–Levich-, the Cottrell- and the Tafel-analysis will be sufficient to gather conclusive remarks on the respective electrode kinetics. This was, however, not the case. In contrast, it was found that particularly the Randles–Ševčík analysis will result in an incorrect interpretation of the electrode kinetics. Furthermore, the Koutecký–Levich analysis revealed a very specific feature — a non-zero ordinate intercept — which cannot be explained in terms of the classical model. These two, very specific findings led to the concept of finite heterogeneous electron transfer kintics, which deviate from the classical Butler–Volmer behaviour and which account for the experimental findings. This new model will be presented in

brief in this sub-chapter. Furthermore, a *'master equation'*, which accounts for finite electrode kinetics and which is slightly different from the one presented in the original publication will be derived in order to provide a uniform notation and nomenclature throughout this thesis. A discussion of experimental details of this study will not be included in the main part of this chapter. For experimental details the reader is referred to the original publication in the section 6.1.

Theory of finite electron transfer kinetics

The kinetics and hydrodynamics of an electrochemically irreversible reaction which takes place at a planar electrode surface in a semi-infinite diffusion domain might be investigated by utilizing the relations given in tables 5.1 and 5.2. These are either derived from or equivalent to the expressions named in the previous chapters of this thesis and are assembled here to improve the readibility. Hence, table 5.1 includes all the expressions for an electrochemical reaction at a stationary electrode. In contrast, table 5.2 lists the expressions for an electrode reaction involving the forced convection of a rotating disc electrode.

Table 5.1: Equations for extracting kinetic and hydrodynamic parameters of an electrochemically irreversible reaction taking place at a planar electrode in a semi-infinite diffusion domain in a stagnant electrolyte solution.

Name	Equation
Randles–Ševčík	$I_{\mathrm{p,irr}} = 0.496\, nFAc\sqrt{\frac{nFD\nu\alpha}{RT}}$
Matsuda–Ayabe (I)	$\alpha = \frac{1.85\, RT}{nF(E_{\mathrm{p,irr}/2} - E_{\mathrm{p,irr}})}$
Matsuda–Ayabe (II)	$\alpha = \frac{RT}{2\, nF}\left(\frac{\partial E_{\mathrm{p,irr}}}{\partial \ln(\nu)}\right)^{-1}$
Nicholson–Shain	$k^0 = 2.182\sqrt{\frac{\alpha nFD\nu}{RT}} \cdot \exp\left(\frac{\alpha nF(E_{\mathrm{p,irr}} - E^0)}{RT}\right)$
Cottrell	$I = \frac{nFAc\sqrt{D}}{\sqrt{\pi t}}$

Table 5.2: Equations for extracting kinetic and hydrodynamic parameters of an electrochemically irreversible reaction taking place at a planar electrode in a semi-infinite diffusion domain under forced convection (rotating disc electrode).

Name	Equation
Koutecký–Levich	$\frac{1}{I} = \frac{1}{I_{\mathrm{kin}}} + \frac{1}{I_{\mathrm{lim}}}$
Levich	$I_{\mathrm{lim}} = 0.201\, nFAcD^{2/3}\eta^{-1/6}\sqrt{\omega}$
Tafel	$\ln\left(I_{\mathrm{kin}}\right) = \ln\left(\frac{I \cdot I_{\mathrm{lim}}}{I_{\mathrm{lim}} - I}\right) = \ln\left(I^{\mathrm{eq}}\right) + \frac{\alpha n F (E - E^{\mathrm{eq}})}{RT}$
Butler–Volmer	$I^{\mathrm{eq}} = nFAck^0 \exp\left(\frac{\alpha n F (E^{\mathrm{eq}} - E^0)}{RT}\right)$

The first intention in this study was to accurately assess the diffusion coefficient of the oxovanadyl cation in the supporting electrolyte solution (sulfuric acid). For this purpose, the Levich equation and the Cottrell equation were combined in a very specific and novel way which eliminates the concentration dependence and surface area dependence of the current and also does not require for an a-priori knowledge of n. By conducting all experiments at four different electrolyte concentrations, the second partial derivatives of the Cottrell equation and the Levich equation could be calculated from experimental data according to

$$I''_{\mathrm{lim}} = \frac{\partial^2 I_{\mathrm{lim}}}{\partial c \partial \omega^{1/2}} = 0.201\, nFAD^{2/3}\eta^{-1/6} \tag{5.1}$$

and

$$I''_{\mathrm{Cot}} = \frac{\partial^2 I_{\mathrm{Cot}}}{\partial c \partial t^{-1/2}} = \frac{nFA\sqrt{D}}{\sqrt{\pi}}, \tag{5.2}$$

where I_{Cot} denotes the time dependent current of a Cottrellian potential step experiment[1]. Combining these two expressions resulted in

$$D = 489\,\eta \left(\frac{I''_{\mathrm{lim}}}{I''_{\mathrm{Cot}}} \right)^6 . \tag{5.3}$$

In this manner, the diffusion coefficient of the oxovanadyl cation was accurately calculated as $D = 2.26 \cdot 10^{-6}$ cm^2/s. In an analogue way combining the second partial derivative of the irreversible Randles–Ševčík equation as

$$I''_{\mathrm{p,irr}} = \frac{\partial^2 I_{\mathrm{p,irr}}}{\partial c \partial \nu^{1/2}} = 0.496\, nFA \sqrt{\frac{nFD\alpha}{RT}} \tag{5.4}$$

with the second partial derivative of the Cottrell equation (equation 5.2) allowed for an estimation of α as

$$\alpha = 1.294\, \frac{RT}{nF} \left(\frac{I''_{\mathrm{p,irr}}}{I''_{\mathrm{Cot}}} \right)^2 . \tag{5.5}$$

Following equation 5.5 and assuming $n = 1$, the electron transfer coefficient for the electrochemical oxidation of the oxovanadyl cation at a glassy carbon surface was obtained as $\alpha = 0.32$. In order to scrutinize this result, α was also calculated by the Matsuda and Ayabe relations [74], given in table 5.1 and via Tafel-analysis according to the equation given in table 5.2. For details on this procedure, the reader is referred to the original publication in section 6.1. In contrast to the value of $\alpha = 0.32$, obtaind from the Randles–Ševčík approach, all these analysis consistently resulted in $\alpha \approx 0.38$.

This contradictive value for the electron transfer coefficient, even for the most simple electrode geometry, was one motivation for the development of an extended model of electrode kinetics. The second motivation emerged from a careful look on the Koutecký–Levich analysis[2] (cf. figure 2B in the original publication). There it was seen that the so-called Levich–line does not intersect the origin. The Levich line basically corresponds to the Koutecký–Levich equation at large overpotentials such that the hydrodynamic limiting current should already be established.

[1] The index denotes the Cottrellian current and is introduced here to distinguish this particular quantity from the total current of an RDE experiment.

[2] The so-called Koutecký–Levich analysis consists of a plot of the reciprocal limiting current versus the reciprocal square root of the angular rotation frequency of the working electrode in the case of an RDE experiment.

Mathematically, this implies that $I_{\mathrm{kin}} \approx \infty$. Experimentally it is, however, sufficient if $I_{\mathrm{kin}} \gg I_{\mathrm{lim}}$, which should hold true for large overpotentials. Under this circumstance, the Koutecký–Levich equation will reduce to the Levich equation (cf. table 5.2). Now, extrapolating to an infinite rotation rate (to zero of the abscissia in a Koutecký–Levich plot), implies that also the term $I_{\mathrm{lim}}^{-1} \to 0$. Therefore, one would expect a zero ordinate intercept from a theoretical point of view. However, non-zero ordinate intercepts in Koutecký-Levich analysis have been also reported for thin-film coated electrodes which are subjected to finite mass transfer across the film/solution interface [119]. Nevertheless, since the electrodes utilized in this study were not subjected to any coating, the experimental results required for additional investigations. These will be discussed right now.

The only way to achieve a non-zero ordinate intercept in a Koutecký–Levich plot in a mathematical sense will be the assumption that $I_{\mathrm{kin}} \ll \infty$ or better, $I_{\mathrm{kin}} = const = I_{\mathrm{kin,\,max}}$. This assumption does, however, demand that the electrode kinetics will approach a plateau which is independent of the applied potential and which finally translates to the term — *finite heterogeneous reaction rates* or *kinetic limiting current*. Since all the analysis related to this publication had been performed at four different analyte concentrations, a hypothetical concentration dependence of this kinetic limiting current could be investigated with ease. Indeed, a linear concentration dependence of this particular quantity could be verified which finally allowed to define $I_{\mathrm{kin,\,max}} = nFAck_{\mathrm{max}}$, with k_{max} as maximum heterogeneous rate constant.

Since such a finite reaction rate can be expected to significantly affect the current response under any kind of mass transfer conditions the influence on a stationary potential-sweep experiment and on the related Randles–Ševčík analysis had been revisited. Furthermore, also the Koutecký–Levich equation has been significantly modified. For this purpose, an alternative version of the Butler–Volmer equation has been introduced at first, which can be formulated as

$$I = nFAk^0 \left\{ c_{\mathrm{R,S}} \frac{k_{\mathrm{max}} \mathrm{e}^{\alpha\xi}}{k_{\mathrm{max}} + k^0\, \mathrm{e}^{\alpha\xi}} - c_{\mathrm{O,S}} \frac{k_{\mathrm{max}} \mathrm{e}^{-(1-\alpha)\xi}}{k_{\mathrm{max}} + k^0\, \mathrm{e}^{-(1-\alpha)\xi}} \right\}, \tag{5.6}$$

where ξ is the dimension less electrode potential as defined by equation 3.87 in chapter 3.5. It is readily seen that as $k_{\mathrm{max}} \to \infty$, equation 5.6 reduces to the classical, kinetically unlimited Butler–Volmer equation as given by equation 3.87. Treating equation 5.6 in analogy to equation 3.32 and following the exact same derivation as defined by equations 3.36–3.41, one obtains a three-term Koutecký-

Levich like expression which can be stated as

$$\frac{1}{I} = \frac{1}{I_{\mathrm{kin}}} + \frac{1}{I_{\mathrm{kin,\ max}}} + \frac{1}{I_{\mathrm{lim}}}. \tag{5.7}$$

For details on this derivation[3], the reader is referred to the original publication in section 6.1. The third additive term in equation 5.7 can be regarded as the cause of the ordinate intercept in the Koutecký–Levich plots, which cannot be explained by the classical model and therefore as the first proof of concept.

The second validation of the new model follows by introducing the finite heterogeneous reaction rates into the theory of stationary CV/LSV and to explain the inadequacy of the Randles–Ševčík equation. For this purpose, the surface concentrations in equation 5.6 are replaced by their respective convolution integral expressions. These were defined by equations 3.84 and 3.85 for a planar electrode in a semi-infinite diffusion domain or more general by equations 3.103 and 3.104 for an electrode of arbitrary geometry in an arbitrary diffusion domain. Following this strategy, a modified version of the master equation which was given by equation 3.105 is obtained. This new expression incorporates the information on the finite heterogeneous electron transfer kinetics and can be stated as

$$I(i\Delta t) \approx \frac{\mathfrak{f}_{\mathrm{an}}(i\Delta t)\left[nFAc_{\mathrm{R,B}}\sqrt{D_{\mathrm{R}}} - \mathfrak{S}_{\mathrm{R}}\right] - \mathfrak{f}_{\mathrm{ca}}(i\Delta t)\sqrt{\frac{D_{\mathrm{R}}}{D_{\mathrm{O}}}}\mathrm{e}^{-\xi(i\Delta t)}\mathfrak{S}_{\mathrm{O}}}{\frac{\sqrt{D_{\mathrm{R}}}\,\mathrm{e}^{-\alpha\xi(i\Delta t)}}{k^0} + \mathfrak{f}_{\mathrm{an}}(i\Delta t)\,M_{\mathrm{R}}(\Delta t) + \mathfrak{f}_{\mathrm{ca}}(i\Delta t)\,M_{\mathrm{O}}(\Delta t)\sqrt{\frac{D_{\mathrm{R}}}{D_{\mathrm{O}}}}\mathrm{e}^{-\xi(i\Delta t)}}. \tag{5.8}$$

Again, $\mathfrak{S}_{\mathrm{R}}$ and $\mathfrak{S}_{\mathrm{O}}$ denote the convolution of lists of the reduced and oxidized species as defined by equations 3.106 and 3.107. The only difference to equation 3.105 remains in the $\mathfrak{f}_{\mathrm{an}}(i\Delta t)$ and $\mathfrak{f}_{\mathrm{ca}}(i\Delta t)$ terms which are defined by

$$\mathfrak{f}_{\mathrm{an}}(i\Delta t) = \frac{k_{\max}}{k_{\max} + k^0\,\mathrm{e}^{\alpha\xi(i\Delta t)}} \tag{5.9}$$

and

$$\mathfrak{f}_{\mathrm{ca}}(i\Delta t) = \frac{k_{\max}}{k_{\max} + k^0\,\mathrm{e}^{-(1-\alpha)\xi(i\Delta t)}}. \tag{5.10}$$

[3]This derivation is not included here, since this thesis emphasizes the diffusion phenomena in stagnant electrolyte solutions. Nevertheless, the three-term Koutecký–Levich equation has been included here, since it gave rise to the concept of finite kinetics.

A detailed derivation was omitted here since it will be analog to the strategy outlined in the theoretical fundamentals of chapter 3 section 3.5. However, it should be noted that equation 5.8 reduces to equation 3.105, if $k_{\max} \to \infty$. For this reason, equation 5.8 can be regarded as a generalized version of equation 3.105 which accounts for electron transfer kinetics at any degree of limitation.

Since computing CV/LSV on the base of equation 5.8 and evaluating the respective simulated data in terms of the classical Randles-Ševčík relation reproduces the experimentally observed mismatch in the electron transfer coefficient, equation 5.8 can be regarded as the closing validation of the concept of finite electron transfer kinetics. Hence, by carefully reconsidering all the previous results it was found that the electrochemical oxidation of the oxovanadyl-cation at glassy carbon surfaces possesses an electron transfer coefficient of $\alpha = 0.38$, a standard heterogeneous rate constant of $k^0 = 1.35 \times 10^{-5}$cm/s and a maximum heterogeneous rate constant of $k_{\max} = 2.60 \times 10^{-2}$cm/s.

Finally, by regarding equation 5.8 the exceptional power of convolutive modeling in the context of electrochemistry emerges once more. This implies that convolutive modeling is capable to incorporate an entirely new concept of electrode kinetics, by introducing two factors at very specific positions in the respective master equation. Ultimately, the values for D, k^0, α and $k_{\max}$ together with the generalized master equation 5.8 can be regarded as a reference for all the following studies which are dedicated to the electrochemcial oxidation of VO^{2+} at porous electrodes and therefore close this sub-chapter.

5.2 Quantifying Parasitic Reactions

The second publication related to this cumulative thesis, which is entitled

'Rotating Ring-Disc Electrode Measurements for the Quantitative Electrokinetic Investigation of the V^{3+}-Reduction at Modified Carbon Electrodes'

is dedicated to an in depth investigation of the negative VRFB half cell reaction at well-defined model electrodes in order to generate a reference for following studies involving porous electrode structures. Well-defined model electrodes imply that the issue of electrode porosity is avoided experimentally by utilizing planar electrodes in a semi-infinite diffusion domain. The particular use of a rotating ring-disc electrode allowed for a separation of the desired electrochemical reduction of V^{3+} and the parasitic hydrogen evolution. In this manner, an accurate value for the diffusion coefficient of the V^{3+} cation was obtained for the very first time. With the konwledge of this particular quantity, CV simulations were performed in order to fit experimentally acquired data. This allowed for a quantitative interpretation of the electrode kinetics of the desired and parasitic electrochemical reactions simultaneously. Furthermore, selected examples of the *'carbon activation methods'* which are proposed in the literature and which are typically conducted in porous electrodes only, were thoroughly revisited under well-defined diffusion conditions. This revealed that only one out of four of these methods really enhanced the electrode kinetics. Finally, it could be shown that the reduction rate of V^{3+} has an optimum at $E - E_{\mathrm{RHE}} = -0.45$ V and decreases when the electrode potential is swept more negative. Since electrode potentials below $E - E_{\mathrm{RHE}} = -0.6$ V are detrimental to the electrode kinetics, the results of this study are of utmost experimental relevance.

Motivation

The main motivation for the work presented in this section emerged from the model of finite heterogeneous electron transfer kinetics which was introduced in the previous section. Since in this case the finite reaction rate has led to an underestimation of the electron transfer coefficient, α, due to a lowered peak current in a Randles–Ševčík analysis, the opposite trend was expected here. This presumption was based on the fact that the negative VRFB reaction is always accompanied by a parasitic hydrogen evolution which contributes to the Faradaic current. For this reason the measured current will always be larger than the actual pure V^{3+} reduction current which renders a classical estimation of α, k^0

and D impossible. Consequently, the aim of this study was to first separate parasitic and desired electrochemical reactions and to subsequently characterize them individually. For this purpose, the rotating ring-disc electrode (RRDE) technique was first ever employed in the context of VRFB research. Furthermore, two additional advanced electroanalytical techniques, namely electrochemical impedance spectroscopy in combination with the distribution of relaxation times (DRT) analysis and Fourier transform alternating current cyclic voltammetry (FT-ACCV) have been applied. In this manner it was possible to clearly distinguish between parasitic and desired current contributions.

The implementation and fundamentals of the RRDE technique will be outlined in brief next. In contrast, a description of EIS/DRT and FT-ACCV is not included as it would be out of the scope of this thesis. Since these two techniques served, however, as an additional support of the RRDE data, the reader is referred to the original publication attached in section 6.2 for further details.

The RRDE technique

The method of the rotating ring-disc electrode can be thought of as a modification of a classical rotating disc electrode which has been introduced and schematically depicted in the theory section (cf figure 3.1).

A RRDE basically consists of a ring-shaped electrode surrounding the disc of a classical RDE (cf figure 5.1). Disc and ring electrode are thereby separated by an electrically insulating gap and can be subjected to a different potential program each. The device which controls the time dependent potential of disc and ring simultaneously is known as bipotentiostat. An RRDE allows for re-oxidizing or re-reducing the product species which is formed during the reaction at the disc, at the ring. In case the desired reaction which occurs at the disc is accompanied by a parasitic reaction, the RRDE enables that the rate of product formation can be investigated selectively by deliberately detecting one species which passes the ring. In the present study, the RRDE was used in a way that the V^{2+} produced at the disc electrode gets re-oxidized at the ring. In contrast, any hydrogen which is evolved as the product of a parasitic reaction at the disc is not detected at the ring. Consequently, the ring current can be regarded as the quantity related to the desired vanadium reaction and allows for calculating the related diffusion coefficient to high accuracy.

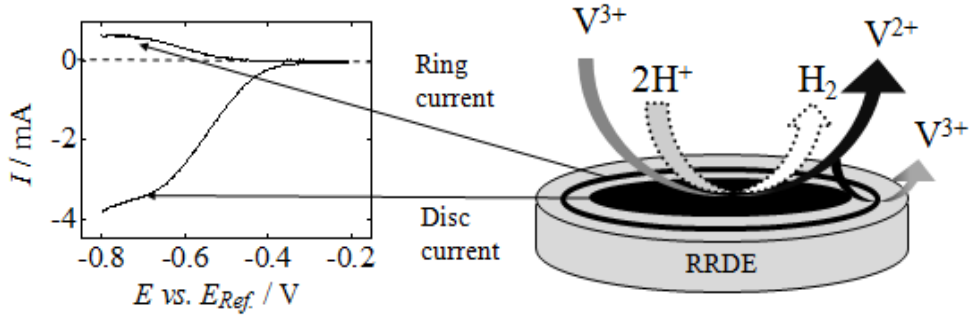

Figure 5.1: Sketch of a rotating ring-disc electrode utilized for separating the desired reduction of V^{3+} from the parasitic hydrogen evolution which occur in parallel at the disc electrode. V^{2+} which is produced at the disc gets re-oxidized at the ring electrode. This enforces a ring-current which is related to vanadium species only.

Results and discussion

Three common methods of carbon surface activation were investigated throughout this study. These fall under the category of chemical etching techniques and involve I) alkaline etching (with concentrated KOH), II) acidic etching (with H_2SO_4/HNO_3) and III) surface oxidation (with H_2O_2). All surface modifications were performed at standard vulcan XC72 carbon. Pristine vulcan XC72 carbon served as reference material. For experimental details the reader is referred to the original publication in the section 6.2 of this thesis.

By thoroughly investigating the ring currents of the RRDE experiments, the diffusion coefficient of the V^{3+}-cation was obtained as $D = 3.51 \times 10^{-6} \pm 0.22\,\mathrm{cm}^2/\mathrm{s}$. Since the ring current excludes all contributions from a parasitic hydrogen evolution, the respective D can be regarded as a highly accurate reference value. Consequently, it was utilized in a fitting routine of experimentally acquired CV responses. The actual CV fitting process was performed manually by minimizing the standard deviation of experimentally acquired to simulated data. The respective CV simulations were performed on the base of equation 5.8. However, since it was set $k_{\max} = 1000$ cm/s, also equations 3.90 or 3.105 could have been employed. This is indeed an important remark, since it suggests that the negative VRFB reaction does not obey a kinetic limitation like its positive analogon. The parasitic hydrogen evolution was considered as a parallel reaction which is independent of any vanadium redox process. Consequently, the related current was also calculated on the base of equations 3.90 or 3.105. Since fitting the CV responses will therefore account for both, desired and undesired reactions, it will provide the respective

kinetic information simultaneously. The thus obtained kinetic data is summarized for the carbon materials investigated in this study in table 5.3. It can be seen that among the chemical surface modification techniques, only an etching with hydrogen peroxide led to a minor enhancement of the V^{3+}/V^{2+} redox kinetics. In contrast, the rate of the hydrogen evolution was changed significantly by up to three orders of magnitude. Furthermore, it is worth to note that an acidic etching with H_2SO_4/HNO_3 significantly decreases the electrode activity for both, desired and parasitic reactions, which contradicts the findings in the literature. The highest selectivity for the desired vanadium reaction was offered by the pristine carbon material.

Table 5.3: Kinetic data in terms of α and k^0 obtained for the surface modified carbon electrodes investigated in this study.

	Vanadium reaction		Hydrogen evolution	
	α	$k^0/\mathrm{cm\,s^{-1}}$	α	$k^0/\mathrm{cm\,s^{-1}}$
Pristine XC72	0.54	9.0×10^{-4}	0.36	9.0×10^{-10}
H_2SO_4/HNO_3 XC72	0.55	3.5×10^{-5}	0.31	3.1×10^{-9}
KOH XC72	0.52	6.0×10^{-4}	0.28	2.3×10^{-8}
H_2O_2 XC72	0.51	1.0×10^{-3}	0.32	3.6×10^{-9}

The final conclusion of this study was therefore that the common surface modification techniques — typically performed at porous electrodes — do not enhance the catalytic activity for the negative VRFB reaction at all. In contrast, it is much more likely that the observed enhancement effect is caused by an increased hydrogen evolution rate or an increased wettability of the porous electrodes which leads to a lowered total charge transfer resistance.

Now, bearing in mind the more decent model of electrode kinetics which was introduced in section 5.1, as well as the remarks on the diffusion coefficients and electrode kinetics of the positive and negative VRFB reactions, the experimental reference for the following three publications related to cyclic voltammetry at porous electrodes is finally established.

5.3 The Diffusion Domain Approximation for Felt Electrodes

The first study on the theory of cyclic voltammetry at porous electrodes which is related to this thesis is entitled

'Theory of Cyclic Voltammetry in Random Arrays of Cylindrical Microelectrodes Applied to Carbon Felt Electrodes for Vanadium Redox-Flow Batteries'.

In this publication the carbon felt electrodes, typically employed in a VRFB are regarded as an array of cylindrical microelectrodes in a finite external cylindrical diffusion domain with a statistically fluctuating size. This publication was the very first combined experimental and theoretical study on cyclic voltammetry at carbon felt electrodes which accounts for the cylindrical symmetry of the fibers of a felt electrode. Furthermore, it was the first publication on the simulation of cyclic voltammetry at cylindrical electrodes in a finite external cylindrical diffusion domain on the base of convolutive modeling in general. It was shown that the novel theoretical concept can be exploited readily for a simultaneous evaluation of electrode kinetics and pore size distribution of carbon felt electrodes. In this manner, the inherent ambiguity of CV at porous electrodes was finally overcome.

Motivation

The motivation of this particular publication emerged from the plethora of studies on cyclic voltammetry at porous carbon felt electrodes in the context of VRFB research and the contradictive findings on the electrode kinetics. It was intended to create a reliable strategy for the interpretation of CV data, even in case of porous electrodes. Furthermore, it was assumed that a decent diffusion model should allow for a simultaneous investigation of electrode kinetics and electrode porosity. Despite that some publications which attempted to include the effect of electrode porosity by considering arrays of electrode sheets [67] or hollow-spherical electrodes [66], a sophisticated theoretical model for felt electrodes was not accessible a priori. In order to create a respective diffusion model the fibers of a carbon felt were assumed as cylindrical microelectrodes in a finite external cylindrical diffusion domain with a statistically fluctuating size. The entire felt electrode was in turn regarded as an array of these individual sub-structures. To account for an even broader range of experimental circumstances it was considered that the electrochemical reaction might be coupled to preceeding and following homogeneous chemical equilibria. In order to benefit from the master-equation approach outlined in the theory

section (section 3.5 equation 3.105), the simulations of the CV responses of the individual cylindrical microelectrodes have been performed on the base of Laplace integral transformation techniques and convolutive modeling. Since the respective Laplace-domain solution for the mass transfer function does, however, not possess an analytic inversion, the concept of numerical inverse Laplace transformation was exploited. This idea was first ever introduced in the context of electrochemistry in a series of publications by Montella [120]–[122] who suggested the use of the Gaver–Stehfest [123] inversion formula. Alternatively, in this work, a modified Talbot-contour was first ever utilized for electrochemical simulations. Adopting the idea of reference [124], a strategy for evaluating cyclic voltammetry at carbon felt electrodes was presented. This routine is based on a manual fitting routine of experimentally acquired CV data for the positive VRFB half cell reaction.

The mass transfer function of a cylindrical external finite diffusion domain coupled to homogeneous kinetics

The considerable challenges of convolutive modeling related to this publication were a) to compute the time-dependent mass transfer functions related to an external cylindrical finite diffusion domain and b) to include the preceding and following homogeneous chemical reactions. Since this exceptionally lengthy derivation could not be included in the original publication[4], but is, however, one of the major highlights of this thesis it will be included in its whole beauty here. The pre-processing step in this derivation is roughly oriented on the idea of Koutecký and Brdička [125] and starts with the following sequence of reactions

$$E \underset{k_{-\mathrm{p}}}{\overset{k_{\mathrm{p}}}{\rightleftharpoons}} R \tag{5.11}$$

$$R \underset{+ne^-}{\overset{-ne^-}{\rightleftharpoons}} O \tag{5.12}$$

$$O \underset{k_{-\mathrm{f}}}{\overset{k_{\mathrm{f}}}{\rightleftharpoons}} P. \tag{5.13}$$

[4]Only the results were given as equations 1 and 2 in the publication — cf chapter 6.

Considering the reactions take place at a cylindrical (micro)electrode, the respective partial differential equations for the species E and R, linked by a preceeding chemical equilibrium can be formulated as follows:

$$\frac{\partial c_{\mathrm{E}}(r,t)}{\partial t} = D_{\mathrm{R}}\left[\frac{\partial^2 c_{\mathrm{E}}(r,t)}{\partial r^2} + \frac{1}{r}\frac{\partial c_{\mathrm{E}}(r,t)}{\partial r}\right] - k_{\mathrm{p}}c_{\mathrm{E}}(r,t) + k_{-\mathrm{p}}c_{\mathrm{R}}(r,t). \tag{5.14}$$

$$\frac{\partial c_{\mathrm{R}}(r,t)}{\partial t} = D_{\mathrm{R}}\left[\frac{\partial^2 c_{\mathrm{R}}(r,t)}{\partial r^2} + \frac{1}{r}\frac{\partial c_{\mathrm{R}}(r,t)}{\partial r}\right] - k_{-\mathrm{p}}c_{\mathrm{R}}(r,t) + k_{\mathrm{p}}c_{\mathrm{E}}(r,t). \tag{5.15}$$

Likewise, the partial differential equations for the species O and P can be stated as:

$$\frac{\partial c_{\mathrm{O}}(r,t)}{\partial t} = D_{\mathrm{O}}\left[\frac{\partial^2 c_{\mathrm{O}}(r,t)}{\partial r^2} + \frac{1}{r}\frac{\partial c_{\mathrm{O}}(r,t)}{\partial r}\right] - k_{\mathrm{f}}c_{\mathrm{O}}(r,t) + k_{-\mathrm{f}}c_{\mathrm{P}}(r,t). \tag{5.16}$$

$$\frac{\partial c_{\mathrm{P}}(r,t)}{\partial t} = D_{\mathrm{O}}\left[\frac{\partial^2 c_{\mathrm{P}}(r,t)}{\partial r^2} + \frac{1}{r}\frac{\partial c_{\mathrm{P}}(r,t)}{\partial r}\right] - k_{-\mathrm{f}}c_{\mathrm{P}}(r,t) + k_{\mathrm{f}}c_{\mathrm{O}}(r,t). \tag{5.17}$$

These four expressions are derived from Ficks second law in one-dimensional cylindrical symmetry, which was given by equation 3.48 in section 3.3. They consider that species E and R have the common diffusion coefficient D_{R} and species O and P have the common diffusion coefficient D_{O}. The next step is to unify the two partial differential equations of the preceeding and following chemical reactions to one combined expression each. This is shown exemplary for the preceding equilibrium.

Pre-processing of the differential equations

Considering the equilibrium constant of the preceeding chemical reaction as

$$K_{\mathrm{p}} = \frac{k_{\mathrm{p}}}{k_{-\mathrm{p}}} = \frac{c_{\mathrm{R}}(r,0)}{c_{\mathrm{E}}(r,0)} = \frac{c_{\mathrm{R,B}}}{c_{\mathrm{E,B}}}, \tag{5.18}$$

one can substitute k_{p} in equations 5.14 and 5.16 such that

$$\frac{\partial c_{\mathrm{E}}(r,t)}{\partial t} = D_{\mathrm{R}}\left[\frac{\partial^2 c_{\mathrm{E}}(r,t)}{\partial r^2} + \frac{1}{r}\frac{\partial c_{\mathrm{E}}(r,t)}{\partial r}\right] + k_{-\mathrm{p}}\left[(c_{\mathrm{R}}(r,t) - K_{\mathrm{p}}c_{\mathrm{E}}(r,t)\right] \tag{5.19}$$

$$\frac{\partial c_{\mathrm{R}}(r,t)}{\partial t} = D_{\mathrm{R}}\left[\frac{\partial^2 c_{\mathrm{R}}(r,t)}{\partial r^2} + \frac{1}{r}\frac{\partial c_{\mathrm{R}}(r,t)}{\partial r}\right] - k_{-\mathrm{p}}\left[(c_{\mathrm{R}}(r,t) - K_{\mathrm{p}}c_{\mathrm{E}}(r,t)\right]. \tag{5.20}$$

Introducing two new variables in a way that

$$\psi_{\mathrm{p}}(r,t) = c_{\mathrm{E}}(r,t) + c_{\mathrm{R}}(r,t) \tag{5.21}$$

and

$$\phi_{\mathrm{p}}(r,t) = c_{\mathrm{R}}(r,t) - K_{\mathrm{p}} c_{\mathrm{E}}(r,t), \tag{5.22}$$

one obtains the following two expressions

$$\frac{\partial c_{\mathrm{E}}(r,t)}{\partial t} = \frac{\partial \psi_{\mathrm{p}}(r,t)}{\partial t} - \frac{\partial c_{\mathrm{R}}(r,t)}{\partial t} \tag{5.23}$$

$$\begin{aligned}\frac{\partial^2 c_{\mathrm{E}}(r,t)}{\partial r^2} + \frac{1}{r}\frac{\partial c_{\mathrm{E}}(r,t)}{\partial r} = \frac{\partial^2 \psi_{\mathrm{p}}(r,t)}{\partial r^2} \\ + \frac{1}{r}\frac{\partial \psi_{\mathrm{p}}(r,t)}{\partial r} - \frac{\partial^2 c_{\mathrm{R}}(r,t)}{\partial r^2} - \frac{1}{r}\frac{\partial c_{\mathrm{R}}(r,t)}{\partial r}.\end{aligned} \tag{5.24}$$

Substituting equation 5.22 into equations 5.19 and 5.20 one arrives at

$$\frac{\partial c_{\mathrm{E}}(r,t)}{\partial t} = D_{\mathrm{R}}\left[\frac{\partial^2 c_{\mathrm{E}}(r,t)}{\partial r^2} + \frac{1}{r}\frac{\partial c_{\mathrm{E}}(r,t)}{\partial r}\right] + k_{-\mathrm{p}}\phi_{\mathrm{p}}(r,t) \tag{5.25}$$

$$\frac{\partial c_{\mathrm{R}}(r,t)}{\partial t} = D_{\mathrm{R}}\left[\frac{\partial^2 c_{\mathrm{R}}(r,t)}{\partial r^2} + \frac{1}{r}\frac{\partial c_{\mathrm{R}}(r,t)}{\partial r}\right] - k_{-\mathrm{p}}\phi_{\mathrm{p}}(r,t). \tag{5.26}$$

Now, eliminating $c_{\mathrm{E}}(r,t)$ in equation 5.25 by substituting equations 5.23 and 5.24 gives

$$\begin{aligned}\frac{\partial \psi_{\mathrm{p}}(r,t)}{\partial t} - \frac{\partial c_{\mathrm{R}}(r,t)}{\partial t} = D_{\mathrm{R}}\Bigg[\frac{\partial^2 \psi_{\mathrm{p}}(r,t)}{\partial r^2} \\ + \frac{1}{r}\frac{\partial \psi_{\mathrm{p}}(r,t)}{\partial r} - \frac{\partial^2 c_{\mathrm{R}}(r,t)}{\partial r^2} - \frac{1}{r}\frac{\partial c_{\mathrm{R}}(r,t)}{\partial r}\Bigg] + k_{-\mathrm{p}}\phi_{\mathrm{p}}(r,t).\end{aligned} \tag{5.27}$$

This expression is rearranged once more which yields

$$\begin{aligned}\frac{\partial \psi_{\mathrm{p}}(r,t)}{\partial t} = D_{\mathrm{R}}\left[\frac{\partial^2 \psi_{\mathrm{p}}(r,t)}{\partial r^2} + \frac{1}{r}\frac{\partial \psi_{\mathrm{p}}(r,t)}{\partial r}\right] + k_{-\mathrm{p}}\phi_{\mathrm{p}}(r,t) \\ + \frac{\partial c_{\mathrm{R}}(r,t)}{\partial t} - D_{\mathrm{R}}\left[\frac{\partial^2 c_{\mathrm{R}}(r,t)}{\partial r^2} + \frac{1}{r}\frac{\partial c_{\mathrm{R}}(r,t)}{\partial r}\right].\end{aligned} \tag{5.28}$$

It is now readily seen that a substitution of the second line of equation 5.28 with equation 5.26 will result in the very handy expression of

$$\frac{\partial \psi_{\mathrm{p}}(r,t)}{\partial t} = D_{\mathrm{R}}\left[\frac{\partial^2 \psi_{\mathrm{p}}(r,t)}{\partial r^2} + \frac{1}{r}\frac{\partial \psi_{\mathrm{p}}(r,t)}{\partial r}\right]. \tag{5.29}$$

Equation 5.29 is almost identical to equation 3.48 in the theory section (it is written in terms of the variable $\psi_{\mathrm{p}}(r,t)$ only). The next step is to generate a similar expression in terms of the variable $\phi_{\mathrm{p}}(r,t)$ as well. Starting with equation 5.22 one can note that

$$\frac{\partial c_{\mathrm{R}}(r,t)}{\partial t} = \frac{\partial \phi_{\mathrm{p}}(r,t)}{\partial t} + K_{\mathrm{p}}\frac{\partial c_{\mathrm{E}}(r,t)}{\partial t} \tag{5.30}$$

and

$$\frac{\partial^2 c_{\mathrm{R}}(r,t)}{\partial r^2} + \frac{1}{r}\frac{\partial c_{\mathrm{R}}(r,t)}{\partial r} = \frac{\partial^2 \phi_{\mathrm{p}}(r,t)}{\partial r^2} + \frac{1}{r}\frac{\partial \phi_{\mathrm{p}}(r,t)}{\partial r} + K_{\mathrm{p}}\left\{\frac{\partial^2 c_{\mathrm{E}}(r,t)}{\partial r^2} + \frac{1}{r}\frac{\partial c_{\mathrm{E}}(r,t)}{\partial r}\right\}. \tag{5.31}$$

Inserting these two expressions in equation 5.26 results in

$$\frac{\partial \phi_{\mathrm{p}}(r,t)}{\partial t} + K_{\mathrm{p}}\frac{\partial c_{\mathrm{E}}(r,t)}{\partial t} = D_{\mathrm{R}}\left[\frac{\partial^2 \phi_{\mathrm{p}}(r,t)}{\partial r^2} + \frac{1}{r}\frac{\partial \phi_{\mathrm{p}}(r,t)}{\partial r} + K_{\mathrm{p}}\left\{\frac{\partial^2 c_{\mathrm{E}}(r,t)}{\partial r^2} + \frac{1}{r}\frac{\partial c_{\mathrm{E}}(r,t)}{\partial r}\right\}\right] - k_{-\mathrm{p}}\phi_{\mathrm{p}}(r,t) \tag{5.32}$$

Collecting all terms which contain $c_{\mathrm{E}}(r,t)$ on the right hand side of equation 5.32 and substituting with equation 5.25 results in

$$\frac{\partial \phi_{\mathrm{p}}(r,t)}{\partial t} = D_{\mathrm{R}}\left[\frac{\partial^2 \phi_{\mathrm{p}}(r,t)}{\partial r^2} + \frac{1}{r}\frac{\partial \phi_{\mathrm{p}}(r,t)}{\partial r}\right] - (K_{\mathrm{p}}k_{-\mathrm{p}} + k_{-\mathrm{p}})\phi_{\mathrm{p}}(r,t). \tag{5.33}$$

This equation can be simplified even further by the definition given in equation 5.18. Introducing another variable p as apparent rate constant of the preceding homogeneous chemical equilibrium as $p = k_{\mathrm{p}} + k_{-\mathrm{p}}$, one finally obtains

$$\frac{\partial \phi_{\mathrm{p}}(r,t)}{\partial t} = D_{\mathrm{R}}\left[\frac{\partial^2 \phi_{\mathrm{p}}(r,t)}{\partial r^2} + \frac{1}{r}\frac{\partial \phi_{\mathrm{p}}(r,t)}{\partial r}\right] - p\phi_{\mathrm{p}}(r,t). \tag{5.34}$$

Solution via Laplace transformation

Equations 5.29 and 5.34 are solved right now by means of Laplace integral transformation techniques. Applying the Laplace transformation to equations 5.29 and 5.34 as outlined in the theory section results in

$$\bar{\psi_{\mathrm{p}}}(r,s) = \frac{D_{\mathrm{R}}}{s}\left[\frac{\partial^2\bar{\psi_{\mathrm{p}}}(r,s)}{\partial r^2} + \frac{1}{r}\frac{\partial\bar{\psi_{\mathrm{p}}}(r,s)}{\partial r}\right] + \frac{\psi_{\mathrm{p}}^*}{s} \tag{5.35}$$

and

$$\bar{\phi_{\mathrm{p}}}(r,s+p) = \frac{D_{\mathrm{R}}}{s+p}\left[\frac{\partial^2\bar{\phi_{\mathrm{p}}}(r,s+p)}{\partial r^2} + \frac{1}{r}\frac{\partial\bar{\phi_{\mathrm{p}}}(r,s+p)}{\partial r}\right] + \frac{\phi_{\mathrm{p}}^*}{s+p}, \tag{5.36}$$

where the property of the Laplace transformation given in equation 3.61 in the theory section was utilized in equation 5.36. Furthermore, it was introduced $\psi_{\mathrm{p}}^* = \psi_{\mathrm{p}}(r,0) = c_{\mathrm{R,B}} + c_{\mathrm{E,B}}$ and $\phi_{\mathrm{p}}^* = \phi_{\mathrm{p}}(r,0) = c_{\mathrm{R,B}} - K_{\mathrm{p}}c_{\mathrm{E,B}}$. The general solutions of equations 5.35 and 5.36 are given in terms of modified Bessel functions of the first and of the second kind and of order zero which are denoted as $\mathcal{I}_0$ and $\mathcal{K}_0$, respectively. By recognizing that $\phi_{\mathrm{p}}^* = 0$ and $\psi_{\mathrm{p}}^* = c_{\mathrm{tot}}$[5] these solutions can be stated as

$$\bar{\psi_{\mathrm{p}}}(r,s) = C_{\psi,+}\mathcal{I}_0\left(r\sqrt{\frac{s}{D_{\mathrm{R}}}}\right) + C_{\psi,-}\mathcal{K}_0\left(r\sqrt{\frac{s}{D_{\mathrm{R}}}}\right) + \frac{c_{\mathrm{tot}}}{s} \tag{5.37}$$

and

$$\bar{\phi_{\mathrm{p}}}(r,s) = C_{\phi,+}\mathcal{I}_0\left(r\sqrt{\frac{s+p}{D_{\mathrm{R}}}}\right) + C_{\phi,-}\mathcal{K}_0\left(r\sqrt{\frac{s+p}{D_{\mathrm{R}}}}\right). \tag{5.38}$$

The next step is to perform a Laplace transformation on equations 5.21 and 5.22 which yields

$$\bar{\psi_{\mathrm{p}}}(r,s) = \bar{c}_{\mathrm{E}}(r,s) + \bar{c}_{\mathrm{R}}(r,s) \tag{5.39}$$

and

$$\bar{\phi_{\mathrm{p}}}(r,s+p) = \bar{c}_{\mathrm{R}}(r,s+p) - K_{\mathrm{p}}\bar{c}_{\mathrm{E}}(r,s+p). \tag{5.40}$$

[5]Caution, $\psi_{\mathrm{p}}^* = c_{\mathrm{tot}}$ is a valid assumption if only species E and R are initially present in the electrolyte. Then, c_{tot} denotes the total concentration of the analyte.

By combining equations 5.39 and 5.40 one can obtain the Laplace transformed concentration of the reduced species as

$$\bar{c}_{\mathrm{R}}(r,s) = \frac{K_{\mathrm{p}}\bar{\psi}_{\mathrm{p}}(r,s) + \bar{\phi}_{\mathrm{p}}(r,s+p)}{1+K_{\mathrm{p}}}. \tag{5.41}$$

In order to use equation 5.41, the functions $\bar{\psi}_{\mathrm{p}}(r,s)$ and $\bar{\phi}_{\mathrm{p}}(r,s+p)$ need to be determined next. This follows from the symmetry of the finite external cylindrical diffusion domain which is depicted in figure 5.2. In order to obtain $\bar{\psi}_{\mathrm{p}}(r,s)$, the constants $C_{\psi,+}$ and $C_{\psi,-}$ need to be calculated. This is performed similar to the procedure outlined in section 3.5. The spatial derivative of $\bar{\psi}_{\mathrm{p}}(r,s)$, evaluated at the electrode surface ($r=a$) can be stated as

$$\left.\frac{\partial\bar{\psi}_{\mathrm{p}}(r,s)}{\partial r}\right|_{r=a} = \left.\frac{\partial\bar{c}_{\mathrm{R}}(r,s)}{\partial r}\right|_{r=a} + \left.\frac{\partial\bar{c}_{\mathrm{E}}(r,s)}{\partial r}\right|_{r=a}. \tag{5.42}$$

Since species E is not directly consumed at the electrode surface, a no-flux boundary can be assumed. Consequently, it holds

$$\left.\frac{\partial\bar{c}_{\mathrm{E}}(r,s)}{\partial r}\right|_{r=a} = 0. \tag{5.43}$$

Therefore, equation 5.42 reduces to

$$\left.\frac{\partial\bar{\psi}_{\mathrm{p}}(r,s)}{\partial r}\right|_{r=a} = \left.\frac{\partial\bar{c}_{\mathrm{R}}(r,s)}{\partial r}\right|_{r=a} = \frac{\bar{I}(s)}{nFAD_{\mathrm{R}}}. \tag{5.44}$$

Performing the spatial derivative on equation 5.37 and rearranging the result yields

$$\frac{\bar{I}(s)}{nFA\sqrt{sD_{\mathrm{R}}}} = C_{\psi,+}\mathcal{I}_1\left(a\sqrt{\frac{s}{D_{\mathrm{R}}}}\right) - C_{\psi,-}\mathcal{K}_1\left(a\sqrt{\frac{s}{D_{\mathrm{R}}}}\right), \tag{5.45}$$

where $\mathcal{I}_1$ and $\mathcal{K}_1$ are first order modified Bessel functions of the first and of the second kind. Now, considering a no-flux boundary for both species E and R at $r = a+d = u$, which follows from the definition of an impermeable wall surrounding the cylindrical electrode one can also state that

$$\left.\frac{\partial\bar{\psi}_{\mathrm{p}}(r,s)}{\partial r}\right|_{r=u} = 0. \tag{5.46}$$

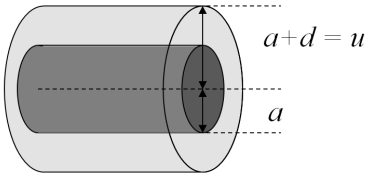

Figure 5.2: Sketch of a finite external cylindrical diffusion domain. The electrode surface is located at $r = a$, whereas the impermeable outer boundary is located at $r = d$.

It immediately follows that

$$C_{\psi,+}\mathcal{I}_1\left(u\sqrt{\frac{s}{D_\mathrm{R}}}\right) - C_{\psi,-}\mathcal{K}_1\left(u\sqrt{\frac{s}{D_\mathrm{R}}}\right) = 0. \tag{5.47}$$

By substituting equation 5.47 into equation 5.45, the constants $C_{\psi,+}$ and $C_{\psi,-}$ are obtained as

$$C_{\psi,+} = \frac{\bar{I}(s)}{nFA\sqrt{D_\mathrm{R}}}\frac{1}{\sqrt{s}}\times \left[\frac{\mathcal{K}_1\left(u\sqrt{\frac{s}{D_\mathrm{R}}}\right)}{\mathcal{K}_1\left(u\sqrt{\frac{s}{D_\mathrm{R}}}\right)\mathcal{I}_1\left(a\sqrt{\frac{s}{D_\mathrm{R}}}\right) - \mathcal{K}_1\left(a\sqrt{\frac{s}{D_\mathrm{R}}}\right)\mathcal{I}_1\left(u\sqrt{\frac{s}{D_\mathrm{R}}}\right)}\right] \tag{5.48}$$

$$C_{\psi,-} = \frac{\bar{I}(s)}{nFA\sqrt{D_\mathrm{R}}}\frac{1}{\sqrt{s}}\times \left[\frac{\mathcal{I}_1\left(u\sqrt{\frac{s}{D_\mathrm{R}}}\right)}{\mathcal{K}_1\left(u\sqrt{\frac{s}{D_\mathrm{R}}}\right)\mathcal{I}_1\left(a\sqrt{\frac{s}{D_\mathrm{R}}}\right) - \mathcal{K}_1\left(a\sqrt{\frac{s}{D_\mathrm{R}}}\right)\mathcal{I}_1\left(u\sqrt{\frac{s}{D_\mathrm{R}}}\right)}\right]. \tag{5.49}$$

These can be substituted readily into equation 5.37 to provide the function $\bar{\psi}_{\mathrm{p}}(r,s)$ as

$$\bar{\psi}_{\mathrm{p}}(r,s) = \frac{c_{\mathrm{tot}}}{s} - \frac{\bar{I}(s)}{nFA\sqrt{D_{\mathrm{R}}}}\frac{1}{\sqrt{s}}\times \left[\frac{\mathcal{K}_1\left(u\sqrt{\frac{s}{D_{\mathrm{R}}}}\right)\mathcal{I}_0\left(r\sqrt{\frac{s}{D_{\mathrm{R}}}}\right) + \mathcal{I}_1\left(u\sqrt{\frac{s}{D_{\mathrm{R}}}}\right)\mathcal{K}_0\left(r\sqrt{\frac{s}{D_{\mathrm{R}}}}\right)}{\mathcal{K}_1\left(a\sqrt{\frac{s}{D_{\mathrm{R}}}}\right)\mathcal{I}_1\left(u\sqrt{\frac{s}{D_{\mathrm{R}}}}\right) - \mathcal{K}_1\left(u\sqrt{\frac{s}{D_{\mathrm{R}}}}\right)\mathcal{I}_1\left(a\sqrt{\frac{s}{D_{\mathrm{R}}}}\right)}\right]. \quad (5.50)$$

The next step is to determine the function $\bar{\phi}_{\mathrm{p}}(r,s)$. Subsequently to starting with

$$\left.\frac{\partial\bar{\phi}_{\mathrm{p}}(r,s)}{\partial r}\right|_{r=a} = \left.\frac{\partial\bar{c}_{\mathrm{R}}(r,s)}{\partial r}\right|_{r=a} - K_{\mathrm{p}}\left.\frac{\partial\bar{c}_{\mathrm{E}}(r,s)}{\partial r}\right|_{r=a} = \frac{\bar{I}(s)}{nFAD_{\mathrm{R}}}. \quad (5.51)$$

and

$$\left.\frac{\partial\bar{\phi}_{\mathrm{p}}(r,s)}{\partial r}\right|_{r=u} = 0 \quad (5.52)$$

the derivation follows the exact same way like the derivation of $\bar{\psi}_{\mathrm{p}}(r,s)$, i.e determining the constants $C_{\phi,+}$ and $C_{\phi,-}$ and substituting them back into equation 5.38. Doing so, one arrives at

$$\bar{\phi}_{\mathrm{p}}(r,s) = -\frac{\bar{I}(s)}{nFA\sqrt{D_{\mathrm{R}}}}\frac{1}{\sqrt{s+p}}\times \left[\frac{\mathcal{K}_1\left(u\sqrt{\frac{s+p}{D_{\mathrm{R}}}}\right)\mathcal{I}_0\left(r\sqrt{\frac{s+p}{D_{\mathrm{R}}}}\right) + \mathcal{I}_1\left(u\sqrt{\frac{s+p}{D_{\mathrm{R}}}}\right)\mathcal{K}_0\left(r\sqrt{\frac{s+p}{D_{\mathrm{R}}}}\right)}{\mathcal{K}_1\left(a\sqrt{\frac{s+p}{D_{\mathrm{R}}}}\right)\mathcal{I}_1\left(u\sqrt{\frac{s+p}{D_{\mathrm{R}}}}\right) - \mathcal{K}_1\left(u\sqrt{\frac{s+p}{D_{\mathrm{R}}}}\right)\mathcal{I}_1\left(a\sqrt{\frac{s+p}{D_{\mathrm{R}}}}\right)}\right]. \quad (5.53)$$

Finally, substituting equations 5.50 and 5.53 into equation 5.41, and evaluating the resulting expression at $r = a$ provides the Laplace transformed surface concentration of the reduced species according to

$$\bar{c}_{\mathrm{R,S}} = \bar{c}_{\mathrm{R}}(a,s) = \frac{c_{\mathrm{tot}} K_{\mathrm{p}}}{s(1+K_{\mathrm{p}})} - \frac{K_{\mathrm{p}}}{(1+K_{\mathrm{p}})nFA\sqrt{D_{\mathrm{R}}}} \frac{\bar{I}(s)}{\sqrt{s}} \times$$

$$\left[\frac{\mathcal{K}_1\left(u\sqrt{\frac{s}{D_{\mathrm{R}}}}\right)\mathcal{I}_0\left(a\sqrt{\frac{s}{D_{\mathrm{R}}}}\right) + \mathcal{I}_1\left(u\sqrt{\frac{s}{D_{\mathrm{R}}}}\right)\mathcal{K}_0\left(a\sqrt{\frac{s}{D_{\mathrm{R}}}}\right)}{\mathcal{K}_1\left(a\sqrt{\frac{s}{D_{\mathrm{R}}}}\right)\mathcal{I}_1\left(u\sqrt{\frac{s}{D_{\mathrm{R}}}}\right) - \mathcal{K}_1\left(u\sqrt{\frac{s}{D_{\mathrm{R}}}}\right)\mathcal{I}_1\left(a\sqrt{\frac{s}{D_{\mathrm{R}}}}\right)} \right]$$

$$- \frac{1}{(1+K_{\mathrm{p}})nFA\sqrt{D_{\mathrm{R}}}} \frac{\bar{I}(s)}{\sqrt{s+p}} \times$$

$$\left[\frac{\mathcal{K}_1\left(u\sqrt{\frac{s+p}{D_{\mathrm{R}}}}\right)\mathcal{I}_0\left(a\sqrt{\frac{s+p}{D_{\mathrm{R}}}}\right) + \mathcal{I}_1\left(u\sqrt{\frac{s+p}{D_{\mathrm{R}}}}\right)\mathcal{K}_0\left(a\sqrt{\frac{s+p}{D_{\mathrm{R}}}}\right)}{\mathcal{K}_1\left(a\sqrt{\frac{s+p}{D_{\mathrm{R}}}}\right)\mathcal{I}_1\left(u\sqrt{\frac{s+p}{D_{\mathrm{R}}}}\right) - \mathcal{K}_1\left(u\sqrt{\frac{s+p}{D_{\mathrm{R}}}}\right)\mathcal{I}_1\left(a\sqrt{\frac{s+p}{D_{\mathrm{R}}}}\right)} \right], \quad (5.54)$$

which is identical to equation 1 in the original publication. Following an analogue derivation of equations 5.18 to 5.54, the surface concentration of the oxidized species could be obtained as well. However, there is a much more decent way by comparing the equilibrium term (the "$s+p$"-term in equation 5.54). Considering a preceeding equilibrium which lies entirely on the side of species R, the equilibrium constant K_{p} will become large. Therefore, the "$s+p$"-term in equation 5.54 will approach zero due to the factor of $1/(1+K_{\mathrm{p}})$. In contrast, the $K_{\mathrm{p}}/(1+K_{\mathrm{p}})$-term will approach one. The resulting expression corresponds therefore to the scenario without a preceeding equilibrium.

Now, considering the apparent rate constant of a following chemical equilibrium as $f = k_{\mathrm{f}} + k_{-\mathrm{f}}$ and the respective equilibrium constant as $K_{\mathrm{f}} = k_{\mathrm{f}}/k_{-\mathrm{f}}$ as introduced in equation 5.13, one can recognize that K_{f} will be very small in case of an equilibrium located at the side of species O. Consequently, the respective equilibrium terms of the oxidized species have to be paired in the opposite way, when compared to the reduced species. Thus, it directly follows that the Laplace transformed surface concentration of the oxidized species is given by

$$\bar{c}_{\mathrm{O,S}} = \bar{c}_{\mathrm{O}}(a,s) = \frac{1}{(1+K_{\mathrm{f}})nFA\sqrt{D_{\mathrm{O}}}}\frac{\bar{I}(s)}{\sqrt{s}}\times$$

$$\left[\frac{\mathcal{K}_1\left(u\sqrt{\frac{s}{D_{\mathrm{O}}}}\right)\mathcal{I}_0\left(a\sqrt{\frac{s}{D_{\mathrm{O}}}}\right)+\mathcal{I}_1\left(u\sqrt{\frac{s}{D_{\mathrm{O}}}}\right)\mathcal{K}_0\left(a\sqrt{\frac{s}{D_{\mathrm{O}}}}\right)}{\mathcal{K}_1\left(a\sqrt{\frac{s}{D_{\mathrm{O}}}}\right)\mathcal{I}_1\left(u\sqrt{\frac{s}{D_{\mathrm{O}}}}\right)-\mathcal{K}_1\left(u\sqrt{\frac{s}{D_{\mathrm{O}}}}\right)\mathcal{I}_1\left(a\sqrt{\frac{s}{D_{\mathrm{O}}}}\right)}\right]$$

$$+\frac{K_{\mathrm{f}}}{(1+K_{\mathrm{f}})nFA\sqrt{D_{\mathrm{O}}}}\frac{\bar{I}(s)}{\sqrt{s+f}}\times$$

$$\left[\frac{\mathcal{K}_1\left(u\sqrt{\frac{s+f}{D_{\mathrm{O}}}}\right)\mathcal{I}_0\left(a\sqrt{\frac{s+f}{D_{\mathrm{O}}}}\right)+\mathcal{I}_1\left(u\sqrt{\frac{s+f}{D_{\mathrm{O}}}}\right)\mathcal{K}_0\left(a\sqrt{\frac{s+f}{D_{\mathrm{O}}}}\right)}{\mathcal{K}_1\left(a\sqrt{\frac{s+f}{D_{\mathrm{O}}}}\right)\mathcal{I}_1\left(u\sqrt{\frac{s+f}{D_{\mathrm{O}}}}\right)-\mathcal{K}_1\left(u\sqrt{\frac{s+f}{D_{\mathrm{O}}}}\right)\mathcal{I}_1\left(a\sqrt{\frac{s+f}{D_{\mathrm{O}}}}\right)}\right], \quad (5.55)$$

Equation 5.55 is now identical to equation 2 in the original publication, such that the derivation of the Laplace domain solution is completed.

Since equations 5.54 and 5.55 do not possess an analytic time domain solution (at least no such solution was found during extensive research), the concept of a numerical inverse Laplace transformation was introduced. For this purpose, a modified Talbot contour was first ever utilized in the context of electrochemistry. In this manner, the respective time domain solution was approximated to high accuracy. Before introducing the Talbot-inversion, the respective mass transfer functions will be defined implicitly in the following.

In order to preserve a uniform notation throughout this thesis, the mass transfer functions $m_{\mathrm{R}}(t)$ and $m_{\mathrm{O}}(t)$ which were introduced in section 3.5, are implicitly defined for a cylindrical electrode in a finite external diffusion domain as

$$m_{\mathrm{R}}(t) = \mathcal{L}^{-1}\left\{\frac{1}{\sqrt{s}}\times\right.$$

$$\left.\left[\frac{\mathcal{K}_1\left(u\sqrt{\frac{s}{D_{\mathrm{R}}}}\right)\mathcal{I}_0\left(a\sqrt{\frac{s}{D_{\mathrm{R}}}}\right)+\mathcal{I}_1\left(u\sqrt{\frac{s}{D_{\mathrm{R}}}}\right)\mathcal{K}_0\left(a\sqrt{\frac{s}{D_{\mathrm{R}}}}\right)}{\mathcal{K}_1\left(a\sqrt{\frac{s}{D_{\mathrm{R}}}}\right)\mathcal{I}_1\left(u\sqrt{\frac{s}{D_{\mathrm{R}}}}\right)-\mathcal{K}_1\left(u\sqrt{\frac{s}{D_{\mathrm{R}}}}\right)\mathcal{I}_1\left(a\sqrt{\frac{s}{D_{\mathrm{R}}}}\right)}\right]\right\}(t) \quad (5.56)$$

and

$$m_{\mathrm{O}}(t) = \mathcal{L}^{-1}\left\{ \frac{1}{\sqrt{s}} \times \right.$$

$$\left. \left[\frac{\mathcal{K}_1\left(u\sqrt{\frac{s}{D_{\mathrm{O}}}}\right)\mathcal{I}_0\left(a\sqrt{\frac{s}{D_{\mathrm{O}}}}\right) + \mathcal{I}_1\left(u\sqrt{\frac{s}{D_{\mathrm{O}}}}\right)\mathcal{K}_0\left(a\sqrt{\frac{s}{D_{\mathrm{O}}}}\right)}{\mathcal{K}_1\left(a\sqrt{\frac{s}{D_{\mathrm{O}}}}\right)\mathcal{I}_1\left(u\sqrt{\frac{s}{D_{\mathrm{O}}}}\right) - \mathcal{K}_1\left(u\sqrt{\frac{s}{D_{\mathrm{O}}}}\right)\mathcal{I}_1\left(a\sqrt{\frac{s}{D_{\mathrm{O}}}}\right)} \right] \right\}(t). \quad (5.57)$$

With the property of the Laplace transformation which was given in equation 3.61, one can directly note the magnificent simplification of

$$m_{\mathrm{R}}(t)\,\mathrm{e}^{-pt} = \mathcal{L}^{-1}\left\{ \frac{1}{\sqrt{s+p}} \times \right.$$

$$\left. \left[\frac{\mathcal{K}_1\left(u\sqrt{\frac{s}{D_{\mathrm{R}}}}\right)\mathcal{I}_0\left(a\sqrt{\frac{s+p}{D_{\mathrm{R}}}}\right) + \mathcal{I}_1\left(u\sqrt{\frac{s+p}{D_{\mathrm{R}}}}\right)\mathcal{K}_0\left(a\sqrt{\frac{s+p}{D_{\mathrm{R}}}}\right)}{\mathcal{K}_1\left(a\sqrt{\frac{s+p}{D_{\mathrm{R}}}}\right)\mathcal{I}_1\left(u\sqrt{\frac{s+p}{D_{\mathrm{R}}}}\right) - \mathcal{K}_1\left(u\sqrt{\frac{s+p}{D_{\mathrm{R}}}}\right)\mathcal{I}_1\left(a\sqrt{\frac{s+p}{D_{\mathrm{R}}}}\right)} \right] \right\}(t) \quad (5.58)$$

and

$$m_{\mathrm{O}}(t)\mathrm{e}^{-ft} = \mathcal{L}^{-1}\left\{ \frac{1}{\sqrt{s+f}} \times \right.$$

$$\left. \left[\frac{\mathcal{K}_1\left(u\sqrt{\frac{s+f}{D_{\mathrm{O}}}}\right)\mathcal{I}_0\left(a\sqrt{\frac{s+f}{D_{\mathrm{O}}}}\right) + \mathcal{I}_1\left(u\sqrt{\frac{s+f}{D_{\mathrm{O}}}}\right)\mathcal{K}_0\left(a\sqrt{\frac{s+f}{D_{\mathrm{O}}}}\right)}{\mathcal{K}_1\left(a\sqrt{\frac{s+f}{D_{\mathrm{O}}}}\right)\mathcal{I}_1\left(u\sqrt{\frac{s+f}{D_{\mathrm{O}}}}\right) - \mathcal{K}_1\left(u\sqrt{\frac{s+f}{D_{\mathrm{O}}}}\right)\mathcal{I}_1\left(a\sqrt{\frac{s+f}{D_{\mathrm{O}}}}\right)} \right] \right\}(t). \quad (5.59)$$

Therefore, the time-dependent surface concentrations can be stated implicitly in terms of convolution integrals as outlined in section 3.5. Since $m_{\mathrm{R}}(t)$ and $m_{\mathrm{O}}(t)$ both posses a weak singularity at the upper integration limit of $\tau = t$, an

integration by parts is performed in analogy to equations 3.82 - 3.85 in the theory section. This yields

$$\bar{c}_{\mathrm{R,S}} = \frac{c_{\mathrm{tot}} K_{\mathrm{p}}}{(1+K_{\mathrm{p}})} - \frac{K_{\mathrm{p}}}{(1+K_{\mathrm{p}}) nFA\sqrt{D_{\mathrm{R}}}} \int_0^t I(\tau) M_{\mathrm{R}}(t-\tau)\mathrm{d}\tau$$
$$- \frac{1}{(1+K_{\mathrm{p}}) nFA\sqrt{D_{\mathrm{R}}}} \int_0^t I(\tau) M_{\mathrm{R}}(t-\tau)\mathrm{e}^{-p(t-\tau)}\mathrm{d}\tau, \quad (5.60)$$

and

$$\bar{c}_{\mathrm{O,S}} = \frac{1}{(1+K_{\mathrm{f}}) nFA\sqrt{D_{\mathrm{O}}}} \int_0^t I(\tau) M_{\mathrm{O}}(t-\tau)\mathrm{d}\tau$$
$$+ \frac{K_{\mathrm{f}}}{(1+K_{\mathrm{f}}) nFA\sqrt{D_{\mathrm{O}}}} \int_0^t I(\tau) M_{\mathrm{O}}(t-\tau)\mathrm{e}^{-f(t-\tau)}\mathrm{d}\tau, \quad (5.61)$$

with $M_{\mathrm{R}}(t)$ and $M_{\mathrm{O}}(t)$ being the antiderivatives of $m_{\mathrm{R}}(t)$ and $m_{\mathrm{O}}(t)$. These can be evaluated easily by exploiting the relation 3.56, which was derived in the theory section. Hence, it is

$$M_{\mathrm{R}}(t) = \mathcal{L}^{-1}\left\{ \frac{1}{s^{3/2}} \times \right.$$
$$\left. \left[\frac{\mathcal{K}_1\left(u\sqrt{\frac{s}{D_{\mathrm{R}}}}\right)\mathcal{I}_0\left(a\sqrt{\frac{s}{D_{\mathrm{R}}}}\right) + \mathcal{I}_1\left(u\sqrt{\frac{s}{D_{\mathrm{R}}}}\right)\mathcal{K}_0\left(a\sqrt{\frac{s}{D_{\mathrm{R}}}}\right)}{\mathcal{K}_1\left(a\sqrt{\frac{s}{D_{\mathrm{R}}}}\right)\mathcal{I}_1\left(u\sqrt{\frac{s}{D_{\mathrm{R}}}}\right) - \mathcal{K}_1\left(u\sqrt{\frac{s}{D_{\mathrm{R}}}}\right)\mathcal{I}_1\left(a\sqrt{\frac{s}{D_{\mathrm{R}}}}\right)} \right] \right\}(t) \quad (5.62)$$

and

$$M_{\mathrm{O}}(t) = \mathcal{L}^{-1}\left\{ \frac{1}{s^{3/2}} \times \right.$$
$$\left. \left[\frac{\mathcal{K}_1\left(u\sqrt{\frac{s}{D_{\mathrm{O}}}}\right)\mathcal{I}_0\left(a\sqrt{\frac{s}{D_{\mathrm{O}}}}\right) + \mathcal{I}_1\left(u\sqrt{\frac{s}{D_{\mathrm{O}}}}\right)\mathcal{K}_0\left(a\sqrt{\frac{s}{D_{\mathrm{O}}}}\right)}{\mathcal{K}_1\left(a\sqrt{\frac{s}{D_{\mathrm{O}}}}\right)\mathcal{I}_1\left(u\sqrt{\frac{s}{D_{\mathrm{O}}}}\right) - \mathcal{K}_1\left(u\sqrt{\frac{s}{D_{\mathrm{O}}}}\right)\mathcal{I}_1\left(a\sqrt{\frac{s}{D_{\mathrm{O}}}}\right)} \right] \right\}(t). \quad (5.63)$$

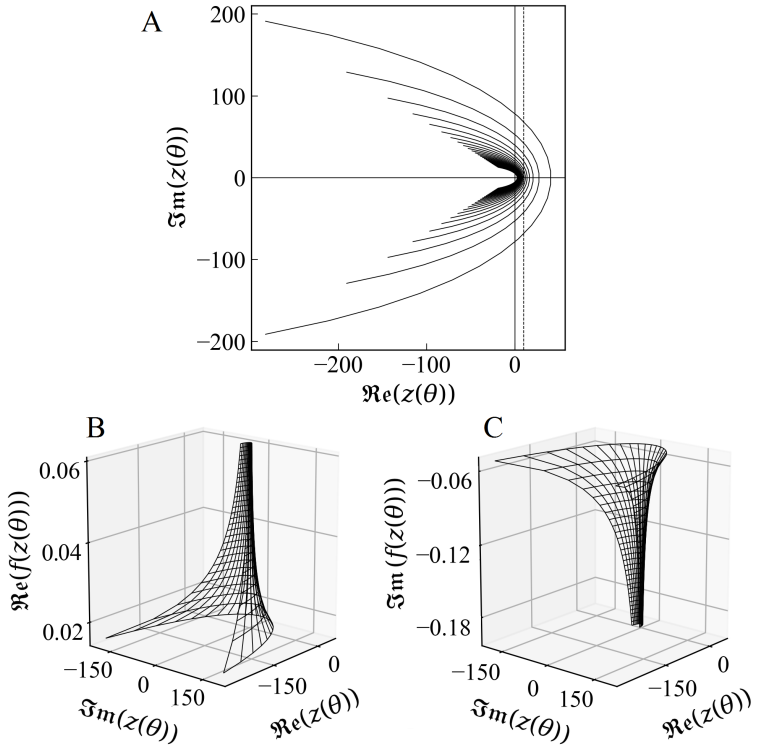

Figure 5.3: (A), modified Talbot contour which is based on equation 5.64 for ten values of t linearly spaced between $t_{\min} = 0.1$ s and $t_{\max} = 1.0$ s. The dotted vertical line corresponds to the Bromwich contour defined by equation 3.60 in the theory section with $\gamma = 10$. (B) and (C), real and imaginary part of the exemplary function $f(z) = z^{-1/2}$ which are associated to the values of z defined by equation 5.64. The function chosen as an example corresponds to the Laplace domain solution of the derivative of the mass transfer function for a planar semi-infinite diffusion domain.

The inverse Laplace transformation in equations 5.62 and 5.63 is performed subsequently, by using the modified Talbot countour suggested by Weideman and Dingfelder[126], which is depicted in figure 5.3A. The Talbot contour basically distorts the Bromwich-line which was defined by equation 3.60 in the theory section into a parabola-like shape [126]–[128]. In this manner, it defines a path in the complex plane along which a numerical integration can be performed readily. The parameterized integration path is given by

$$z(\Theta) = \frac{24}{t}(-0.6122 + 0.5017\Theta \cdot \cot(0.6407\Theta) + \mathrm{i} \cdot 0.2339\Theta), \tag{5.64}$$

The time domain solution can be approximated subsequently via

$$f(t) \approx \mathfrak{Re}\left(\sum_{k=1}^{24} \bar{F}(z(\Theta_k))\mathrm{e}^{tz(\Theta_k)}\frac{\mathrm{d}z(\Theta)}{\mathrm{d}\Theta}\Big|_{\Theta=\Theta_k}\right). \tag{5.65}$$

where the nodes are located at

$$\Theta_k = -\pi + \frac{2\pi}{24}\cdot\left(k-\frac{1}{2}\right). \tag{5.66}$$

Since the contour defined by equation 5.64 adapts its width according to the respective value of t, it provides a maximum accuracy. In figure 5.3B and C, the real and imaginary part of the test function $f(z(\theta)) = z(\theta)^{-1/2}$ are depicted. This function has a singularity at $z = 0$, which is enclosed by the Talbot contour. Since this fulfills Cauchys integral theorem, the inverse Laplace transformation can be approximated. In case of a function whose singularities are located far away from the real axis, i.e. outside of the contour[6] the Talbot contour cannot be applied for a numerical inversion of the Laplace transformation. For more details on the Talbot contour, the reader is referred to the original publication by Weidemann and Dingfelder [126].

Now, treating equations 5.60 and 5.61 in analogy to equation 3.84 and 3.85, one obtains a modified master equation, which accounts for preceeding and following homogeneous chemical equilibria. This expression can be formulated as

$$\begin{aligned} I(i\Delta t) \approx\ & \\ & \frac{\frac{1}{1+K_\mathrm{p}}\left[K_\mathrm{p} nFAc_\mathrm{tot}\sqrt{D_\mathrm{R}} - \sum_{j=1}^{i-1} I(j\Delta t)\delta M_\mathrm{R}(i,j)[K_\mathrm{p} + \mathrm{e}^{-p[i-j]\Delta t}]\right]}{\frac{\sqrt{D_\mathrm{R}}\,\mathrm{e}^{-\alpha\xi(i\Delta t)}}{k^0} + M_\mathrm{R}(\Delta t) + M_\mathrm{O}(\Delta t)\sqrt{\frac{D_\mathrm{R}}{D_\mathrm{O}}}\mathrm{e}^{-\xi(i\Delta t)}} \\ & - \frac{\frac{\mathrm{e}^{-\xi(i\Delta t)}}{1+K_\mathrm{f}}\sqrt{\frac{D_\mathrm{R}}{D_\mathrm{O}}}\sum_{j=1}^{i-1} I(j\Delta t)\delta M_\mathrm{O}(i,j)[1+K_\mathrm{f}\mathrm{e}^{-f[i-j]\Delta t}]}{\frac{\sqrt{D_\mathrm{R}}\,\mathrm{e}^{-\alpha\xi(i\Delta t)}}{k^0} + M_\mathrm{R}(\Delta t) + M_\mathrm{O}(\Delta t)\sqrt{\frac{D_\mathrm{R}}{D_\mathrm{O}}}\mathrm{e}^{-\xi(i\Delta t)}}. \end{aligned} \tag{5.67}$$

[6] Such a function possesses oscillatory behaviour in the time domain.

In equation 5.67, it is defined that

$$\delta M_{\mathrm{R}}(i,j) = M_{\mathrm{R}}((i-j+1)\Delta t) - M_{\mathrm{R}}((i-j)\Delta t) \tag{5.68}$$

and

$$\delta M_{\mathrm{O}}(i,j) = M_{\mathrm{O}}((i-j+1)\Delta t) - M_{\mathrm{O}}((i-j)\Delta t). \tag{5.69}$$

By exploiting equation 5.67, with the respective $M_{\mathrm{R}}(t)$ and $M_{\mathrm{O}}(t)$ defined by equations 5.62 and 5.63, it was finally possible to simulate a CV response for one single electrode in an external cylindrical finite diffusion domain with coupled preceeding and following chemical equilibria.

The diffusion domain approximation

The final step was to implement the effect of a statistically distributed finiteness of the diffusion domain inside of a felt electrode. For this purpose, the porous structure was assumed as an array of cylindrical microelectrodes as depicted in figure 5.4. This implies that a certain fraction of the void volume of the entire felt electrode was assigned to each individual electrode fiber. Since all the fibers inside of a felt electrode possess approximately the same diameter, the simulations were performed by considering a variable distance d and a constant a only. Since very large and very low values of d are rather improbable, the respective individual CV responses required for a statistical weightning. For this purpose a suitably chosen density distribution function was assumed. For details on the statistical weightning process, the reader is referred to the original publication in section 6.3. However, schematically, it is depicted in figure 5.5 and can be summarized as follows.

At first, individual CV responses are simulated for different values of the diffusion domain size. This is depicted in figure 5.5A for the diffusion domain sizes shown in figure 5.5B. It can be seen that for a large diffusion domain size the magnitude and peak-to-peak separation of the individual CV responses are increased, which is typical for a finite diffusion domain model. In figure 5.5B, the density distribution function, which was assumed to describe the individual fiber distances inside of a felt electrode is depicted. The integral of each interval of this paricular distribution function corresponds to the probability of finding a pair of cylindrical microelectrodes (fibers) at a certain distance to each other.

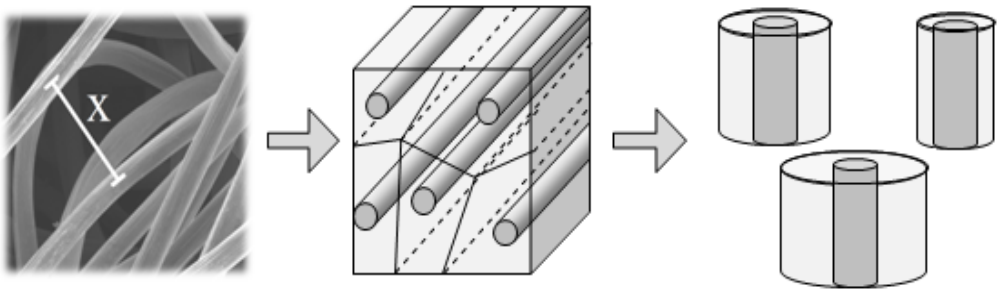

Figure 5.4: Diffusion domain approximation for a carbon felt electrode. The felt (cf SEM image) is assumed as an array of cylindrical microelectrodes. By assigning a certain fraction of the felt volume to each individual microelectrode, CV simulations are performed on the base of equation 5.67, Thereby a variable finiteness of d is considered.

Consequently, the current magnitudes of the individual CV responses which are calculated in figure 5.5A, need to be multiplied by this particular statistical weights. This is depicted in figure 5.5C. It can be seen that — especially for curve (d) — a low statistical weight decreases the current contribution significantly. Finally, the individual CV responses which are depicted in figure 5.5C are added to yield the superimposed CV response of the entire felt electrode which is depicted in figure 5.5D.

Now, following this routine, a novel strategy for simulating CV responses of carbon felt electrodes was created. In the original publication it is shown furthermore, that manually fitting experimentally acquired CV data for the positive VRFB half-cell reaction provides a fairly good agreement with the kinetic reference data presented in section 5.1. Furthermore, the distance distributions which were utilized throughout the fitting process agree with porosimetry measurements of the particular felt electrode type. Therefore, it was finally concluded that the novel strategy overcomes the inherent ambiguity of CV in porous structures and finally provides a reliable way for analyzing electrode kinetics and electrode porosities of felt electrodes simultaneously.

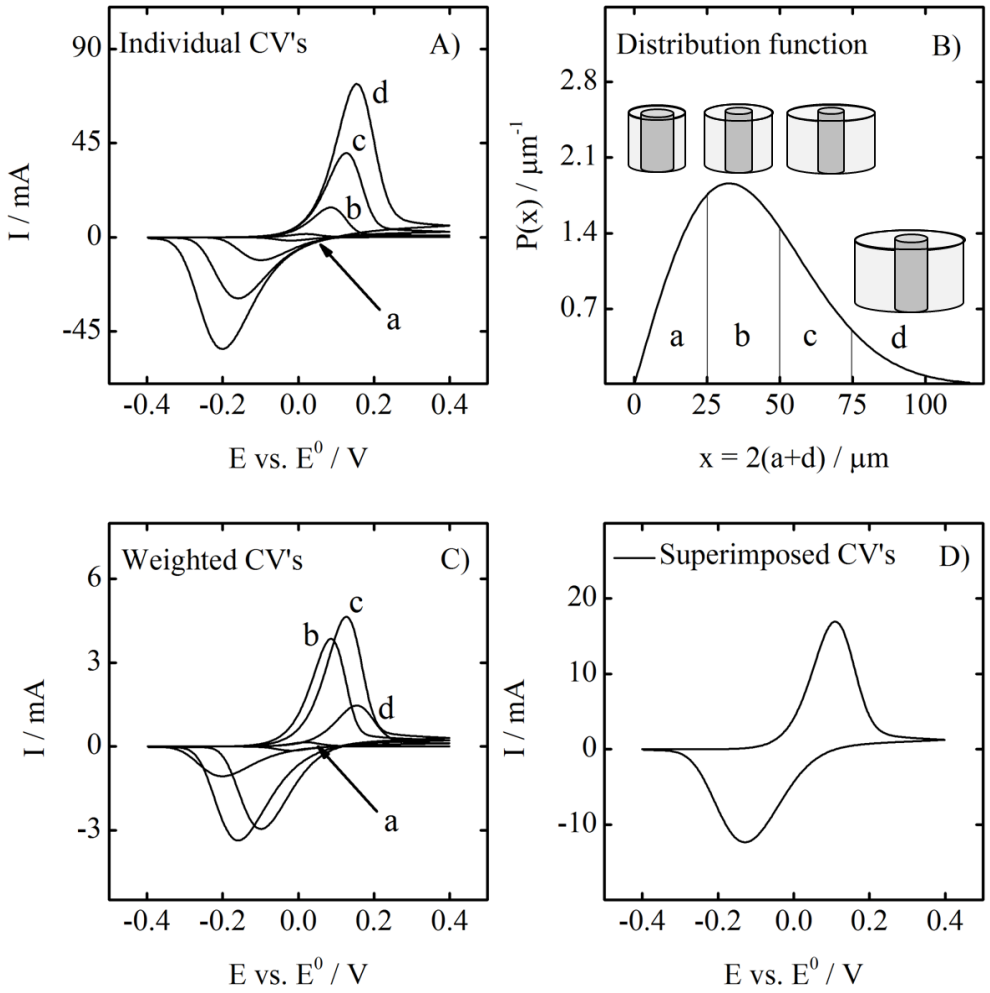

Figure 5.5: Qualitative sketch of the statistical weightning process of the diffusion domain approximation for a carbon felt electrode. (A) Individual CV responses at four different diffusion domain sizes, where the diffusion domain size increases from (a) to (d). (B) Weibull-like density distribution function for describing the nearest neighbor distances inside of a felt electrode. The integral segments below the curve correspond to the probability of finding a pair of cylindrical microelectrodes in the distances of (a) to (d), respectively. (C) Individual CV curves of panel (A) multiplied by their respective statistical weight which was obtained from panel (B). (D) Superimposed, statistically weighted CV responses, i.e. the entire CV response of a felt electrode.

5.4 The Generalized Diffusion Domain Approximation

In the fourth publication related to this thesis which is entitled

> *'Universal Algorithm for Simulating and Evaluating Cyclic Voltammetry at Macroporous Electrodes by Considering Random Arrays of Microelectrodes'*,

all the previous concepts were combined. The diffusion domain approximation which was introduced in section 5.3 was extended to layered structures, electrodes with hollow-cylindrical pore structures and electrode foams. For this purpose, random 1D, 2D, and 3D arrays of planar, hollow-cylindrical and hollow-spherical microelectrodes were considered. Furthermore, the effect of preceeding and following homogeneous chemical equilibria and finite heterogeneous electron transfer kinetics was included. This accounts for an exceptionally broad range of experimental cirumstances. In order to provide the experimentalists community with an alternative way of interpreting CV data at porous and non-porous electrodes a powerful open source tool, named *Polarographica*[7], was created. This program provides a graphical user interface and therefore allows for a facile simulation and evaluation of electroanalytical experiments which will eventually result in a more reliable interpretation of CV data. Since detailed derivations are provided in the original publication, this section will mainly introduce *Polarographica* in brief.

Motivation

The motivation of this particular publication was to generalize the diffusion domain approximation presented in section 5.3 to any kind of porous electrode structure. In order to provide an overview on the complex interplay of diffusive mass transfer at porous electrodes, coupled chemical kinetics and modified heterogeneous electrode kinetics, numerous simulations were performed. Furthermore, the effect of electrode porosity on the CV response is emphasized in order to explain the tailing in experimental CV data which is not captured by the classical finite diffusion domain models. However, since a purely theoretical model does not provide a significant benefit to the experimentalists community, a software tool for facile simulation and interpretation of CV at porous electrodes was desired and finally created. This program will be introduced as the result of the related publication in this sub-chapter.

[7] The name *'Polarographica'* is derived from *'polarography'* and *'graphical user interface'*

Polarographica

The software tool *Polarographica* was mainly created to allow for an evaluation of cyclic voltammetry data at porous electrode structures by a manual fitting routine. Nevertheless, it also supports an automated version of the classical evaluations (Randles–Ševčík, Cottrell, Koutecký–Levich, Tafel) as well as simulation and fitting routines for a whole series of other electroanalytical techniques. Among them are voltamperometric methods such as chronoamperometry, large-sine amplitude cyclic voltammetry, Fourier transformation alternating current cyclic voltammetry, cyclic-staircase voltammetry and random input voltammetry as well as impedance methods such as potentiostatic electrochemical impedance spectroscopy and the distribution of relaxation times analysis. The main graphical user interface of *Polarographica* is depicted in figure 5.6. Figure 5.7 in turn depicts the simulation mode for a CV experiment at a porous carbon felt electrode in analogy to the theory presented in section 5.3.

Figure 5.8 shows the *'superposition mode'* of *Polarographica* which can be used for a) overlaying up to 50 CV experiments at different potential sweep rates (referred to as Randles–Ševčík mode) or b) for superimposing up to 50 different CV curves (referred to as additive mode). An ancestory version of the additive mode was utilized for superimposing the desired vanadium reduction and the hydrogen evolution reaction in the study which was presented in section 5.2.

Since this thesis is restricted to the theory of cyclic voltammetry experiments at porous electrodes, the additional electroanalytical methods supported by *Polarographica* will not be discussed in detail. However, it is worth to note that all the voltamperometric simulations are based on the same master equation. This particular equation resulted from a combination of equation 5.8 in section 5.1 as well as equation 5.67 from section 5.3. It therefore accounts for an electrochemical reaction which is coupled to homogeneous chemical equilibria and optionally possesses finite heterogeneous electron transfer kinetics. This provides a maximum flexibility which captures an exceptionally broard range of experimental circumstances. This — so to say — final master equation of this thesis is given by equation 5.70. The definition of $\mathfrak{f}_{\mathrm{an}}(i\Delta t)$ and $\mathfrak{f}_{\mathrm{ca}}(i\Delta t)$ is identical to equations 5.9 and 5.10 and the definition of $\delta M_{\mathrm{R}}(i,j)$ and $\delta M_{\mathrm{O}}(i,j)$ follows from equations 5.68 and 5.69, respectively. The time-dependent mass transfer functions $M_{\mathrm{R}}(t)$ and M_{O} which are individually required for each diffusion model which is supported by *Polarographica* are calculated from their respective Laplace domain solutions by means of numerical inverse Laplace transformation. For this purpose, the modified Talbot contour proposed by Dingfelder and Weideman was exploited as outlined in section 5.3.

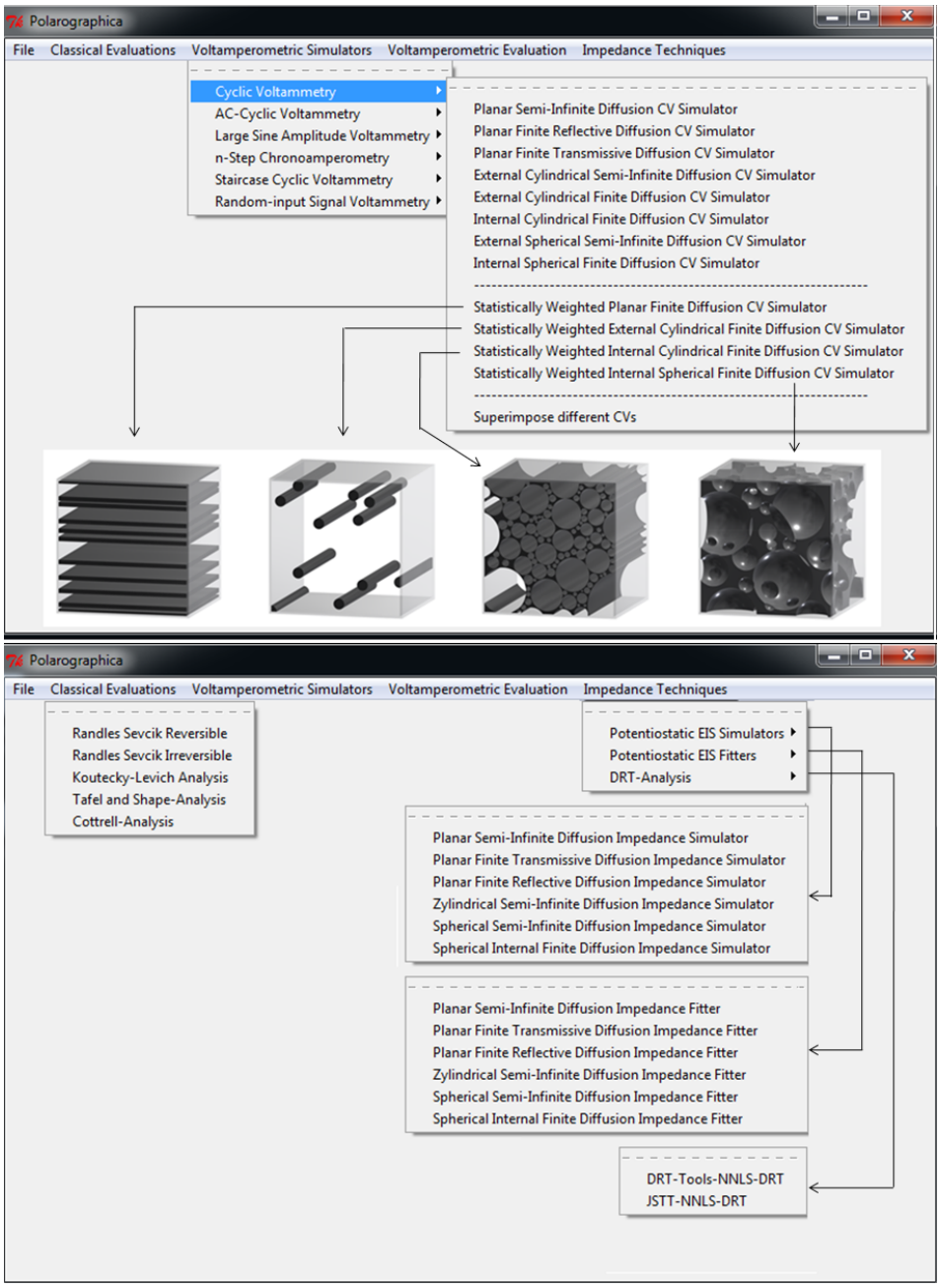

Figure 5.6: Main menu of *Polarographica* with all supported functions and electroanalytical techniques. The four diffusion models for cyclic voltammetry at porous electrodes which were derived in the related publication are depicted schematically.

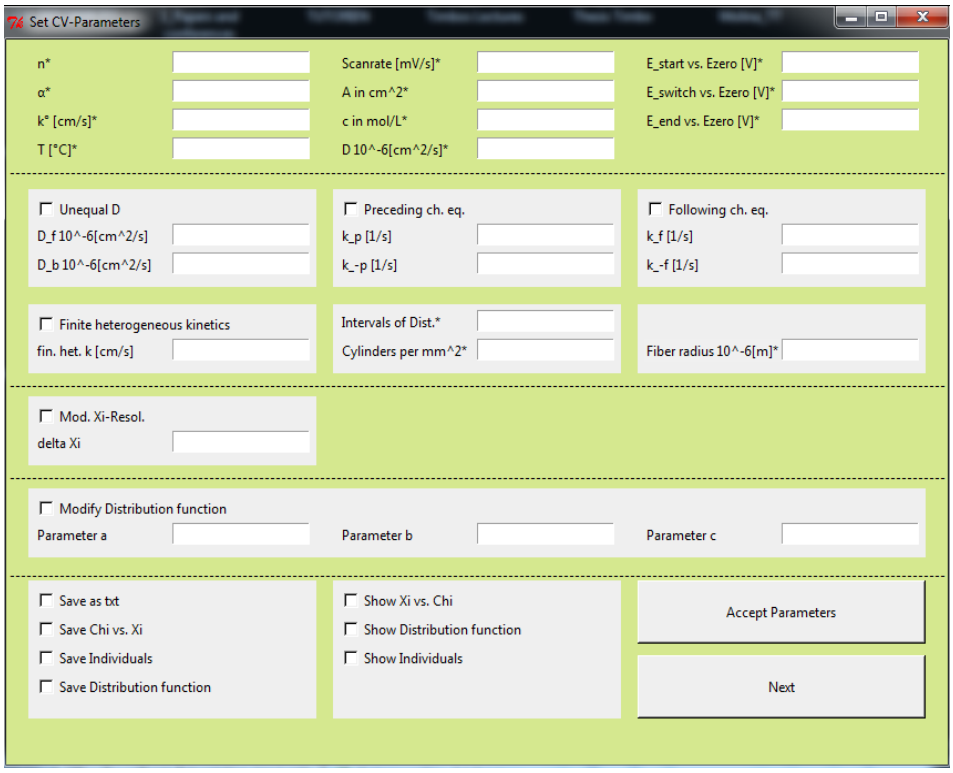

Figure 5.7: CV simulation mode of *Polarographica* for a carbon felt electrode which is considered as an array of cylindrical microelectrodes. This model is equivalent to the theory presented in section 5.3.

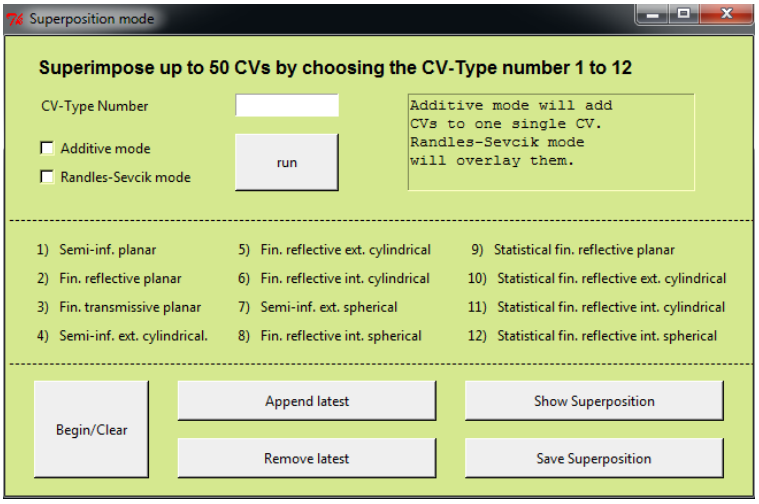

Figure 5.8: Superposition mode of *Polarographica*. This feature allows for adding (additive mode) or overlaying (Randles–Ševčík mode) up to 50 different CV curves.

For details on the numerical inversion of the Laplace transformation, the reader is referred to the original publication attached in section 6.4 of this thesis. The respective Laplace domain solutions of the mass transfer functions are also given in the appendix of this particular publication.

$$
\begin{aligned}
I(i\Delta t) \approx & \\
& \frac{\frac{\mathfrak{f}_{\mathrm{an}}(i\Delta t)}{1+K_{\mathrm{p}}}\left[K_{\mathrm{p}} nFAc_{\mathrm{tot}}\sqrt{D_{\mathrm{R}}} - \sum_{j=1}^{i-1} I(j\Delta t)\delta M_{\mathrm{R}}(i,j)[K_{\mathrm{p}} + \mathrm{e}^{-p[i-j]\Delta t}]\right]}{\frac{\sqrt{D_{\mathrm{R}}}\,\mathrm{e}^{-\alpha\xi(i\Delta t)}}{k^0} + \mathfrak{f}_{\mathrm{an}}(i\Delta t)\, M_{\mathrm{R}}(\Delta t) + \mathfrak{f}_{\mathrm{ca}}(i\Delta t)\, M_{\mathrm{O}}(\Delta t)\sqrt{\frac{D_{\mathrm{R}}}{D_{\mathrm{O}}}}\mathrm{e}^{-\xi(i\Delta t)}} \\
& - \frac{\frac{\mathfrak{f}_{\mathrm{ca}}(i\Delta t)\,\mathrm{e}^{-\xi(i\Delta t)}}{1+K_{\mathrm{f}}}\sqrt{\frac{D_{\mathrm{R}}}{D_{\mathrm{O}}}}\sum_{j=1}^{i-1} I(j\Delta t)\delta M_{\mathrm{O}}(i,j)[1+K_{\mathrm{f}}\mathrm{e}^{-f[i-j]\Delta t}]}{\frac{\sqrt{D_{\mathrm{R}}}\,\mathrm{e}^{-\alpha\xi(i\Delta t)}}{k^0} + \mathfrak{f}_{\mathrm{an}}(i\Delta t)\, M_{\mathrm{R}}(\Delta t) + \mathfrak{f}_{\mathrm{ca}}(i\Delta t)\, M_{\mathrm{O}}(\Delta t)\sqrt{\frac{D_{\mathrm{R}}}{D_{\mathrm{O}}}}\mathrm{e}^{-\xi(i\Delta t)}}.
\end{aligned}
\tag{5.70}
$$

The different electroanalytical techniques which are implemented into *Polarographica* simply rely on subjecting equation 5.70 to different potential programs — i.e. by varying the input signal $\xi(t)$

In case of the random network diffusion models, the effect of electrode porosity was introduced similar to the publication presented in section 5.3. By considering 1D, 2D, and 3D arrays of planar, hollow-cylindrical and hollow-spherical microelectrodes the diffusion domain inside of the porous electrodes is approximated. The respective distance distributions which are required for a proper statistical weightning of the individual CV responses of the microelectrode sub-units inside the porous electrodes are assumed to follow a three-parameter generalized gamma distribution. Details on the respective statistical weightning process can be found in the original publication. Finally, in the supporting information of the original publication, an example for a CV fitting routine can be found. This can be regarded as an instruction on how to use *Polarographica* for the evaluation of experimentally acquired CV data without any programming effort and decent knowledge on the mathematics of diffusion and concludes the respective publication.

5.5 The Unified Mass-Transfer Function and CV in Real-Space

The fifth and final publication related to this cumulative thesis is entitled

'Real-Space Simulation of Cyclic Voltammetry in Carbon Felt Electrodes by Combining Micro X-Ray CT Data, Digital Simulation and Convolutive Modeling'.

In this study the diffusion domain approximation approach — introduced in the two foregoing publications — for the modeling of voltamperometric experiments at porous electrodes was circumvented. The alternative CV simulation strategy consists of four successive steps. At first, by exploiting micro X-ray tomography, the diffusion domain inside of a porous felt electrode is resonstructed. Subsequently, the time-dependent current related to this real-space template is calculated to Cottrellian boundary conditions by means of digital simulation. The third step is to compute the mass transfer function related to the particular porous electrode stucture by an inverse convolution algorithm from the time dependent current wave. Finally, the thus obtained mass transfer function is utilized to compute the related CV experiments on the base of equation 5.70 from section 5.4. Since almost any real electroanalytical experiment involves coupled electrolyte resistances and interfacial double layer capacities, these quantities have been included into the respective model as well. Ultimately, the novel theoretical concept was validated by experimental data acquired for the positive VRFB half-cell reaction which concludes the respective publication.

Motivation

The motivation for the work presented in this section resulted from the diffusion domain approximation for porous electrodes which has been introduced in the latter two publications and which offers two significant drawbacks. Since this approximation considers the porous electrode as an array of individual microelectrodes which are independent of each other, the effect of overlapping diffusion zones inside of the random network was excluded by definition. Furthermore, the effect of mass transport from and towards the porous electrode structures was not considered. This has been caused by the fact that the diffusive part of the system of interest was solved on the base of Laplace integral transformation techniques which require for a symmetrical diffusion domain and therefore a discretization of the porous electrode structure into distinct and symmetrical sub-units. Consequently,

the mathematical treatment of a random network diffusion model, which possesses an inherent anisotropy of the diffusion domain was not yet possible by means of Laplace transformation techniques and the outstanding advantage of using a master equation was never employed in this context either. The emphasis of the study related to this section was now, to create a routine for simulating CV experiments at electrodes with an anisotropic diffusion domain and to preserve the advantage of utilizing a master equation.

Cyclic voltammetry in real-space: The four-step strategy

In order to simulate cyclic voltammetry experiments in an anisotropic diffusion domain, it was mandatory to avoid the direct utilization of Laplace transformation techniques for solving the diffusive part of the system of interest. However, for preserving the advantages of a master equation, a Laplace transformation needs to be involved implicitly. For this purpose, an algorithm of four successive steps was proposed. These can be summarized as follows and are schematically depicted in figure 5.10.

At first, the real-space diffusion domain inside of a porous electrode was reconstructed from micro X-ray tomography data. Subsequently, this template was utilized to simulate the time dependent current of a chronoamperometric experiment to Cottrellian boundary conditions by means of digital simulation. For this purpose, the Douglas–Gunn modification [129] of the three dimensional Crank–Nicolson method was exploited [96]. Since the native Crank-Nicolson method in three spatial dimensions gets exceptionally expensive with respect to the computation time, this particular modification was necessary to render the simulations tracktable. The full Crank–Nicolson method in the three spatial dimension can be derived from equation 3.44 in analogy to the procedure outlined in the theory section. In this manner, the three-dimensional Crank–Nicolson method can be stated as

$$\begin{aligned} -\lambda c_{i,j,k-1,t+\Delta t} - \lambda c_{i,j-1,k,t+\Delta t} - \lambda c_{i-1,j,k,t+\Delta t} + (2+6\lambda)c_{i,j,k,t+\Delta t} \\ - \lambda c_{i+1,j,k,t+\Delta t} - \lambda c_{i,j+1,k,t+\Delta t} - \lambda c_{i,j,k+1,t+\Delta t} \\ = \\ \lambda c_{i,j,k-1,t} + \lambda c_{i,j-1,k,t} + \lambda c_{i-1,j,k,t} + (2-6\lambda)c_{i,j,k,t} \\ + \lambda c_{i+1,j,k,t} + \lambda c_{i,j+1,k,t} + \lambda c_{i,j,k+1,t}. \end{aligned} \tag{5.71}$$

where the parameter λ has its usual definition and $i,\ j\ k$ represent the counting of spatial grid points in the $x,\ y$ and z direction, respectively. Unfortunately,

this procedure results in a heptadiagonal sparse matrix whose rang scales with the third power of grid points. This renders the computation of realistic sample volumes impossible. The banded structure of the respective full Crank–Nicolson matrix (of rang 64) is depicted for a $4 \times 4 \times 4$ voxels diffusion field in figure 5.9.

To overcome the computational expense of the three dimensional Crank–Nicolson method, the Douglas–Gunn modification was introduced. This approach basically splits each individual time march of the Crank–Nicolson method in three sub-steps. Since step I is implicit in x-direction and explicit in y- and z-directions, step II is implicit along the y direction and step III along the z-direction, this particular method is termed alternating direction implicit (ADI). The three steps can be stated as follows: Step I:

$$\begin{aligned} -\lambda c_{i-1,j,k,t+\Delta t/3} + 2(1+\lambda) c_{i,j,k,t+\Delta t/3} - \lambda c_{i+1,j,k,t+\Delta t/3} = \\ [\lambda \cdot (c_{i-1,j,k,t} + c_{i+1,j,k,t} + 2c_{i,j-1,k,t} + 2c_{i,j+1,k,t} + \\ 2c_{i,j,k-1,t} + 2c_{i,j,k+1,t} - 10c_{i,j,k,t}) + 2c_{i,j,k,t}] \cdot c_{i,j,k,t=0} \end{aligned} \tag{5.72}$$

Step II:

$$\begin{aligned} -\lambda c_{i,j-1,k,t+2\Delta t/3} + 2(1+\lambda) c_{i,j,k,t+2\Delta t/3} - \lambda c_{i,j+1,k,t+2\Delta t/3} = \\ [\lambda \cdot (c_{i-1,j,k,t+\Delta t/3} - 2c_{i,j,k,t+\Delta t/3} + c_{i+1,j,k,t+\Delta t/3} + \\ c_{i-1,j,k,t} + c_{i+1,j,k,t} c_{i,j-1,k,t} + c_{i,j+1,k,t} + \\ 2c_{i,j,k-1,t} + 2c_{i,j,k+1,t} - 8c_{i,j,k,t}) + 2c_{i,j,k,t}] \cdot c_{i,j,k,t=0} \end{aligned} \tag{5.73}$$

Step III:

$$\begin{aligned} -\lambda c_{i,j,k-1,t+\Delta t} + 2(1+\lambda) c_{i,j,k,t+\Delta t} - \lambda c_{i,j,k+1,t+\Delta t} = \\ [\lambda \cdot (c_{i-1,j,k,t+\Delta t/3} - 2c_{i,j,k,t+\Delta t/3} + c_{i+1,j,k,t+\Delta t/3} + \\ c_{i,j-1,k,t+2\Delta t/3} - 2c_{i,j,k,t+2\Delta t/3} + c_{i,j+1,k,t+2\Delta t/3} + \\ c_{i-1,j,k,t} + c_{i+1,j,k,t} c_{i,j-1,k,t} + c_{i,j+1,k,t} + \\ c_{i,j,k-1,t} + c_{i,j,k+1,t} - 6c_{i,j,k,t}) + 2c_{i,j,k,t}] \cdot c_{i,j,k,t=0} \end{aligned} \tag{5.74}$$

Since each of these three successive steps is involves tridiagonal matrices only, which can be solved very efficiently by utilizing the Thomas algorithm [100], the ADI method is substantially faster than the full Crank-Nicolson scheme.

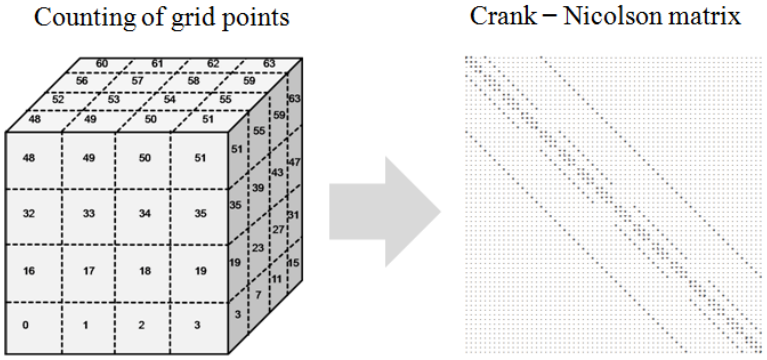

Figure 5.9: Counting of spatial grid points and the resulting structure of the heptadiagonal full Crank–Nicolson matrix which corresponds to a $4 \times 4 \times 4$ voxels diffusion field with outer no-flux boundaries.

Subsequently to solving the time dependent concentration profile inside of the real-space network, the chronoamperometric current is calculated according to Ficks first law. Based on this chronoamperometric current response, the time dependent mass transfer function related to the real-space diffusion domain of the porous electrode is calculated. For this purpose, an inverse convolution algorithm was designed, which is basically the reverse computation of equation 3.74. It was obtained by rearranging equation 3.73 in terms of $M(t)$ instead of $I(t)$. Once the mass transfer function was computed, the simulation of cyclic voltammetry experiments could be performed readily, by utilizing equation 5.70. In order to implement the current contributions of interfacial double layer capacities and the non-linear effects of coupled ohmic resistances into the convolution algorithm, the master equation approach represented by equation 5.70 was refined by the model proposed by Montalla [130]. For details on this extended model, the reader is referred to the original publication in section 6.5 of this thesis. In this manner, a final model for the simulation of cyclic voltammetry experiments at porous electrodes is created which

- accounts for anisotropic diffusion domains in macroporous electrodes,
- preserves all the advantages of convolutive modeling and allows for the use of a master equation,
- optionally accounts for homogeneous chemical reactions and finite heterogeneous kinetics which deviate from Butler–Volmer behaviour,
- includes the non-linear effects of coupled ohmic resistances and interfacial double layer capacities.

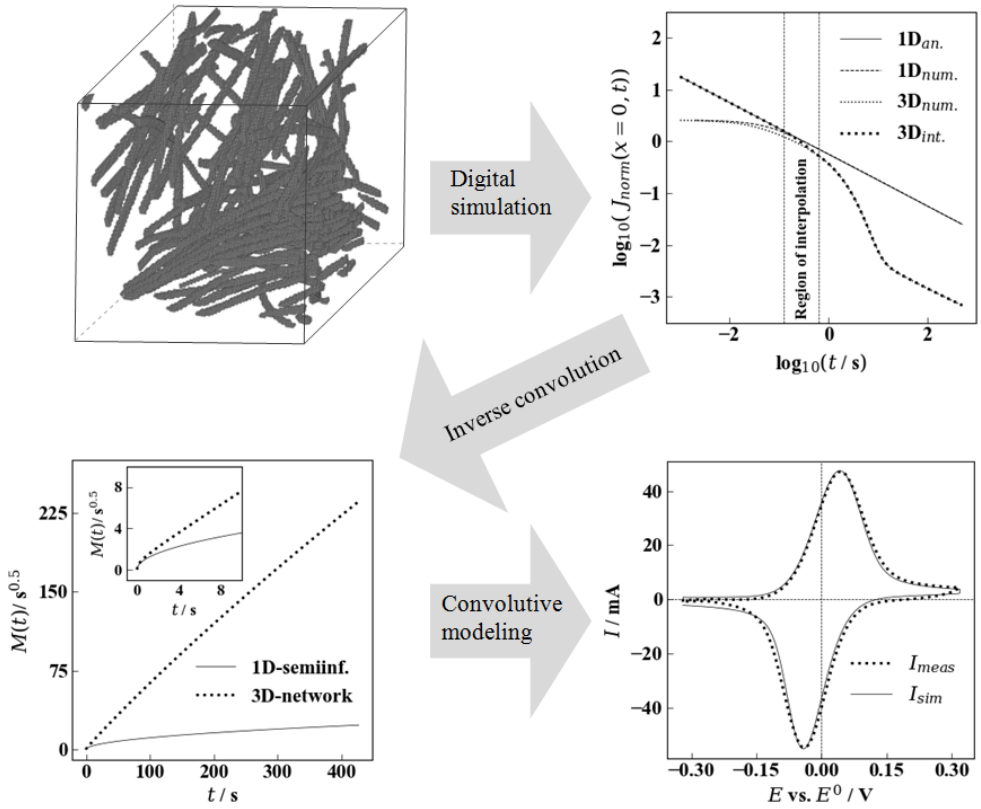

Figure 5.10: Sketch of the novel four-step strategy for simulating cyclic voltammetry experiments at porous electrodes. At first, the diffusion domain inside of the porous structure is reconstructed from micro X-ray tomography measurements. Subsequently, the Cottrellian current response of this real-space network is computed by means of digital simulation. In the third step, the mass transfer function related to the porous electrode is calculated by an inverse convolution algorithm. Finally, this mass transfer function is utilized for simulating CV via classical convolutive modeling.

Since a manual fitting of simulated data to experimentally acquired data, which is based on the novel four-step strategy provides an excellent agreement with the reference data which was acquired in the first publication of this cumulative thesis, it can be concluded that the inherent ambiguity of cyclic voltammetry of porous electrodes was finally overcome.

Chapter 6

Original Publications

This chapter comprises all the original publications related to this cumulative thesis. All manuscripts were translated to original TEX language to provide a uniform style. The original publications can be accessed by their respective DOI.

FINITE HETEROGENEOUS RATE CONSTANTS FOR THE ELECTROCHEMICAL OXIDATION OF VO^{2+} AT GLASSY CARBON ELECTRODES

Tim Tichter, Jonathan Schneider, Christina Roth

DOI: 10.3389/fenrg.2020.00155

Individual contributions

Tim Tichter:
Conceptualization, Developing the theory, Methodology, Software, Writing – original draft, Writing – review

Jonathan Schneider:
Scientific discussion, Writing – review & editing

Christina Roth:
Supervision, scientific discussion

FINITE HETEROGENEOUS RATE CONSTANTS FOR THE ELECTROCHEMICAL OXIDATION OF VO^{2+} AT GLASSY CARBON ELECTRODES

Tim Tichter[a,*], Jonathan Schneider[a], Christina Roth[b]

Abstract

The electrochemical oxidation of VO^{2+} at planar glassy carbon electrodes is investigated via stationary and rotating linear sweep voltammetry as well as via chronoamperometry. It is demonstrated that introducing finite kinetic rate constants into the Butler-Volmer equation captures the experimentally observed concentration dependence of the ordinate intercept in Koutecký-Levich plots, that cannot be explained by using the classical model. This new concept leads to a three-term Koutecky-Levich equation considering mass transport limitations, Butler-Volmer kinetics as well as finite heterogeneous kinetics simultaneously. Based on these findings it is pointed out that stationary linear sweep voltammetry followed by an irreversible Randles-Ševčík analysis is not sufficient for deducing the electrode kinetics of the VO^{2+}-oxidation. In contrast, it is verified experimentally and theoretically that a Tafel analysis will still provide reasonable values of $k^0 = 1.35 \cdot 10^{-5}$ cm/s and $\alpha = 0.38$, respectively. Finally, it is shown that introducing the concept of finite heterogeneous kinetics into the theory of stationary linear sweep voltammetry also explains the failure of the irreversible Randles-Sevcik relation leading to an extension of the classical model and providing insights into the electrochemical oxidation reaction of VO^{2+}.

Keywords: Vanadium redox-flow batteries; Rotating disc electrode; Linear sweep voltammetry; Koutecky-Levich analysis; Tafel analysis

Journal: Frontiers in Energy Research; DOI: 10.3389/fenrg.2020.00155
Submitted on 27 March 2020; accepted on 22 June 2020

[a] *Freie Universität Berlin, Arnimallee 22, 14195 Berlin, Germany*

[b] *Universität Bayreuth, Universitätsstr. 30, 95447 Bayreuth, Germany*

[*] *Correspondence: Tim Tichter, t.tichter@fu-berlin.de*

ROTATING RING-DISC ELECTRODE MEASUREMENTS FOR THE QUANTITATIVE ELECTROKINETIC INVESTIGATION OF THE V^{3+}-REDUCTION AT MODIFIED CARBON ELECTRODES

Tim Tichter, Jonathan Schneider, Duc Nguyen Viet,
Alvaro Diaz Duque, Christina Roth

DOI: 10.1016/j.jelechem.2020.113843

Individual contributions

Tim Tichter:
Conceptualization, Methodology, Software, Writing – original draft, Writing – review & editing, Visualization

Jonathan Schneider:
Conceptualization, Software, Writing – review & editing

Duc Nguyen Viet:
Investigation, Validation

Alvaro Diaz Duque:
Conceptualization, Writing - review & editing, Software

Christina Roth:
Supervision, Funding acquisition, Writing – review & editing

ROTATING RING-DISC ELECTRODE MEASUREMENTS FOR THE QUANTITATIVE ELECTROKINETIC INVESTIGATION OF THE V^{3+}-REDUCTION AT MODIFIED CARBON ELECTRODES

Tim Tichter[a,*], Jonathan Schneider[a], Duc Nguyen Viet[a], Alvaro Diaz Duque[a], Christina Roth[b]

Abstract

Thin film rotating-ring disc electrode (RRDE) technique is exploited to quantify the parasitic hydrogen evolution reaction (HER) competing with the desired V^{3+}-reduction at surface modified carbon nanoparticles for application as electrocatalysts in the negative half-cell of vanadium redox-flow batteries (VRFB). Carbon based electrode materials are derived from standard Vulcan XC-72 carbon, treated by chemical surface etching techniques proposed for carbon felt-electrodes in the literature. Additional electrochemical characterization is performed using stationary cyclic voltammetry (CV) followed by fitting of CV data, Fourier-transform alternating-current cyclic voltammetry (FT-ACCV) and electrochemical impedance spectroscopy (EIS) followed by distribution of relaxation times (DRT) analysis. To our knowledge the present paper is the first study using the RRDE technique for separating HER and V^{3+}-reduction reactions. It is demonstrated that the ratio of HER to V^{3+}-reduction significantly depends on the chemical pretreatment of the carbon electrodes and that the V^{3+}-reduction proceeds at an optimum rate at $E - E_{RHE} = -0.45$ V. Separating the HER from the V^{3+}-reduction also allows us to provide highly accurate values for the diffusion coefficient of the V^{3+}-ion in sulfuric acid solutions.

Keywords: Vanadium redox-flow batteries; Rotating ring-disc electrode; Cyclic voltammetry fitting; Distribution of relaxation times analysis; Carbon based electrodes

Journal: J. Electroanal. Chem.; DOI: 10.1016/j.jelechem.2020.113843
Submitted on 30 September 2019; accepted on 09 January 2020

[a] *Freie Universität Berlin, Arnimallee 22, 14195 Berlin, Germany*

[b] *Universität Bayreuth, Universitätsstr. 30, 95447 Bayreuth, Germany*

[*] *Correspondence: Tim Tichter, t.tichter@fu-berlin.de*

THEORY OF CYCLIC VOLTAMMETRY IN RANDOM ARRAYS OF CYLINDRICAL MICROELECTRODES APPLIED TO CARBON FELT ELECTRODES FOR VANADIUM REDOX FLOW BATTERIES

Tim Tichter, Dirk Andrae, Jacob Mayer, Jonathan Schneider, Marcus Gebhard, Christina Roth

DOI: 10.1039/C9CP00548J

Individual contributions

Tim Tichter:
Conceptualization, Developing the theory, Methodology, Scientific programming, Writing – original draft, Writing – review & editing

Dirk Andrae:
Scientific discussion (mathematics), Writing – original draft

Jacob Mayer:
Data acquisition (electrochemistry)

Jonathan Schneider:
Data acquisition (electrochemistry)

Marcus Gebhard:
Data acquisition (scanning electron microscopy)

Christina Roth:
Supervision, Funding acquisition

THEORY OF CYCLIC VOLTAMMETRY IN RANDOM ARRAYS OF CYLINDRICAL MICROELECTRODES APPLIED TO CARBON FELT ELECTRODES FOR VANADIUM REDOX FLOW BATTERIES

Tim Tichter[a,*], Dirk Andrae[a], Jacob Mayer[a], Jonathan Schneider[a], Marcus Gebhard[b], Christina Roth[b]

Abstract

In order to quantitatively investigate the kinetic performance and the pore size distribution of carbon felt electrodes for the application in vanadium redox flow batteries, the theory of cyclic voltammetry (CV) is derived for a random network of cylindrical microelectrodes on the base of convolutive modeling. In this context we present an algorithm based on the use of a modified Talbot contour for inverse Laplace transformation, providing the mass transfer functions required for the calculation of the CV responses in external cylindrical finite diffusion space. First order homogenous chemical kinetics preceding and/or following the electrochemical reactions are implemented in this algorithm as well. The VO^{2+} oxidation is investigated as model reaction at pristine and electrochemically aged commercial carbon felt electrodes. A fit of simulated data to experimental data clearly shows that an electrochemical aging predominantly affects the kinetics of the electron transfer reaction and that internal electrode surfaces and pore size distributions remain constant. The estimated pore size distributions are in excellent agreement with porosimetry measurements, validating our theory and providing a new strategy to determine electrode porosities and electrode kinetics simultaneously via CV.

Keywords: Modified Talbot contour; convolution; finite external cylindrical diffusion space; vanadium redox flow batteries; felt electrodes

Journal: PCCP; DOI: 10.1039/C9CP00548J
Submitted on 28 January 2019; accepted on 01 March 2019

[a] *Freie Universität Berlin, Arnimallee 22, 14195 Berlin, Germany*

[b] *Universität Bayreuth, Universitätsstr. 30, 95447 Bayreuth, Germany*

[*] *Correspondence: Tim Tichter, t.tichter@fu-berlin.de*

UNIVERSAL ALGORITHM FOR SIMULATING AND EVALUATING CYCLIC VOLTAMMETRY AT MACROPOROUS ELECTRODES BY CONSIDERING RANDOM ARRAYS OF MICROELECTRODES

Tim Tichter, Jonathan Schneider, Dirk Andrae,
Marcus Gebhard, Christina Roth

DOI: 10.1002/cphc.201901113

Individual contributions

Tim Tichter:
Conceptualization, Developing the theory, Methodology, Scientific programming, Writing – original draft, Writing – review, Developing the related software, Data acquisition (electrochemistry)

Jonathan Schneider:
Data acquisition (electrochemistry), Scientific discussion (electrochemistry)

Dirk Andrae:
Scientific discussion (mathematics), Writing – original draft

Marcus Gebhard:
Data acquisition (scanning electron microscopy), Visualization

Christina Roth:
Supervision, Funding acquisition

UNIVERSAL ALGORITHM FOR SIMULATING AND EVALUATING CYCLIC VOLTAMMETRY AT MACROPOROUS ELECTRODES BY CONSIDERING RANDOM ARRAYS OF MICROELECTRODES

Tim Tichter[a,*], Jonathan Schneider[a], Dirk Andrae[a], Marcus Gebhard[b], Christina Roth[b]

Abstract

An algorithm for the simulation and evaluation of cyclic voltammetry (CV) at macroporous electrodes such as felts, foams, and layered structures is presented. By considering 1D, 2D, and 3D arrays of electrode sheets, cylindrical microelectrodes, hollow cylindrical microelectrodes, and hollow-spherical microelectrodes the internal diffusion domains of the macroporous structures are approximated. A universal algorithm providing the time-dependent surface concentrations of the electrochemically active species, required for simulating cyclic voltammetry responses of the individual planar, cylindrical, and spherical microelectrodes, is presented as well. An essential ingredient of the algorithm, which is based on Laplace integral transformation techniques, is the use of a modified Talbot contour for the inverse Laplace transformation. It is demonstrated that first-order homogeneous chemical kinetics preceding and/or following the electrochemical reaction and electrochemically active species with non-equal diffusion coefficients can be included in all diffusion models as well. The proposed theory is supported by experimental data acquired for a reference reaction, the oxidation of $[Fe(CN)_6]^{4-}$ at platinum electrodes as well as for a technically relevant reaction, the oxidation of VO^{2+} at carbon felt electrodes. Based on our calculation strategy, we provide a powerful open source tool for simulating and evaluating CV data implemented into a Python graphical user interface (GUI).

Keywords: convolution; cyclic voltammetry; diffusion; porous electrodes; modified Talbot contour

Journal: ChemPhysChem; DOI: 10.1002/cphc.201901113
Submitted on 20 November 2019; accepted on 16 December 2019

[a] *Freie Universität Berlin, Arnimallee 22, 14195 Berlin, Germany*

[b] *Universität Bayreuth, Universitätsstr. 30, 95447 Bayreuth, Germany*

[*] *Correspondence: Tim Tichter, t.tichter@fu-berlin.de*

REAL-SPACE SIMULATION OF CYCLIC VOLTAMMETRY IN CARBON FELT ELECTRODES BY COMBINING MICRO X-RAY CT DATA, DIGITAL SIMULATION AND CONVOLUTIVE MODELING

Tim Tichter, Dirk Andrae, Jonathan Schneider, Marcus Gebhard, André Hilger, Ingo Manke, Christina Roth

DOI: 10.1016/j.electacta.2020.136487

Individual contributions

Tim Tichter:
Conceptualization, Methodology, Data acquisition (electrochemistry), Software, Writing original draft, Writing review

Dirk Andrae:
Methodology, Scientific Discussion (Mathematics), Writing original draft, Writing review & editing.

Jonathan Schneider:
Conceptualization, Scientific discussion (electrochemistry), Software, Writing original draft, Writing review & editing

Marcus Gebhard:
Scientific discussion (electrochemistry), Visualization

André Hilger:
X-ray tomography measurements and data processing

Ingo Manke:
X-ray tomography measurements and data processing

Christina Roth:
Supervision, Funding acquisition

REAL-SPACE SIMULATION OF CYCLIC VOLTAMMETRY IN CARBON FELT ELECTRODES BY COMBINING MICRO X-RAY CT DATA, DIGITAL SIMULATION AND CONVOLUTIVE MODELING

Tim Tichter[a,*], Dirk Andrae[a], Jonathan Schneider[a], Marcus Gebhard[b], André Hilger[c], Ingo Manke[c], Christina Roth[b]

Abstract

A novel four-step strategy for real-space simulation of cyclic voltammetry (CV) at carbon felt electrodes is presented, circumventing the diffusion domain approximation approach used so far for CV simulation at porous electrodes. At first, the three-dimensional template of the internal electrode structure is constructed from micro X-ray tomography measurements. Subsequently, by exploiting the Douglas–Gunn modification of the three-dimensional Crank–Nicolson algorithm to Cottrellian boundary conditions, the mass transfer controlled current of this "true" network is obtained. Based on this current, the third step is to compute the mass transfer functions related to the electrode under investigation by an inverse convolution algorithm. In this manner, the spatial dimensionality of the system is reduced from three to one, resulting in significant savings in computation time. The fourth and final step is then to simulate CV experiments via classical convolution methods, featuring the great advantage that any degree of electrochemical reversibility, coupled homogeneous reactions, electrolyte resistances and double layer capacities can be inplemented readily. As a proof of concept, the simulations are supported by experimental data acquired for the oxidation of VO^{2+} in carbon felt electrodes.

Keywords: Convolution; Crank–Nicolson technique; Douglas–Gunn algorithm; Porous electrodes; Vanadium redox-flow batteries

Journal: Electrochimica Acta; DOI: 10.1016/j.electacta.2020.136487
Submitted on 11 April 2020; accepted on 20 May 2020

[a] *Freie Universität Berlin, Arnimallee 22, 14195 Berlin, Germany*

[b] *Universität Bayreuth, Universitätsstr. 30, 95447 Bayreuth, Germany*

[c] *Helmholtz-Zentrum Berlin, Hahn-Meitner-Platz 1, 14109 Berlin, Germany*

[*] *Correspondence: Tim Tichter, t.tichter@fu-berlin.de*

Chapter 7

Conclusion and Future Perspectives

In this cumulative thesis, the classical theory of cyclic voltammetry was extended to (macro)porous electrode structures. In particular, two different models for describing carbon felt electrodes were developed which are summarized graphically in figure 7.1. At first, by regarding felt electrodes as an array of individual cylindrical microelectrodes in a finite external cylindrical diffusion domain with a statistically fluctuating size, a method oriented approach for describing porous electrode structures was provided. This model was referred to as diffusion domain approximation. Since the CV responses of the individual microelectrodes were simulated on the base of Laplace integral transformation techniques and convolutive modeling, implementing the effects of homogeneous chemical reactions preceeding and/or following the heterogeneous electron transfer was readily possible by exploiting the so-called master equation approach. In this context, the Laplace domain solution of the mass transfer function of an electrode reaction which occurs in a finite external cylindrical diffusion domain and which is coupled to homogeneous chemical reactions was derived for the first time. Since no analytic function in the time-domain, related to this particular Laplace domain solution, could be found the concept of numerical inverse Laplace transformation was exploited. For this purpose, a modified Talbot contour was first ever utilized in the context of electrochemistry. In this manner, it was possible to readily simulate cyclic voltammetry experiments at carbon felt electrodes to high accuracy. As a proof of

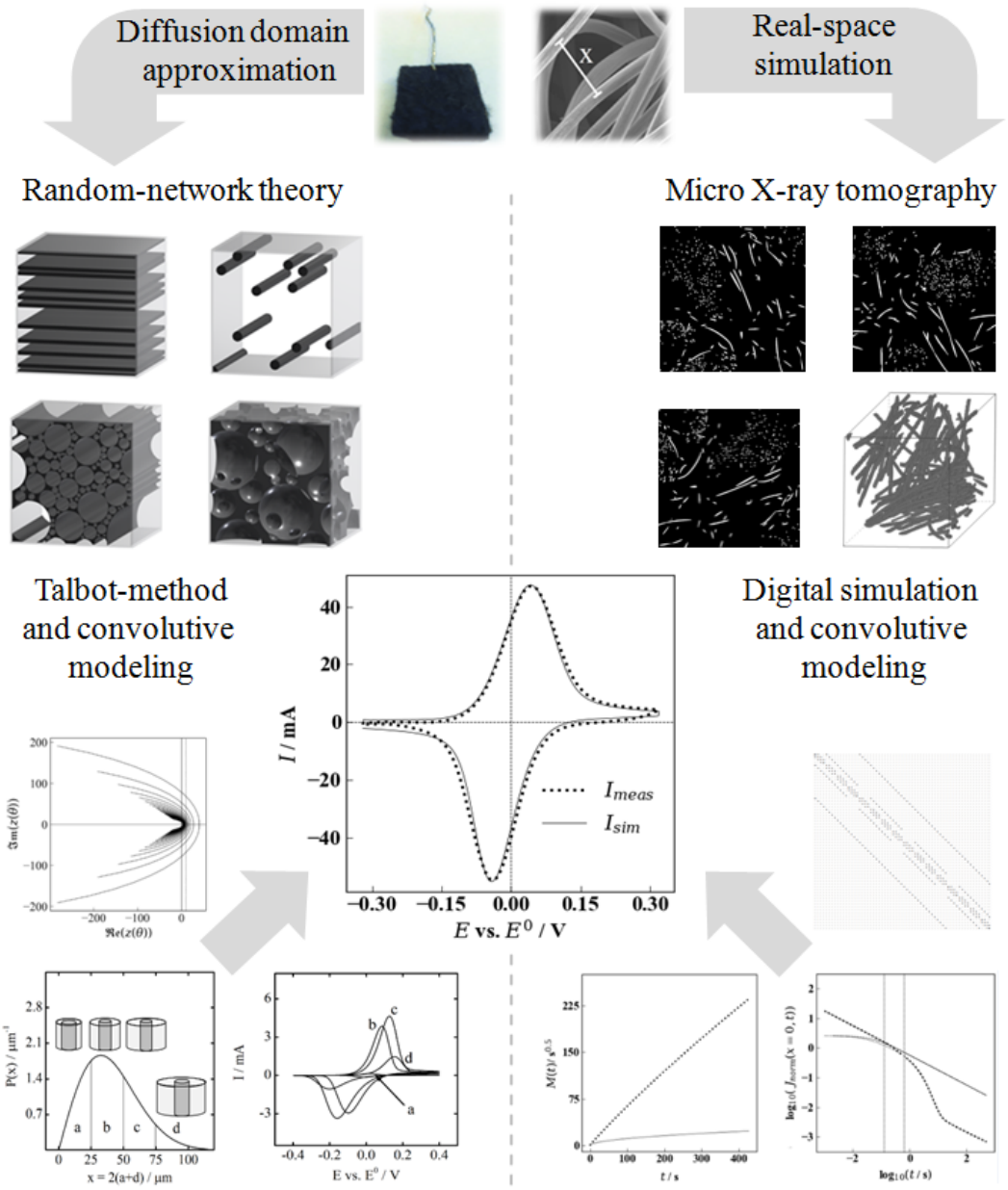

Figure 7.1: Graphical summary of the two strategies for the simulation and evaluation of cyclic voltammetry experiments at macroporous electrodes which have been developed throughout this thesis.

concept, the simulations were supported by experimental data acquired for the electrochemical oxidation of the oxovanadyl cation at carbon felt electrodes.

In a follow up study, the diffusion domain approximation approach which was initially designed for carbon felt electrodes was generalized to layered electrode structures, electrodes with a hollow cylindrical pore structure and electrode foams. In order to provide the experimentalists community with a novel and reliable way of interpreting cyclic voltammetry data at porous electrode sturctures, this generalized diffusion domain approximation was implemented into a powerful open source tool for simulating and evaluating electroanalytical experiments, which was named *Polarographica*.

Since any diffusion domain approximation excludes the effect of overlapping diffusion zones inside of the random network by definition, a second — yet much more sophisticated — model for cyclic voltammetry at carbon felt electrodes was created in the final publication related to this thesis. This model utilizes the real-space template of the diffusion domain, which was experimentally acquired by means of micro X-ray tomography. Based on a novel four-step strategy which involves digital simulation and convolutive modeling, the CV responses related to this real-space template of the diffusion domain were simulated. Since this strategy implicitly involves the Laplace transformation technique, it preserves the advantages of convolutive modeling. It therefore features that a master equation can be utilized even in case of the anisotropic diffusion domain of a porous electrode. In order to cover an even broader range of experimental cicumstances, the contributions of interfacial double layer capacities and the non-linear effects of coupled ohmic resistances, present in almost any realistic electroanalytical experiment, have been included as well. Together with the effects of coupled homogeneous chemical reactions and the concept of finite heterogeneous electron transfer kinetics which has been developed in this thesis, the novel model provides a maximum flexibility for simulating and evaluating cyclic voltammetry experiments at porous electrodes. Since interpreting CV experimental data at porous electrodes on the base of this novel model provides an excellent agreement with reference measurements under well-defined diffusion conditions it was concluded that the inherent ambiguity of cyclic voltammetry at porous electrodes was finally overcome.

However, since any theoretical model captures a limited extent of experimental circumstances only, also the concepts presented in this thesis require for continuous improvements and refinements. In this context, particularly the real-space simulation technique might be extended to account for internal Ohmic drop effects inside of porous electrode structures according to a transmission line model. Furthermore, the implementation of parasitic reactions might be performed in terms of convoluted currents rather than by the recent superposition approach. Finally,

complex reaction mechanisms and more decent theories of the electron transfer might be incorporated in the recent model. These can eventually account for almost any experimental situation and draw a conclusive picture on the electrode kinetics in each and every occasion.

In order to provide experimentalists with all the novel strategies for simulating and evaluating electroanalytical experiments at (macro)porous electrode structures, the ultimate target remains in continuously implementing future developments into *Polarographica*. This will allow for a facile, GUI-supported and standardized evaluation of experimentally acquired data which will eventually lead to a reliable interpretation of electrode kinetics and might be therefore beneficial for the entire electrochemistry community.

Bibliography

[1] L. Lu, X. Han, J. Li, J. Hua, and M. Ouyang, A review on the key issues for lithium-ion battery management in electric vehicles, *Journal of Power Sources*, 226, 272–288, **2013**. doi: 10.1016/j.jpowsour.2012.10.060.

[2] B. Zhao, R. Ran, M. Liu, and Z. Shao, A comprehensive review of $Li_4Ti_5O_{12}$-based electrodes for lithium-ion batteries: The latest advancements and future perspectives, *Materials Science and Engineering R*, 98, 1–71, **2015**. doi: 10.1016/j.mser.2015.10.001.

[3] G. Zubi, R. Dufo-López, M. Carvalho, and G. Pasaoglu, The lithium-ion battery: State of the art and future perspectives, *Renewable and Sustainable Energy Reviews*, 89, 292–308, **2018**. doi: 10.1016/j.rser.2018.03.002.

[4] G. J. May, A. Davidson, and B. Monahov, Lead batteries for utility energy storage: A review, *Journal of Energy Storage*, 15, 145–157, **2018**. doi: 10.1016/j.est.2017.11.008.

[5] A. Yilanci, I. Dincer, and H. K. Ozturk, A review on solar-hydrogen/fuel cell hybrid energy systems for stationary applications, *Progress in Energy and Combustion Science*, 35, 231–244, **2009**. doi: 10.1016/j.pecs.2008.07.004.

[6] C. Ziogou, D. Ipsakis, C. Elmasides, F. Stergiopoulos, S. Papadopoulou, P. Seferlis, and S. Voutetakis, Automation infrastructure and operation control strategy in a stand-alone power system based on renewable energy sources, *Journal of Power Sources*, 196, 9488– 9499, **2011**. doi: 10.1016/j.jpowsour.2011.07.029.

[7] S. Tesfahunegn, O. Ulleberg, P. Vie, and T. Undeland, Optimal shifting of Photovoltaic and load fluctuations from fuel cell and electrolyzer to lead acid battery in a Photovoltaic/hydrogen standalone power system for improved performance and life time, *Journal of Power Sources*, 196, 10401– 10414, **2011**. doi: 10.1016/j.jpowsour.2011.06.037.

[8] G. Gahleitner, Hydrogen from renewable electricity: An international review of power-to-gas pilot plants for stationary applications, *International Journal of Hydrogen Energy*, 38, 2039–2061, **2013**. doi: 10.1016/j.ijhydene.2012.12.010.

[9] A. González, E. Goikolea, J. A. Barrena, and R. Mysyk, Review on supercapacitors: Technologies and materials, *Renewable and Sustainable Energy Reviews*, 58, 1189–1206, **2016**. doi: 10.1016/j.rser.2015.12.249.

[10] Q. Li, M. Horn, Y. Wang, J. MacLeod, N. Motta, and J. Liu, A Review of Supercapacitors Based on Graphene and Redox-Active Organic Materials, *Materials*, 12, 1–30, **2019**. doi: 10.3390/ma12050703.

[11] Poonam, K. Sharma, A. Arora, and S. K. Tripathi, Review of supercapacitors: Materials and devices, *Journal of Energy Storage*, 21, 801–825, **2019**. doi: 10.1016/j.est.2019.01.010.

[12] T. Surawan and P. S. Priambodo, Supercapacitor Based On Active Carbon Electrode: Review, *2019 16th International Conference on Quality in Research (QIR): International Symposium on Electrical and Computer Engineering*, 1–8, **2019**. doi: 10.1109/QIR.2019.8898254.

[13] R. Dubey and V. Guruviah, Review of carbon-based electrode materials for supercapacitor energy storage, *Ionics*, 25, 1419–1445, **2019**. doi: 10.1007/s11581-019-02874-0.

[14] G. Kear, A. A. Shah, and F. C. Walsh, Development of the all - vanadium redox flow battery for energy storage: a review of technological, financial and policy aspects, *International Journal of Energy Research*, 36, 1105–1120, **2011**. doi: 10.1002/er.1863.

[15] W. Wang, Q. Luo, B. Li, X. Wei, L. Li, and Z. Yang, Recent Progress in Redox Flow Battery Research and Development, *Advanced Functional Materials*, 23, 970–986, **2012**. doi: 10.1002/adfm.201200694.

[16] K. J. Kim, M.-S. Park, Y.-J. Kim, J. H. Kim, S. X. Dou, and M. Skyllas-Kazacos, A technology review of electrodes and reaction mechanisms in vanadium redox flow batteries, *Journal of Materials Chemistry A*, 3, 16913–16933, **2015**. doi: 10.1039/C5TA02613J.

[17] F. Pan and Q. Wang, Redox Species of Redox Flow Batteries: A Review, *Molecules*, 20, 20499–20517, **2015**. doi: 10.3390/molecules201119711.

[18] M. Park, J. Ryu, W. Wang, and J. Cho, Material design and engineering of next-generation flow battery technologies, *Nature Reviews Materials*, 2, 2058–8437, **2016**. doi: 10.1038/natrevmats.2016.80.

[19] M. Skyllas-Kazacos, L. Cao, M. Kazacos, N. Kausar, and A. Mousa, Vanadium Electrolyte Studies for the Vanadium Redox Battery—A Review, *ChemSusChem*, 9, 1–24, **2016**. doi: 10.1002/cssc.201600102.

[20] C. Choi, S. Kim, R. Kim, Y. Choi, S. Kim, H.-y. Jung, J. H. Yang, and H.-T. Kim, A review of vanadium electrolytes for vanadium redox flow batteries, *Renewable and Sustainable Energy Reviews*, 69, 263–274, **2017**. doi: 10.1016/j.rser.2016.11.188.

[21] H. R. Jiang, J. Sun, L. Wei, M. C. Wu, W. Shyy, and T. S. Zhao, A high power density and long cycle life vanadium redox flow battery, *Energy Storage Materials*, 24, 529–540, **2020**. doi: 10.1016/j.ensm.2019.07.005.

[22] T. Wu, K. Huang, S. Liu, and S. Zhuang, Hydrothermal ammoniated treatment of PAN-graphite felt for vanadium redox flow battery, *Journal of Solid State Electrochemistry*, 16, 579–585, **2012**. doi: 10.1007/s10008-011-1383-y.

[23] C. Flox, J. Rubio-García, M. Skoumal, T. Andreu, and J. R. Morante, Thermo–chemical treatments based on NH_3 / O_2 for improved graphite-based fiber electrodes in vanadium redox flow batteries, *Carbon*, 60, 280–288, **2013**. doi: 10.1016/j.carbon.2013.04.038.

[24] Z. Zhang, J. Xi, H. Zhou, and X. Qiu, KOH etched graphite felt with improved wettability and activity for vanadium flow batteries, *Electrochimica Acta*, 218, 15–23, **2016**. doi: 10.1016/j.electacta.2016.09.099.

[25] L. Dai, Y. Jiang, W. Meng, H. Zhou, L. Wang, and Z. He, Improving the electrocatalytic performance of carbon nanotubes for $VO^{2+}/VO_2{}^{+}$ redox reaction by KOH activation, *Applied Surface Science*, 401, 106–113, **2017**. doi: 10.1016/j.apsusc.2017.01.002.

[26] L. Yue, W. Li, F. Sun, L. Zhao, and L. Xing, Highly hydroxylated carbon fibres as electrode materials of all-vanadium redox flow battery, *Carbon*, 48, 3079–3090, **2010**. doi: 10.1016/j.carbon.2010.04.044.

[27] C. Gao, N. Wang, S. Peng, S. Liu, Y. Lei, X. Liang, S. Zeng, and H. Zi, Influence of Fenton's reagent treatment on electrochemical properties of graphite felt for all vanadium redox flow battery, *Electrochimica Acta*, 88, 193–202, **2013**. DOI: 10.1016/j.electacta.2012.10.021.

[28] K. J. Kim, S. Lee, J. Kim, M. Park, H. Kim, Y.-J. Kim, and M. Skyllas-Kazacos, Superior Electrocatalytic Activity of a Robust Carbon-Felt Electrode with Oxygen-Rich Phosphate Groups for All- Vanadium Redox Flow Batteries, *ChemSusChem*, 9, 1329–1338, **2016**. DOI: 10.1002/cssc.201600106.

[29] Z. He, Y. Jiang, Y. Li, J. Zhu, H. Zhou, W. Meng, L. Wang, and L. Dai, Carbon layer-exfoliated, wettability-enhanced, SO_3H-functionalized carbon paper: A superior positive electrode for vanadium redox flow battery, *Carbon*, 127, 297–304, **2018**. DOI: 10.1016/j.carbon.2017.11.006.

[30] E.-M. Hammer, B. Berger, and L. Komsiyska, Improvement of the Performance of Graphite Felt Electrodes for Vanadium-Redox-Flow-Batteries by Plasma Treatment, *International Journal of Renewable Energy Develoepement*, 3, 7–12, **2014**. DOI: 10.14710/ijred.3.1.7-12.

[31] D. Dixon, D. Babu, J. Langner, M. Bruns, L. Pfaffmann, A. Bhaskar, J. J. Schneider, F. Scheiba, and H. Ehrenberg, Effect of oxygen plasma treatment on the electrochemical performance of the rayon and polyacrylonitrile based carbon felt for the vanadium redox flow battery application, *Journal of Power Sources*, 332, 240 –248, **2016**. DOI: 10.1016/j.jpowsour.2016.09.070.

[32] M. Park, I.-Y. Jeon, J. Ryu, H. Jang, J.-B. Back, and J. Cho, Edge-halogenated graphene nanoplatelets with F , Cl , or Br as electrocatalysts for all-vanadium redox flow batteries, *Nano Energy*, 26, 233–240, **2016**. DOI: 10.1016/j.nanoen.2016.05.027.

[33] Y. Shao, X. Wang, M. Engelhard, C. Wang, S. Dai, J. Liu, Z. Yang, and Y. Lin, Nitrogen-doped mesoporous carbon for energy storage in vanadium redox flow batteries, *Journal of Power Sources*, 195, 4375–4379, **2010**. DOI: 10.1016/j.jpowsour.2010.01.015.

[34] J Jin, X Fu, Q Liu, Y Liu, Z Wei, K Niu, and J Zhang, Identifying the Active Site in Nitrogen-Doped Graphene for the $VO^{2+}/VO_2{}^{+}$ Redox Reaction, *ACS Nano*, 7, 4764–4773, **2013**. DOI: 10.1021/nn3046709.

[35] S. Park and H. Kim, Fabrication of nitrogen-doped graphite felts as positive electrodes using polypyrrole as a coating agent in vanadium redox flow batteries, *Journal of Materials Chemistry A*, 3, 12276–12283, **2015**. doi: 10.1039/C5TA02674A.

[36] L. Wu, Y. Shen, L. Yu, J. Xi, and X. Qiu, Boosting vanadium flow battery performance by Nitrogen-doped carbon nanospheres electrocatalyst, *Nano Energy*, 28, 19–28, **2016**. doi: 10.1016/j.nanoen.2016.08.025.

[37] D.-S. Yang, J. H. Han, J. W. Jeon, J. Y. Lee, D.-G. Kim, D. H. Seo, B. G. Kim, T.-H. Kim, and Y. T. Hong, Multimodal porous and nitrogen-functionalized electrode based on graphite felt modified with carbonized porous polymer skin layer for all-vanadium redox flow battery, *Materials Today Energy*, 11, 159–165, **2019**. doi: 10.1016/j.mtener.2018.11.003.

[38] P. Han, H. Wang, Z. Liu, X. Chen, W. Ma, J. Yao, Y. Zhu, and G. Cui, Graphene oxide nanoplatelets as excellent electrochemical active materials for $VO^{2+}/VO_2{}^{+}$ and V^{2+}/V^{3+} redox couples for a vanadium redox flow battery, *Carbon*, 49, 693–700, **2011**. doi: 10.1016/j.carbon.2010.10.022.

[39] W. Li, J. Liu, and C. Yan, Multi-walled carbon nanotubes used as an electrode reaction catalyst for $VO^{2+}/\ VO_2{}^{+}$ for a vanadium redox flow battery, *Carbon*, 49, 3463–3470, **2011**. doi: 10.1016/j.carbon.2011.04.045.

[40] W. Li, J. Liu, and C. Yan, The electrochemical catalytic activity of single-walled carbon nanotubes towards $VO^{2+}/\ VO_2{}^{+}$ and V^{3+}/V^{2+} redox pairs for an all vanadium redox flow battery, *Electrochimica Acta*, 79, 102–108, **2012**. doi: 10.1016/j.electacta.2012.06.109.

[41] S. Wang, X. Zhao, T. Cochell, and A. Manthiram, Nitrogen-Doped Carbon Nanotube/Graphite Felts as Advanced Electrode Materials for Vanadium Redox Flow Batteries, *Journal of Physical Chemistry Letters*, 3, 2164–2167, **2012**. doi: 10.1021/jz3008744.

[42] Z. González, C. Botas, P. Álvarez, S. Roldán, C. Blanco, R. Santamaría, M. Granda, and R. Menéndez, Thermally reduced graphite oxide as positive electrode in Vanadium Redox Flow Batteries, *Carbon*, 50, 828–834, **2012**. doi: 10.1016/j.carbon.2011.09.041.

[43] W. Li, J. Liu, and C. Yan, Reduced graphene oxide with tunable C/O ratio and its activity towards vanadium redox pairs for an all vanadium redox flow battery, *Carbon*, 55, 313–320, **2013**. DOI: 10.1016/j.carbon.2012.12.069.

[44] M. Park, Y.-J. Jung, J. Kim, H. I. Lee, and J. Cho, Synergistic Effect of Carbon Nano fiber/Nanotube Composite Catalyst on Carbon Felt Electrode for High-Performance All-Vanadium Redox Flow Battery, *Nano Letters*, 13, 4833–4839, **2013**. DOI: 10.1021/nl402566s.

[45] N. Pour, D. G. Kwabi, T. J. Carney, R. M. Darling, M. L. Perry, and Y. Shao-horn, Influence of Edge- and Basal-Plane Sites on the Vanadium Redox Kinetics for Flow Batteries, *Journal of Physical Chemistry C*, 119, 5311–5318, **2015**. DOI: 10.1021/jp5116806.

[46] L Wei, T. S. Zhao, G Zhao, L An, and L Zeng, A high-performance carbon nanoparticle-decorated graphite felt electrode for vanadium redox flow batteries, *Applied Energy*, 176, 74–79, **2016**. DOI: 10.1016/j.apenergy.2016.05.048.

[47] Z. González, C. Flox, C. Blanco, M. Granda, J. R. Morante, R. Menéndez, and R. Santamaría, Outstanding electrochemical performance of a graphene-modified graphite felt for vanadium redox flow battery application, *Journal of Power Sources*, 338, 155–162, **2017**. DOI: 10.1016/j.jpowsour.2016.10.069.

[48] K. M. Tenny, V. S. Lakhanpal, R. P. D. Jr, V. Yarlagadda, and T. V. Nguyen, Impact of Multi-Walled Carbon Nanotube Fabrication on Carbon Cloth Electrodes for Hydrogen-Vanadium Reversible Fuel Cells, *Journal of The Electrochemical Society*, 164, 2534–2538, **2017**. DOI: 10.1149/2.1151712jes.

[49] H. Kabir, I. O. Gyan, and I. F. Cheng, Electrochemical modification of a pyrolytic graphite sheet for improved negative electrode performance in the vanadium redox flow battery, *Journal of Power Sources*, 342, 31–37, **2017**. DOI: 10.1016/j.jpowsour.2016.12.045.

[50] H.-M. Tsai, S.-J. Yang, C.-C. M. Ma, and X. Xie, Preparation and electrochemical activities of iridium-decorated graphene as the electrode for all-vanadium redox flow batteries, *Electrochimica Acta*, 77, 232–236, **2012**. DOI: 10.1016/j.electacta.2012.05.099.

[51] C. Flox, M. Skoumal, J. Rubio-garcia, T. Andreu, and J. R. Morante, Strategies for enhancing electrochemical activity of carbon-based electrodes for all-vanadium redox flow batteries, *Applied Energy*, 109, 344–351, **2013**. doi: 10.1016/j.apenergy.2013.02.001.

[52] T.-M. Tseng, R.-H. Huang, C.-Y. Huang, K.-L. Hsueh, and F.-S. Shieu, Improvement of Titanium Dioxide Addition on Carbon Black Composite for Negative Electrode in Vanadium Redox Flow Battery, *Journal of the Electrochemical Society*, 160, 1269–1275, **2013**. doi: 10.1149/2.082308jes.

[53] B. Li, M. Gu, Z. Nie, X. Wei, C. Wang, V. Sprenkle, and W. Wang, Nanorod Niobium Oxide as Powerful Catalysts for an All Vanadium Redox Flow Battery, *Nano Letters*, 14, 158–165, **2014**. doi: 10.1021/nl403674a.

[54] T.-M. Tseng, R.-H. Huang, C.-Y. Huang, C.-C. Liu, K.-L. Hsueh, and F.-S. Shieu, Carbon Felt Coated with Titanium Dioxide / Carbon Black Composite as Negative Electrode for Vanadium Redox Flow, *Journal of the Electrochemical Society*, 161, 1132–1138, **2014**. doi: 10.1149/2.102406jes.

[55] D. J. Suárez, Z. Gonzalez, C. Blanco, M. Granda, R. Menendez, and S. Ricardo, Graphite Felt Modified with Bismuth Nanoparticles as Negative Electrode in a Vanadium Redox Flow Battery, *ChemSusChem*, 7, 914–918, **2014**. doi: 10.1002/cssc.201301045.

[56] C. Yang, H. Wang, S. Lu, C. Wu, Y. Liu, Q. Tan, D. Liang, and Y. Xiang, Titanium nitride as an electrocatalyst for V(II)/V(III) redox couples in all-vanadium redox flow batteries, *Electrochimica Acta*, 182, 834–840, **2015**. doi: 10.1016/j.electacta.2015.09.155.

[57] T. Liu, X. Li, H. Nie, C. Xu, and H. Zhang, Investigation on the effect of catalyst on the electrochemical performance of carbon felt and graphite felt for vanadium flow batteries, *Journal of Power Sources*, 286, 73–81, **2015**. doi: 10.1016/j.jpowsour.2015.03.148.

[58] H. Zhou, Y. Shen, J. Xi, X. Qiu, and L. Chen, ZrO_2 - Nanoparticle-Modified Graphite Felt: Bifunctional Effects on Vanadium Flow Batteries, *Applied Materials and Interfaces*, 24, 15369–15378, **2016**. doi: 10.1021/acsami.6b03761.

[59] J. J. Park, J. H. Park, O. O. Park, and J. H. Yang, Highly porous graphenated graphite felt electrodes with catalytic defects for high-performance vanadium redox flow batteries produced via NiO/Ni redox reactions, *Carbon*, 110, 17–26, **2016**. DOI: 10.1016/j.carbon.2016.08.094.

[60] Z. He, M. Li, Y. Li, J. Zhu, Y. Jiang, W. Meng, H. Zhou, L. Wang, and L. Dai, Flexible electrospun carbon nanofiber embedded with TiO_2 as excellent negative electrode for vanadium redox flow battery, *Electrochimica Acta*, 281, 601–610, **2018**. DOI: 10.1016/j.electacta.2018.06.011.

[61] P. C. Ghimire, R. Schweiss, N. Wai, T. M. Lim, A. Bhattarai, T. D. Nguyen, and Q. Yan, Titanium carbide-decorated graphite felt as high performance negative electrode in vanadium redox flow batteries, *Journal of Materials Chemistry A*, 6, 6625–6632, **2018**. DOI: 10.1039/C8TA00464A.

[62] Y. Xiang and W. A. Daoud, Investigation of an advanced catalytic effect of cobalt oxide modification on graphite felt as the positive electrode of the vanadium redox flow battery, *Journal of Power Sources*, 416, 175–183, **2019**. DOI: 10.1016/j.jpowsour.2019.01.079.

[63] M.-A. Goulet, M. Skyllas-Kazacos, and E. Kjeang, The importance of wetting in carbon paper electrodes for vanadium redox reactions, *Carbon*, 101, 390–398, **2016**. DOI: 10.1016/j.carbon.2016.02.011.

[64] F. G. Chevallier, L. Jiang, T. G. J. Jones, and R. G. Compton, Mathematical modelling and numerical simulation of cyclic voltammetry at an electrode covered with an insulating film containing cylindrical micropores, *Journal of Electroanalytical Chemistry*, 587, 254–262, **2006**. DOI: 10.1016/j.jelechem.2005.11.016.

[65] D. Menshykau and R. G. Compton, The Influence of Electrode Porosity on Diffusional Cyclic Voltammetry, *Electroanalysis*, 20, 2387–2394, **2008**. DOI: 10.1002/elan.200804334.

[66] E. O. Barnes, X. Chen, P. Li, and R. G. Compton, Voltammetry at porous electrodes: A theoretical study, *Journal of Electroanalytical Chemistry*, 720, 92–100, **2014**. DOI: 10.1016/j.jelechem.2014.03.028.

[67] R. E. Smith, T. J. Davies, N. d. B. Baynes, and R. J. Nichols, The electrochemical characterisation of graphite felts, *Journal of Electroanalytical Chemistry*, 747, 29–38, **2015**. DOI: 10.1016/j.jelechem.2015.03.029.

[68] A. Peinetti, R. Gilardoni, M. Mizrahi, F. Requejo, G. González, and F. Battaglini, Numerical Simulation of the Diffusion Processes in Nanoelectrode Arrays Using an Axial Neighbor Symmetry Approximation, *Analytical Chemistry*, 88, 5752–5759, **2016**. doi: 10.1021/acs.analchem.6b00039.

[69] H. T. Chan, E. Kätelhön, and R. G. Compton, Voltammetry using multiple cycles: Porous electrodes, *Journal of Electroanalytical Chemistry*, 799, 126–133, **2017**. doi: 10.1016/j.jelechem.2017.05.043.

[70] T. Tichter, D. Andrae, J. Mayer, J. Schneider, M. Gebhard, and C. Roth, Theory of cyclic voltammetry in random arrays of cylindrical microelectrodes applied to carbon felt electrodes for vanadium redox flow batteries, *Physical Chemistry Chemical Physics*, 21, 9061–9068, **2019**. doi: 10.1039/C9CP00548J.

[71] T. Tichter, J. Schneider, D. Andrae, M. Gebhard, and C. Roth, Universal algorithm for simulating and evaluating cyclic voltammetry at macroporous electrodes by considering random arrays of microelectrodes, *ChemPhysChem*, 21, 428 –441, **2019**. doi: 10.1002/cphc.201901113.

[72] A. Lasia, Electrochemical Impedance Spectroscopy and its Applications. Springer, **2014**. doi: 10.1007/978-1-4614-8933-7.

[73] R. G. Compton, E. Laborda, and K. R. Ward, Understanding Voltammetry. World Scientific, **2007**. doi: 10.1142/p726.

[74] H. Matsuda and Y. Ayabe, Zur Theorie der Randles-Ševčík'schen Kathodenstrahl-Polarographie, *Zeitschrift für Elektrochemie*, 59, 494–503, **1954**. doi: 10.1002/bbpc.19550590605.

[75] R. S. Nicholson and I. Shain, Theory of Stationary Electrode Polarography Single Scan and Cyclic Methods Applied to Reversible, Irreversible, and Kinetic Systems, *Analytical Chemistry*, 36, 706–723, **1964**. doi: 10.1021/ac60210a007.

[76] R. S. Nicholson, Theory and Application of Cyclic Voltammetry for Measurement of Electrode Reaction Kinetics, *Analytical Chemistry*, 37, 1351–1355, **1965**. doi: 10.1021/ac60230a016.

[77] K. Aoki, K. Honda, K. Tokuda, and H. Matsuda, Voltammetry at microcylinder electrodes: Part I. Linear sweep voltammetry, *Journal of Electroanalytical Chemistry and Interfacial Electrochemistry*, 182, 267 –279, **1985**. doi: 10.1016/0368-1874(85)87005-2.

[78] K. Aoki and H. Kaneko, Theory of irreversible cyclic voltammograms at microcylinder electrodes, *Journal of Electroanalytical Chemistry and Interfacial Electrochemistry*, 247, 17 –27, **1988**. DOI: 10.1016/0022-0728(88)80127-X.

[79] K. Aoki, K. Tokuda, and H. Matsuda, Theory of linear sweep voltammetry with finite diffusion space, *Journal of Electroanalytical Chemistry and Interfacial Electrochemistry*, 146, 417 –424, **1983**. DOI: 10.1016/S0022-0728(83)80601-9.

[80] K. Aoki, K. Tokuda, and H. Matsuda, Theory of linear sweep voltammetry with finite diffusion space: Part II. Totally irreversible and quasi-reversible cases, *Journal of Electroanalytical Chemistry and Interfacial Electrochemistry*, 160, 33 –45, **1984**. DOI: 10.1016/S0022-0728(84)80113-8.

[81] D. H. Evans, Theory for a homogeneous reaction following a quasireversible electrode reaction, *Journal of Physical Chemistry*, 76, 1160–1165, **1972**. DOI: 10.1021/j100652a013.

[82] J. Savéant and D. Tessier, Convolution potential sweep voltammetry: Part IV. Homogeneous follow-up chemical reactions, *Journal of Electroanalytical Chemistry and Interfacial Electrochemistry*, 61, 251–263, **1975**. DOI: 10.1016/S0022-0728(75)80226-9.

[83] L. K. Bieniasz, Automatic solution of integral equations pertinent to diffusion with first order homogeneous reactions at cylindrical wire electrodes, *Journal of Electroanalytical Chemistry*, 674, 38–47, **2012**. DOI: 10.1016/j.jelechem.2012.04.003.

[84] L. K. Bieniasz, Automatic solution of integral equations describing electrochemical transients under conditions of internal cylindrical diffusion, *Journal of Electroanalytical Chemistry*, 700, 30–39, **2013**. DOI: 10.1016/j.jelechem.2013.04.010.

[85] L. K. Bieniasz, Automatic solution of integral equations describing electrochemical transients under conditions of internal spherical diffusion, *Journal of Electroanalytical Chemistry*, 694, 104–113, **2013**. DOI: 10.1016/j.jelechem.2013.01.043.

[86] J. Friedl and U. Stimming, Determining Electron Transfer Kinetics at Porous Electrodes, *Electrochimica Acta*, 227, 235–245, **2017**. DOI: 10.1016/j.electacta.2017.01.010.

[87] M. Becker and T. Turek, Combination of impedance spectroscopy and potential probe sensing to characterize vanadium redox-flow batteries, *Journal of Power Sources*, 446, 227–349, **2020**. doi: 10.1016/j.jpowsour.2019.227349.

[88] A. J. Bard and L. R. Faulkner, Electrochemical Methods: Fundamentals and Applications. Wiley and Sons, **2001**. doi: 10.1023/A:1021637209564.

[89] D. Britz and J. Strutwolf, Digital Simulation in Electrochemistry. Springer International Publishing, Switzerland, **2016**. doi: 10.1007/978-3-319-30292-8.

[90] J. E. B. Randles, A cathode ray polarograph. Part II. — The current-voltage curves, *Transactions of the Faraday Society*, 44, 327–338, **1948**. doi: 10.1039/TF9484400327.

[91] A. Ševčík, Periodic loading oscillographic polygraphy, *Collection of the Czechoslovakian Chemistry Communications*, 13, 349, **1948**.

[92] V. G. Levich, Physicochemical Hydrodynamics. Prentice-Hall Englewood Cliffs, **1962**.

[93] A. E. Fick, Ueber Diffusion, *Annalen der Physik*, 170, 59–86, **1855**. doi: 10.1002/andp.18551700105.

[94] H. S. Carslaw and J. C. Jaeger, Conduction of Heat in Solids. Oxford University Press, **1959**.

[95] S. W. Feldberg and C. Auerbach, Model for Current Reversal Chronopotentiometry with Second - Order Kinetic Complications, *Analytical Chemistry*, 36, 505–509, **1964**. doi: 10.1021/ac60209a055.

[96] J. Crank and P. Nicolson, A practical method for numerical evaluation of solutions of partial differential equations of the heat-conduction type, *Advances in Computational Mathematics*, 6, 207 –226, **1996**. doi: 10.1007/BF02127704.

[97] J. Heinze, M. Störzbach, and J. Mortensen, Digital simulation of cyclic voltammetric curves by the implicit Crank-Nicolson technique, *Journal of Electroanalytical Chemistry and Interfacial Electrochemistry*, 165, 61 –70, **1984**. doi: 10.1016/S0022-0728(84)80086-8.

[98] M. Rudolph, A fast implicit finite difference algorithm for the digital simulation of electrochemical processes, *Journal of Electroanalytical Chemistry and Interfacial Electrochemistry*, 314, 13 –22, **1991**. doi: 10.1016/0022-0728(91)85425-O.

[99] M. Störzbach and J. Heinze, The Crank Nicolson Technique — an efficient algorithm for the simulation of electrode processes at macro- and microelectrodes, *Journal of Electroanalytical Chemistry*, 346, 1–27, **1993**. doi: 10.1016/0022-0728(93)85001-W.

[100] L. H. Thomas, Elliptic Problems in Linear Differential Equations over a Network, *Watson Science Computer Laboratory Report*, **1949**.

[101] G. Stephenson and P. M. Radmore, Advanced Mathematical Methods for Engineering and Science Students. Cambridge University Press, **1990**. doi: 10.1017/CBO9781139168120.

[102] A. M. Cohen, Numerical Methods for Laplace Transform Inversion. Springer US, **2007**. doi: 10.1007/978-0-387-68855-8.

[103] F. G. Cottrell, Der Reststrom bei galvanischer Polarisation betrachtet als ein Diffusionsproblem, *Zeitschrift für Physikalische Chemie*, 42, 386–431, **1903**. doi: 10.1515/zpch-1903-4229.

[104] F. Oberhettinger and L. Badii, Tables of Laplace Transforms. Springer-Verlag Berlin Heidelberg, **1973**. doi: 10.1007/978-3-642-65645-3.

[105] K. B. Oldham, Convolution: a general electrochemical procedure implemented by a universal algorithm, *Analytical Chemistry*, 58, 2296 –2300, **1986**. doi: 10.1021/ac00124a040.

[106] L. K. Bieniasz, Automatic simulation of electrochemical transients assuming finite diffusion space at planar interfaces, by the adaptive Huber method for Volterra integral equations, *Journal of Electroanalytical Chemistry*, 684, 20–31, **2012**. doi: 10.1016/j.jelechem.2012.08.019.

[107] I. Streeter and R. G. Compton, Linear Sweep Voltammetry at Randomly Distributed Arrays of Microband Electrodes, *Journal of Physical Chemistry C*, 111, 15053–15058, **2007**. doi: 10.1021/jp0747205.

[108] D. Menshykau, I. Streeter, and R. G. Compton, Influence of Electrode Roughness on Cyclic Voltammetry, *Journal of Physical Chemistry C*, 112, 14428–14438, **2008**. doi: 10.1021/jp8047423.

[109] I. Streeter, G. G. Wildgoose, L. Shao, and R. G. Compton, Cyclic voltammetry on electrode surfaces covered with porous layers: An analysis of electron transfer kinetics at single-walled carbon nanotube modified electrodes, *Sensors and Actuators B*, 133, 462–466, **2008**. doi: 10.1021/jp8047423.

[110] A. F. Holloway, D. A. Craven, L. Xiao, J. Del-Campo, and G. G. Wildgoose, Developing Random Network Theory for Carbon Nanotube Modified Electrode Voltammetry: Introduction and Application to Estimating the Potential Drop between MWCNT-MWCNT Contacts, *Journal of Physical Chemistry C*, 112, 13729–13738, **2008**. doi: 10.1021/jp804830a.

[111] N. Godino, X. Borrisé, F. X. Munoz, F. J. Del-Campo, and R. G. Compton, Mass Transport to Nanoelectrode Arrays and Limitations of the Diffusion Domain Approach: Theory and Experiment, *Sensors and Actuators B*, 113, 11119–11125, **2009**. doi: 10.1021/jp9031354.

[112] L. H. Thaller, Electrically Rechargable Redox Flow Cell, *U.S. Patent 3 996 064, Dec. 7*, **1976**.

[113] E. Sum and M. Skyllas-Kazacos, A study of the V(II)/V(III) redox couple for redox flow cell applications, *Journal of Power Sources*, 15, 179–190, **1985**. doi: 10.1016/0378-7753(85)80071-9.

[114] E. Sum, M. Rychcik, and M. Skyllas-Kazacos, Investigation of the V(V)/V(IV) system for use in the positive half-cell of a redox battery, *Journal of Power Sources*, 16, 85–95, **1985**. doi: 10.1016/0378-7753(85)80082-3.

[115] M. Skyllas-Kazacos, All-Vanadium Redox Battery, *U.S. Patent 4 786 567, Nov. 22*, **1988**.

[116] A. Bourke, M. A. Miller, R. P. Lynch, X. Gao, J. Landon, J. S. Wainright, R. F. Savinell, and D. N. Buckley, Electrode Kinetics of Vanadium Flow Batteries: Contrasting Responses of V(I)I-V(III) and V(IV)-V(V) to Electrochemical Pretreatment of Carbon, *Journal of the Electrochemical Society*, 163, 5097–5105, **2016**. doi: 10.1149/2.0131601jes.

[117] V. Krikstolaityte, O. E. Y. Joshua, A. Veksha, N. Wai, G. Lisak, and T. M. Lim, Conversion of Spent Coffee Beans to Electrode Material for Vanadium Redox Flow Batteries, *Batteries*, 4, 56–67, **2018**. doi: 10.3390/batteries4040056.

[118] M. Park, J. Ryu, Y. Kim, and J. Cho, Corn protein-derived nitrogen-doped carbon materials with oxygen-rich functional groups: A highly efficient electrocatalyst for the allvanadium redox flow batteries, *Energy and Environmental Science*, 7, 3727–3735, **2014**. doi: 10.1039/C4EE02123A.

[119] J. Leddy, A. J. Bard, J. T. Maloy, and J. M. Savéant, Kinetics of film-coated electrodes: Effect of a finite mass transfer rate of substrate across the film—solution interface at steady state, *Journal of Electroanalytical Chemistry and Interfacial Electrochemistry*, 187, 205–227, **1985**. DOI: 10.1016/0368-1874(85)85779-8.

[120] C. Montella, LSV modelling of electrochemical systems through numerical inversion of Laplace transforms. I – The GS–LSV algorithm, *Journal of Electroanalytical Chemistry*, 614, 121 –130, **2007**. DOI: 10.1016/j.jelechem.2007.11.010.

[121] C. Montella and J. P. Diard, New approach of electrochemical systems dynamics in the time-domain under small-signal conditions. I. A family of algorithms based on numerical inversion of Laplace transforms, *Journal of Electroanalytical Chemistry*, 623, 29 –40, **2008**. DOI: 10.1016/j.jelechem.2007.11.010.

[122] C. Montella, Re-examination of the potential-step chronoamperometry method through numerical inversion of Laplace transforms. I. General formulation and numerical solution, *Journal of Electroanalytical Chemistry*, 633, 35 –44, **2009**. DOI: 10.1016/j.jelechem.2009.04.019.

[123] H. Stehfest, Numerical inversion of Laplace transforms: Algorithm 368, *Communications of the ACM*, 13, 47 –49, **1970**.

[124] M. C. Henstridge and R. G. Compton, Direct extraction of kinetic parameters from experimental cyclic voltammetry, *Journal of Electroanalytical Chemistry*, 681, 109–112, **2012**. DOI: 10.1016/j.jelechem.2012.06.011.

[125] J. Koutecký and R. Brdička, Fundamental equation for the electrolytic current when depending on the formation rate of the depolariser jointly with diffusion and its polarographic verification, *Collection of the Czechoslovakian Chemistry Communications*, 12, 337–355, **1947**. DOI: 10.1135/cccc19470337.

[126] B. Dingfelder and J. A. C. Weideman, An improved Talbot method for numerical Laplace transform inversion, *Numerical Algorithms*, 68, 167 –183, **2015**. DOI: 10.1007/s11075-014-9895-z.

[127] A. Talbot, The Accurate Numerical Inversion of Laplace Transforms, *Journal of Applied Mathemathics*, 23, 97 –120, **1979**. DOI: 10.1093/imamat/23.1.97.

[128] J. A. C. Weideman and N. L. Trefethen, Parabolic and Hyperbolic Contours for Computing the Bromwich Integral, *Mathematics of Computation*, 76, 1341 –1356, **2007**. doi: 10.1090/S0025-5718-07-01945-X.

[129] J. Douglas, Alternating Direction Methods for Three Space Variables, *Numerische Mathematik*, 4, 41–63, **1962**. doi: 10.1007/BF01386295.

[130] C. Montella, LSV/CV modelling of electrochemical reactions with interfacial CPE behaviour, using the generalised Mittag–Leffler function, *Journal of Electroanalytical Chemistry*, 667, 38 –47, **2012**. doi: 10.1016/j.jelechem.2011.12.010.

List of Publications

[1] I. Akhmetova, S. Beyer, K. Schutjajew, **T. Tichter**, M. Wilke, C. Prinz, I. C. B. Martins, D. Al-Sabbagh, C. Roth, and F. Emmerling, Cadmium benzylphosphonates – the close relationship between structure and properties, *CrystEngComm*, 21, 5958–5964, **2019**. doi: 10.1039/c9ce00776h.

[2] **T. Tichter**, D. Andrae, J. Mayer, J. Schneider, M. Gebhard, and C. Roth, Theory of cyclic voltammetry in random arrays of cylindrical microelectrodes applied to carbon felt electrodes for vanadium redox flow batteries, *Physical Chemistry Chemical Physics*, 21, 9061–9068, **2019**. doi: 10.1039/C9CP00548J.

[3] F. Muench, G. A. El-Nagar, **T. Tichter**, A. Zintler, U. Kunz, L. Molina-Luna, V. Sikolenko, C. Pasquini, I. Lauermann, and C. Roth, Conformal Solution Deposition of Pt-Pd Titania Nanocomposite Coatings for Light-Assisted Formic Acid Electro-Oxidation, *Applied Materials and Interfaces*, 11, 43081–43092, **2019**. doi: 10.1021/acsami.9b12783.

[4] **T. Tichter**, J. Schneider, D. Andrae, M. Gebhard, and C. Roth, Universal algorithm for simulating and evaluating cyclic voltammetry at macroporous electrodes by considering random arrays of microelectrodes, *ChemPhysChem*, 21, 428 –441, **2019**. doi: 10.1002/cphc.201901113.

[5] M. Gebhard, **T. Tichter**, D. Franzen, M. C. Paulisch, K. Schutjajew, T. Turek, I. Manke, and C. Roth, Improvement of Oxygen-Depolarized Cathodes in Highly Alkaline Media by Electrospinning of Poly(vinylidene fluoride) Barrier Layers, *ChemElectroChem*, 7, 830–837, **2020**. doi: 10.1002/celc.201902115.

[6] J. Schneider, **T. Tichter**, P. Khadke, R. Zeis, and C. Roth, Deconvolution of electrochemical impedance data for the monitoring of electrode degradation in VRFB, *Electrochimica Acta*, 336, 135510, **2020**. doi: 10.1016/j.electacta.2019.135510.

[7] **T. Tichter**, J. Schneider, D. Nguyen Viet, A. Diaz Duque, and C. Roth, Rotating Ring-Disc Electrode Measurements for the Quantitative Electrokinetic Investigation of the V^{3+}-Reduction at Modified Carbon Electrodes, *Journal of Electroanalytical Chemistry*, 859, 113843, **2020**. doi: 10.1016/j.jelechem.2020.113843.

[8] **T. Tichter**, D. Andrae, J. Schneider, M. Gebhard, A. Hilger, I. Manke, and C. Roth, Real-Space Simulation of Cyclic Voltammetry in Carbon Felt Electrodes by Combining Micro X-Ray CT Data, Digital Simulation and Convolutive Modeling, *Electrochimica Acta*, 353, 136487, **2020**. doi: 10.1016/j.electacta.2020.136487.

[9] **T. Tichter**, J. Schneider, and C. Roth, Finite Heterogeneous Rate Constants for The electrochemical Oxidation of VO^{2+} at Glassy Carbon Electrodes, *Frontiers in Energy Research*, Accepted on 22$^{\text{th}}$ June 2020, pages not yet defined, **2020**. doi: 10.3389/fenrg.2020.00155.

[10] M. Gebhard, **T. Tichter**, J. Schneider, J. Mayer, A. Hilger, M. Osenberg, M. Rahn, I. Manke, and C. Roth, On the stability of bismuth in modified carbon felt electrodes for vanadium redox flow batteries: An in-operando X-ray computed tomography study, *Journal of Power Sources*, Accepted on 25$^{\text{th}}$ July 2020, pages not yet defined, **2020**. doi: 10.1016/j.jpowsour.2020.228695.

[11] P. Khadke, **T. Tichter**, T. Böttcher, F. Münch, W. Ensinger, and C. Roth, Differential Tafel Plots: A Simple yet Effective Strategy for Accurate Interpretation of Tafel Plots, *ChemElectroChem*, Submitted and under revision, **2020**.

[12] M. Maleki, **T. Tichter**, G. El-Nagar, I. Lauermann, and C. Roth, Hybrid Electrospun Nanofibers as Electrocatalyst for Vanadium Redox Flow Batteries: Theory and Experiment, *ACS Applied Materials and Interfaces*, Submitted and under revision, **2020**.

Appendix A

Additional Derivations

The following appendix contains two additional derivations of Laplace transformation/inverse Laplace transformation pairs, which are referred to in the main part of this cumulative thesis and which belog to a planar semi-infinite and a planar finite reflective diffusion domain.

A.1 Planar Semi-Infinite Diffusion

The aim of this section is finding the Laplace transformation of the function $f(t) = (\pi t)^{-1/2}$. Consider

$$\bar{f}(s) = \mathcal{L}\left\{\frac{1}{\sqrt{\pi t}}\right\}(s) = \int_0^\infty \frac{1}{\sqrt{\pi t}}\,\mathrm{e}^{-st}\mathrm{d}t \tag{A.1}$$

and substitute $t^{1/2} = x$, such that $\mathrm{d}t = 2t^{1/2}\mathrm{d}x$. This results in the expression

$$\bar{f}(s) = \frac{2}{\sqrt{\pi}}\int_0^\infty \mathrm{e}^{-sx^2}\mathrm{d}x, \tag{A.2}$$

which can be regarded as Gaussian integral. Since

$$\int_{-\infty}^{\infty} \mathrm{e}^{-ax^2}\mathrm{d}x = \sqrt{\frac{\pi}{a}} \tag{A.3}$$

with a as a constant such that $a > 0$, it can be noticed that

$$\int_0^\infty \mathrm{e}^{-ax^2}\mathrm{d}x = \frac{1}{2}\sqrt{\frac{\pi}{a}}. \tag{A.4}$$

This finally yields

$$\bar{f}(s) = \frac{1}{\sqrt{s}}. \tag{A.5}$$

In this manner, the following Laplace transformation/inverse Laplace transformation pair is defined:

$$\mathcal{L}\left\{\frac{1}{\sqrt{\pi t}}\right\}(s) = \frac{1}{\sqrt{s}} \tag{A.6}$$

$$\mathcal{L}^{-1}\left\{\frac{1}{\sqrt{s}}\right\}(t) = \frac{1}{\sqrt{\pi t}} \tag{A.7}$$

A.2 Planar Finite Reflective Diffusion

The aim of this section is to find the inverse Laplace transformation of the function $\bar{f}(s) = \coth(s^{1/2})/s^{1/2}$, or in particular of $\bar{f}(s) = \coth(as^{1/2})/s^{1/2}$, where a is a constant which fulfills $a > 0$ and which translates to $a^2 = d^2/D$. For this purpose, one might start with the definition of Eulers infinite sine product according to

$$\sin(x) = x \prod_{k=1}^{\infty} \left(1 - \frac{x^2}{k^2\pi^2}\right). \tag{A.8}$$

Noting that the hyperbolic sine function and the sine function are related via

$$\sinh(x) = \frac{\sin(\mathrm{i}x)}{\mathrm{i}}, \tag{A.9}$$

where $\mathrm{i} = \sqrt{-1}$, one can obtain

$$\sinh(x) = x \prod_{k=1}^{\infty} \left(1 + \frac{x^2}{k^2\pi^2}\right). \tag{A.10}$$

Taking the logarithm of equation A.10 results in

$$\ln(\sinh(x)) = \ln(x) + \sum_{k=1}^{\infty} \ln\left(1 + \frac{x^2}{k^2\pi^2}\right). \tag{A.11}$$

Performing a differentiation with respect to x on equation A.11 gives

$$\frac{\partial \ln(\sinh(x))}{\partial x} = \frac{\cosh(x)}{\sinh(x)} = \coth(x) = \frac{1}{x} + \sum_{k=1}^{\infty} \left(\frac{\frac{2x}{\pi^2k^2}}{1 + \frac{x^2}{\pi^2k^2}}\right), \tag{A.12}$$

with $\coth(x)$ being the hyperbolic cotangent function. Now, taking $x = s^{1/2}$ as well as the initial function of $\bar{f}(s) = \coth(s^{1/2})/s^{1/2}$, one arrives at

$$\bar{f}(s) = \frac{1}{s} + 2\sum_{k=1}^{\infty} \left(\frac{1}{s + \pi^2k^2}\right). \tag{A.13}$$

The inverse Laplace transformation can be applied readily on equation A.13. The first term is easily identified as the Laplace transformation of 1. The infinite sum in turn might be inverted term by term by exploiting the relation given in equation 3.61. This finally yields

$$\mathcal{L}^{-1}\left\{\bar{f}(s)\right\}(t) = 1 + 2\sum_{k=1}^{\infty}\exp(-\pi^2 k^2 t). \tag{A.14}$$

The right hand side of equation A.14 can be identified as the Jacobian Θ_3 function. This defines the Laplace transformation/inverse Laplace transformation pair of

$$\mathcal{L}\left\{\Theta_3(0|t)\right\}(s) = \frac{\coth(\sqrt{s})}{\sqrt{s}} \tag{A.15}$$

$$\mathcal{L}^{-1}\left\{\frac{\coth(\sqrt{s})}{\sqrt{s}}\right\}(t) = \Theta_3(0|t) = 1 + 2\sum_{k=1}^{\infty}\exp(-\pi^2 k^2 t), \tag{A.16}$$

which was used along with equation 3.100 in the theory section.

Acknowledgements

The acknowledgements have been removed in the online version.

The acknowledgements have been removed in the online version.